Feasibility Study of Long-Life Micro Fuel Cell Power Supply for Sensor Networks for Space and Terrestrial Applications

By

Kavya Kamal Manyapu

Submitted to the Department of Aeronautics and Astronautics
on May 7th, 2010, in partial fulfillment of the
requirements for the degree of Masters of Science in
Aeronautics and Astronautics

At the

Massachusetts Institute of Technology

May 2010
[June 2010]

Signature of Author .....
Department of Aeronautics and Astronautics
May 7, 2010

Certified by .....
Steven Dubowsky
Professor of Mechanical Engineering
Thesis Supervisor

Accepted by .....
Eytan H. Modiano
Associate Professor of Aeronautics and Astronautics
Chair, Committee on Graduate Students

Dedicated to my loving parents
Raghava Rao Manyapu and Manjulatha

Feasibility Study of Long-Life Micro Fuel Cell Power Supply for Sensor Networks for Space and Terrestrial Applications

By

Kavya Kamal Manyapu

Submitted to the Department of Aeronautics and Astronautics
on May 7th, 2010, in partial fulfillment of the
requirements for the degree of Masters of Science in
Aeronautics and Astronautics

ABSTRACT

Sensor networks used for activities like border security, search and rescue, planetary exploration, commonly operate in harsh environments for long durations, where human supervision is minimal. A major challenge confronting such devices is providing adequate and reliable power supply required for long durations. This research considers the feasibility of a miniature Proton Exchange Membrane (PEM) fuel cell system coupled with battery to supply power for long life missions.

The focus of this research is to prove the feasibility of long-life, self-contained power-supplies using miniature fuel cells for low-power distributed sensor networks. In this research, the performance of fuel cell power-supplies weighing not more than a few hundred grams is studied. The performance of the PEM fuel cell is modeled, analyzed and validated using experimental results. The feasibility of the fuel cell power systems are studied for two reference missions - one on the lunar surface and the other in the desert regions of Negev, Israel. This research analyzes the use of passive methods to achieve thermal, air and water management for PEM fuel cells supplying power to these field sensors.

The results of this study suggest that the proposed fuel cell power system is capable of providing power to sensor modules in challenging field conditions with operational lives extending from many months to years. The scope of this concept can be extended to power devices such as micro-robots and small unmanned aerial vehicles operating in extreme environmental conditions for sustained periods of time.

Thesis Supervisor: Steven Dubowsky
Title: Professor of Mechanical Engineering

ACKNOWLEDGEMENTS

This research was conducted in the MIT Field and Space Robotics lab with funding from NASA's Jet Propulsion Laboratory and Israeli Ministry of Defense

I would like to thank the many people who made this thesis possible:

- Dr. Dubowsky for giving me the opportunity to learn and for his endless and continued advice, guidance and mentoring.
- My family for dedicating their efforts for my career and education over the past 23 years with love and guidance.
- My beloved, Chetan for supporting and motivating me to achieve my goals.
- Amy Bilton for guidance and mentoring.
- Jekanthan Thangavelautham, Danielle Gallardo and Paolo Iora for being supportive team mates and helping me with progressing on my research.
- Kevin Plumer, an Undergraduate Research student for his assistance in fabrication and machining for experimental work.
- Francesco Mazzini and Leah Kelley for helping me hone my technical skills.
- Each of the FSRL members who have spent their valuable time in reviewing my thesis and providing guidance and useful suggestions.
- The entire FSRL for helping me with every challenge I have encountered.

And finally, I would like to thank MIT giving me an opportunity for being a part of their prestigious institution and providing me with the best education in the past 2 years.

TABLE OF CONTENTS

ABSTRACT 3
ACKNOWLEDGEMENTS 4
TABLE OF CONTENTS 5
LIST OF FIGURES 6
LIST OF TABLES 8
CHAPTER 1 INTRODUCTION 9
1.1. Motivation 9
1.2. Background Literature 11
1.3. Fuel Cell Powered Sensor System Concepts for Space and Terrain Applications 12
1.4. Thesis Organization 14
CHAPTER 2 FEASIBILITY OF FUEL CELL POWER SYSTEM 16
2.1 PEM Fuel Cells Overview 16
2.2. Fuel Cell System Components 18
2.3. Feasibility Analysis 21
CHAPTER 3 FUEL CELL MODEL DEVELOPMENT 28
3.1. Models from Literature 28
3.2. Fuel Cell Model Configuration 29
3.3. Model validation 40
3.4. Experimental Characterization 41
CHAPTER 4 THERMAL ARCHITECHTURE FOR FUEL CELL POWERED SENSOR SYSTEMS 46
4.1. Thermal Isolation System for Space Applications 46
4.2. Thermal Isolation System for Terrain Applications 53
4.3. Experimental Validation of the Thermal Model 63
CHAPTER 5 AIR AND WATER MANAGEMENT FOR A TERRESTRIAL APPLICATION 70
5.1. Soils of the Desert Regions 70
5.2. Air Breathing System 72
5.3. Carbon Dioxide Accumulation 76
5.4. Water Management 79
CHAPTER 6 CONCLUSIONS AND RECOMMENDATIONS 85
6.1. Summary of Results 85
6.2 Challenges and Lessons Learnt 85
6.3 Future work 86
REFERENCES 87
APPENDIX A FEASIBILITY ANALYSIS FOR OTHER SMALL SCALE APPLCIATIONS 91
APPENDIX B DETAILS OF FUEL CELL EXPERIMENT 94

LIST OF FIGURES

Figure 1. (Left) Remote site (cave) requiring Border security, (Right) Natural disaster debris requiring search and rescue operations [1] 10
Figure 2. Micro PEM Fuel Cell [7] 10
Figure 3. A conceptual design for fuel cell power system for sensors [18]. 11
Figure 4.Typical duty cycle of small scale environmental sensor. 13
Figure 5. Concept for micro fuel cell power supply for long life applications [19]. 13
Figure 6. A concept of fuel cell-powered sensor system for space applications. 14
Figure 7. (Left) A concept of a buried sensor module with fuel cell power supply. (Right) Internal layout. ..14
Figure 8. PEM Fuel Cell Detailed Operation [54]. 16
Figure 9. Basic PEM Fuel Cell Operation. 17
Figure 10. Fuel cell power supply components [19]. 19
Figure 11. Metal Hydrides operating pressures and temperatures [47] 20
Figure 12. Comparison of energy densities of electrochemical technologies (Ragone chart) [56]. 22
Figure 13. Feasibility analysis results for system mass of 1kg and 0.5W power requirement. 23
Figure 14. Feasibility analysis results for system volume of 1L and 0.5W power requirement 25
Figure 15.Comparison of the mass of the system for various electrochemical technologies. 26
Figure 16. Mass of power supply system verses the operational life of the mission. 26
Figure 17. Schematic of the developed PEM fuel cell model. 30
Figure 18. Cell Polarization Curve [8]. 35
Figure 19. Humidity effect on power generated. 38
Figure 20. Pressure effect on power generated. 39
Figure 21. Temperature effect on power generated. 40
Figure 22. Validation of model results with published literature model. 40
Figure 23. Schematic of the experimental setup [25] 42
Figure 24. Experimental setup in the laboratory [25]. 42
Figure 25. Experimental results of the polarization curve for varying humidity levels in inlet air. 43
Figure 26. Experimental results of the power curve for varying humidity levels in inlet air. 43
Figure 27. Experimental validation of the model for 30% humidity level of air (100% H_2). 44
Figure 28. Experimental validation of the Model for 80% humidity level of air (100% H2). 44
Figure 29. Lower heating value efficiency of PEM fuel cell from model and experiments 45
Figure 30. A concept of a fuel cell-powered sensor network on the lunar surface [39] 47
Figure 31. Three-dimensional representation of thermal architecture concept for sensors on lunar surface. ..48
Figure 32: Inner acrylic ring [Dimensions are in inches]. 48
Figure 33: Outer acrylic ring. 49
Figure 34: Heat transfer modes at each node in the system. 50
Figure 35. Location of Nizzana, Israel [40] 54
Figure 36. Temperature profiles at varying depths during summer and winter at Nizzana, Israel. 56
Figure 37. Three dimensional representation of fuel cell-powered sensor system in a spherical configuration. 56
Figure 38. Representation of the fuel cell-powered sensor system buried underground 57
Figure 39. Heat transfer model of buried sensor system. 58
Figure 40. Temperature profile radially outward into the surrounding during winter. 59

Figure 41. Temperature profile radially outward into the surrounding during summer. 59
Figure 42. Three-dimensional representation of fuel cell-powered sensor system in a rectangular configuration. 60
Figure 43. Representation of the fuel cell powered sensor system buried underground. 60
Figure 44. Representation of the heat transfer model for the rectangular configuration. 62
Figure 45. Temperature profile radially outward into the surrounding soil during summer. 62
Figure 46. Temperature profile radially outward into the surrounding soil during winter. 63
Figure 47. Electrical circuit embedded inside the inner sphere. 64
Figure 48. (Left) External ring holding the outer domes (Right) Completed Assembly. 64
Figure 49. AA Alkaline Battery Performance [19]. 65
Figure 50. Test 1 experimental results: 0.5 W heat production and ambient temperature -15 °C. 66
Figure 51. Test 2 experimental results: 0.5 W heat production and ambient temperature -24°C. 67
Figure 52. Test 3 experimental results: 0.5W heat production and ambient temperature -24°C. 68
Figure 53. Temporal variation in water movement [59]. 72
Figure 54. Air breathing system with hydrophobic material on the surface. 74
Figure 55. (Left) GORE-TEX® material [28], (Right). HST Roll [17]. 75
Figure 56. Model for air breathing analysis of the system buried underground. 76
Figure 57. Model for Carbon dioxide accumulation in the system buried underground. 78
Figure 58. Results from carbon dioxide accumulation analysis. 79
Figure 59. Water management concept for fuel cell powered sensor systems [19]. 81
Figure 60. Air and vapor flow rates through the vapor barrier for water management. 82
Figure 61. Vapor escaped from the system with respect to the vapor barrier surface area. 82
Figure 62. Model for water management analysis. 83
Figure 63. Feasibility analysis results for UAVs. 91
Figure 64. Feasibility analysis results for Terrain robot. 92
Figure 65. Feasibility analysis for AUVs (Fish Robot). 93
Figure 66. Resistance Network values [25]. 95
Figure 67: Electrical Schematic of Resistance Network, Fuel Cells, and Multimeter [25]. 95
Figure 68. Fuel Cell Temperature Sensor Placement [25]. 96

LIST OF TABLES

Table 1. Types of Fuel Cell [8, 41]. 17
Table 2. Hydrogen storage methods and efficiencies [32, 48]. 19
Table 3. Comparison of Energy Densities of Electrochemical technologies [8, 23, 41, 42]. 21
Table 4. Thermal Isolation system parameters. 48
Table 5.Values used in thermal transient analysis. 53
Table 6. Temperatures at Nizzana, Israel [40]. 54
Table 7. Values used for heat transfer analysis. 58
Table 8. Sequence of experimental tests. 65
Table 9. Air permeability values of soil [48]. 71
Table 10. Mass of reactants required for 3 years operation of fuel cell. 73
Table 11. Values of parameters used. 73
Table 12. Dimensions of rectangular configuration system. 73
Table 13. Mass of air in the system. 73
Table 14. Air breathing analysis results. 76
Table 15.Water required and released by fuel cell. 80
Table 16. Parameters used for water management analysis. 82
Table 17. Comparison of water required with and without vapor barrier in the system. 84
Table 18. Connection Guide for RN1 and RN2, and the corresponding resistance [25]. 97

CHAPTER 1
INTRODUCTION

This thesis proves the feasibility of using a miniature, long-life, self-contained fuel cell power-supply system for low-power, long-duration distributed sensor networks. In this research, the performance of fuel cell power-supplies weighing in the order of 100's of grams is studied. These systems are capable of providing power to sensor modules with operational lives extending many months to years. This concept could be extended to power other applications like micro-robots for weeks to months in extreme environmental conditions, such as terrestrial deserts, lunar surface, and other planetary surfaces.

This research demonstrates the feasibility of using fuel cell power systems for sensors operating in two representative missions, 1) lunar surface, and 2) terrestrial deserts (Negev, Israel). Part of this research focuses on feasibility analysis of small scale robotic systems in air, water, and ground. A miniature Proton Exchange Membrane (PEM) fuel cell is proposed as a power supply. The PEM fuel cell consumes hydrogen and oxygen (from air) to produce electrical power. The performance of the fuel cell is modeled, characterized under varying operating conditions via experiments and validated using published results. A passive thermal management system is proposed for the fuel cell power supply and analyzed for the representative missions. Feasibility of using passive air and water management systems are presented for fuel cell power supply system intended for distributed sensors in challenging field conditions.

This research is conducted at the MIT Field and Space Robotics Laboratory (FSRL) under the guidance of Professor Steven Dubowsky with funding from the Israeli Ministry of Defense and NASA's Jet Propulsion Laboratory.

1.1. Motivation

Applications such as planetary exploration, search and rescue, monitoring of remote sites for border security, and other related activities require operating sensors and robots in harsh environments. Environmental conditions like irregular terrain, wide temperature fluctuations, debris from natural and man-made disasters, are not favorable for humans to traverse and achieve mission goals. Figure1 shows examples of environments that are unfavorable to human exploration. Hence for missions in such challenging environments, self operating devices like sensors are used to accomplish the tasks. The current challenge for these devices in such missions is providing adequate onboard power supply to sustain operations for long durations.

Figure 1. (Left) Remote site (cave) requiring Border security, (Right) Natural disaster debris requiring search and rescue operations [1].

These missions require power for long durations, ranging from weeks to months based on the mission goals. It is often critical that field sensors operate for long durations unattended, as it reduces the cost involved in replacing, transporting and deploying these devices.

Presently, such applications use batteries as a power source. Batteries provide sufficient power but not enough energy for long missions. Batteries are electrochemical devices that provide instantaneous power; however they are limited in terms of life, prone to high rates of self-discharge and can leak toxic metals into the environment. Fuel cells are a promising alternative that are very efficient, non-toxic and have the potential of providing power for long durations, on the order of months to years. Although micro fuel cells generate relatively low power, they have high specific energy. Figure 2 shows a commercially available micro PEM fuel cell that can generate 300mW of power [7].

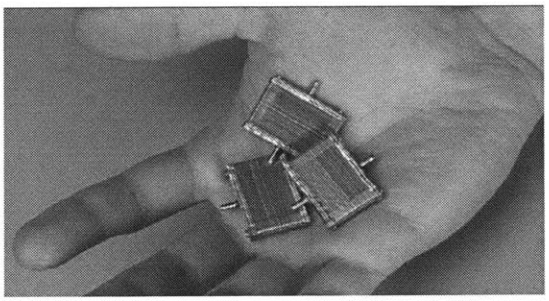

Figure 2. Micro PEM Fuel Cell [7].

Many applications mentioned earlier require small amounts of power (< 1 W) but substantial energy for longer durations. In such cases small, lightweight batteries alone are not sufficient to meet the total energy demand. Hence, a hybrid system is proposed, where micro-fuel cells are coupled with batteries. The combined system provides power to meet the high demands and the energy to sustain long life missions.

Though large fuel cells have been used successfully in applications such as spacecraft for many years, their utility in providing long-life power for very small distributed sensor networks is yet to be investigated. PEM fuel cells are more efficient than conventional batteries and can readily be miniaturized. This research addresses the

use of micro fuel cells for such small scale applications with operational lives on the order of months to years. The purpose of this research is to focus on analyzing the feasibility of using fuel cell power systems for applications in harsh environments. It is shown that matching micro-fuel cells with batteries in a hybrid system can provide long-life power for distributed sensor networks.

The use of micro fuel cells in field conditions presents a number of technical challenges. These challenges include the development of effective passive methods for fuel cell power system thermal management, effective means to store the required hydrogen, and fuel cell power system's reliability in providing long-duration power. These are the basic engineering challenges that are being addressed in this study. Figure 3 shows a conceptual design of the fuel cell power system module for sensor networks. The fuel cell concept is explained in more detail in Section 1.3.

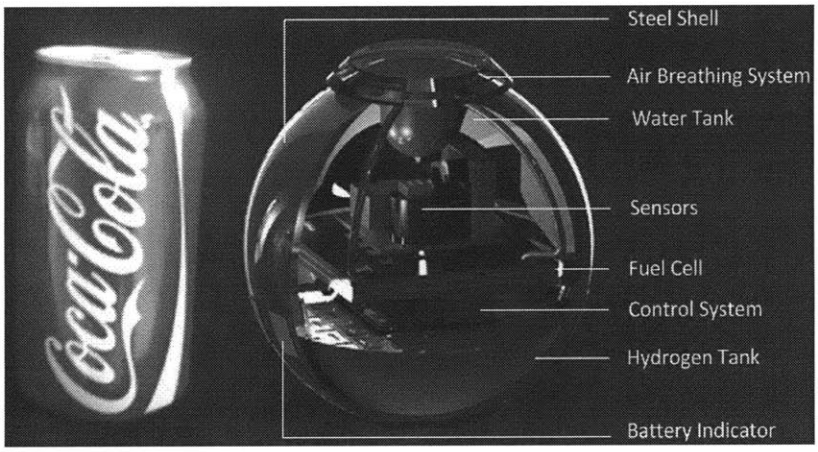

Figure 3. A conceptual design for fuel cell power system for sensors [18].

1.2. Background Literature

Some examples of fuel cell power systems for long-duration applications with low power are [20]:

- Monitoring remote sites for border protection.
- Seismic nets to aid in search and rescue operations after earthquakes.
- Environmental and meteorology sensors for air pollution, radiation, rainfall, forest fires.
- Monitoring tunnels, oil pipelines and water supply systems for potential terrorist activity.
- Sensors networks for surveillance of, hidden chemical and biological threats.

This section presents related literature on fuel cell power supplies for low-power, long duration applications.

1.2.2. Fuel Cell Power Systems for Small Scale Applications

Fuel cells are simple energy conversion devices that convert electrochemical energy into electrical power. A fuel cell consists of an anode, cathode and an electrolyte. Details on the operation of a PEM fuel cell and its components are explained in Chapter 2.

Fuel cells have been used in space exploration since the Gemini spacecraft in 1965 [11, 12]. NASA has opted to use alkaline fuel cells instead of batteries as the primary source of electrical power on human spaceflight systems for over four decades due to their high-reliability and efficiency [11]. Fuel cells provide

electricity, heat and drinking water for the spacecraft crew. However, very little research has been published on the application of fuel cells for low power applications such as small sensor networks.

Previously, a PEM fuel cell power supply concept was demonstrated by members of FSRL to power Microbots with hopping capability [33]. The application was designed for planetary surface and subsurface exploration that required power in the range of 500-700mW. The application was based on studies conducted on using fuel cells for planetary exploration [21, 22, 32]. An experimental fuel cell power system was designed and tested and the feasibility of hopping, rolling and bouncing mobility using the power from fuel cells was demonstrated [21, 22, 32, 33]. This thesis uses the design concept from this previous study and applies it to sensor networks.

Another relevant research using fuel cells for small applications was the work done at the Osaka City University where a PEM fuel cell was shown to power fish robots [53]. The fish robot was tethered to the PEM fuel cell located outside of the fish tank and produced 0.42W of power using hydrogen and ambient air, enough for short range swimming. However the reliability and long life capabilities of fuel cells were not shown in the study.

Aerovironment has broken long-duration flight record using a small unmanned air vehicle (UAV) powered by a fuel cell-battery hybrid system. The 12.5-pound UAV called Puma flew for nine hours, operating at an altitude between 100-500 feet and flew at speeds of 7-14 m/s [3]. The onboard fuel cell-battery hybrid storage system provided three times more energy than with a comparable battery powered system [3]. This study however, has not been able to demonstrate extended missions lasting more than 9 hours.

Ball Aerospace has demonstrated an advanced portable power source using a 50W PEM fuel cell for commercial and military applications. The system was evaluated under different environmental temperatures and humidity conditions [6]. It was concluded that the portable fuel cell system can provide a normal power output of about 50W at 12V, while peak power output could reach 65W. A similar system was used to power PRC-119 radios for communication applications, and a laptop computer, operating continuously for over 25 hours [6]. This study however, focused on particular PEM fuel cells available and does not demonstrate the use of fuel cells for distributed sensor networks for long durations.

1.3. Fuel Cell Powered Sensor System Concepts for Space and Terrain Applications

Portable PEM fuel cells that provide powers less than 1W are available commercially however these fuel cells have not been designed for long-life [19, 30, 3]. The focus of this research is to prove the feasibility of using such small fuel cells for long-life for powering small distributed sensors. This section summarizes the conceptual design of the fuel cell powered sensor system in a hybrid configuration using a battery. Two representative missions are chosen for proving the feasibility of using fuel cell power supply for sensor networks: 1) the polar regions of the lunar surface, and 2) the desert regions of Negev, Israel. For the reference mission in the desert regions, it is assumed that the sensor networks are buried 0.61m (2 feet) below the surface for applications such as border security.

For the representative missions, it is assumed that the sensors require average power within 10mW for 3 years and peak powers up to 100mW. A typical power requirement for a sensor with the average and peak powers demands is shown in Figure 4. Based on our studies, the fuel cells shouldn't be connected directly to the sensors for the specified duty cycle because the life of the fuel cell will be drastically reduced due to power fluctuations [19]. Fuel cells can achieve long lives, when producing constant power. Hence a fuel cell-battery hybrid system is proposed, where the battery supplies power during peak demands and the fuel cell constantly charges the battery.

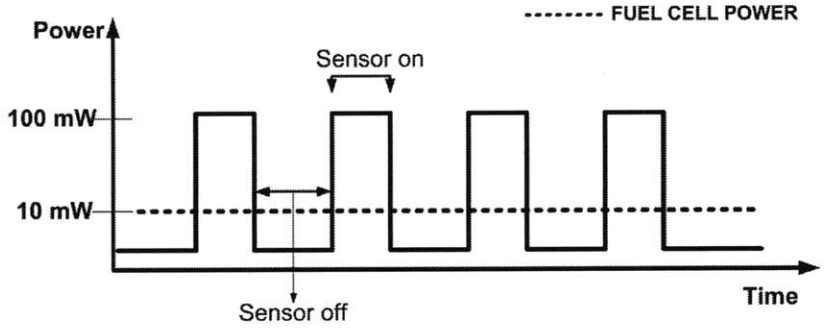

Figure 4.Typical duty cycle of small scale environmental sensor.

The concept for the fuel cell power system for sensor networks proposed in this research is shown in the system block diagram in Figure 5 [19]. The micro fuel cell is optimized to provide uniform average power that will charge a battery which in turn provides power for the sensors, control system and communication. The fuel cell consumes hydrogen stored in metal hydrides with a hydrogen storage-weight efficiency of 5-6 %. For applications on earth, fuel cells obtain oxygen from ambient air, where as for space applications oxygen is supplied by an onboard oxygen carrier.

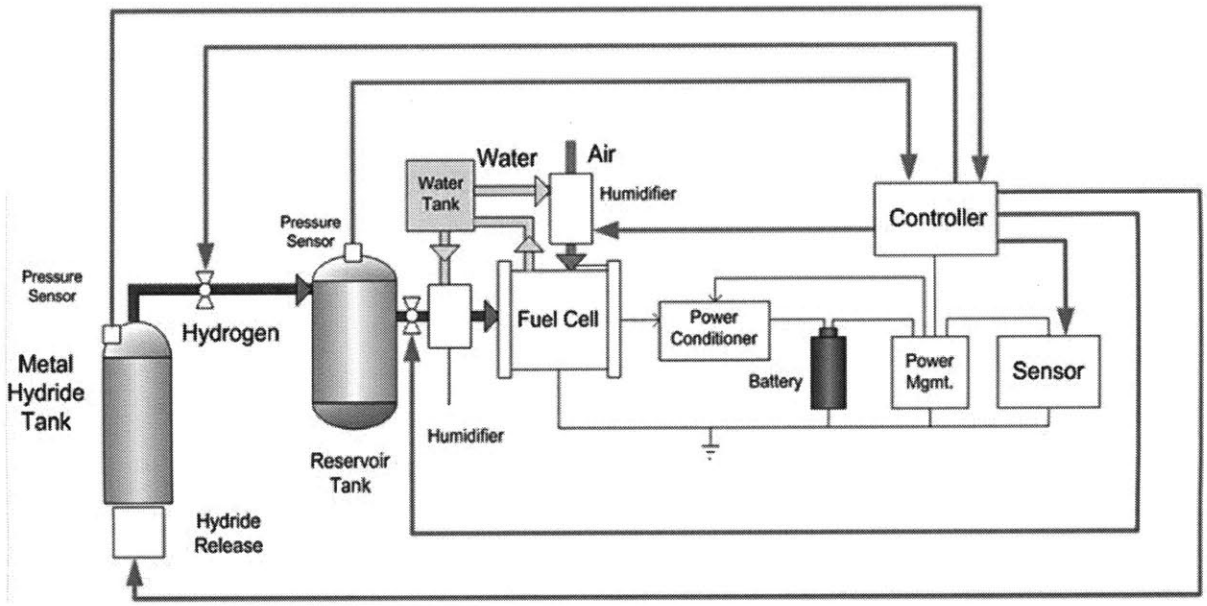

Figure 5. Concept for micro fuel cell power supply for long life applications [19].

The fuel cell powered concept proposed in this research can be implemented for various applications, both for space and terrestrial applications. Figures 6 and 7 show two system designs using the power concept. Figure 6 shows a three dimensional model of the fuel cell powered sensor network concept for space applications. The fuel cell powered sensor module is no larger than a soccer ball, and is thermally insulated to maintain temperatures above 0°C for the operation of fuel cell and other electronics. Figure 7 shows a concept of the fuel cell powered sensor system for use in a field sensor network that is no larger than a typical shoe box. In both configurations, the fuel cell is used to trickle charge a battery and power low power devices.

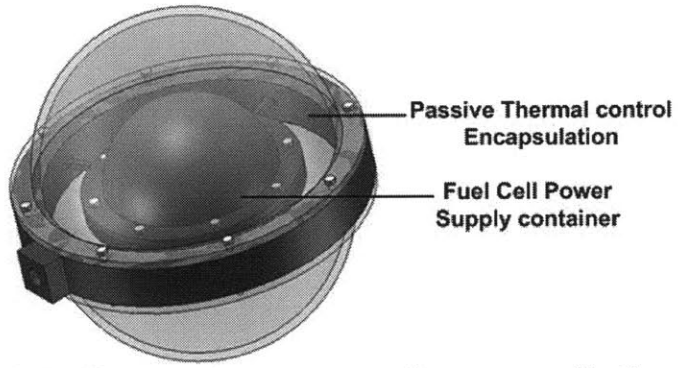

Figure 6. A concept of fuel cell-powered sensor system for space applications.

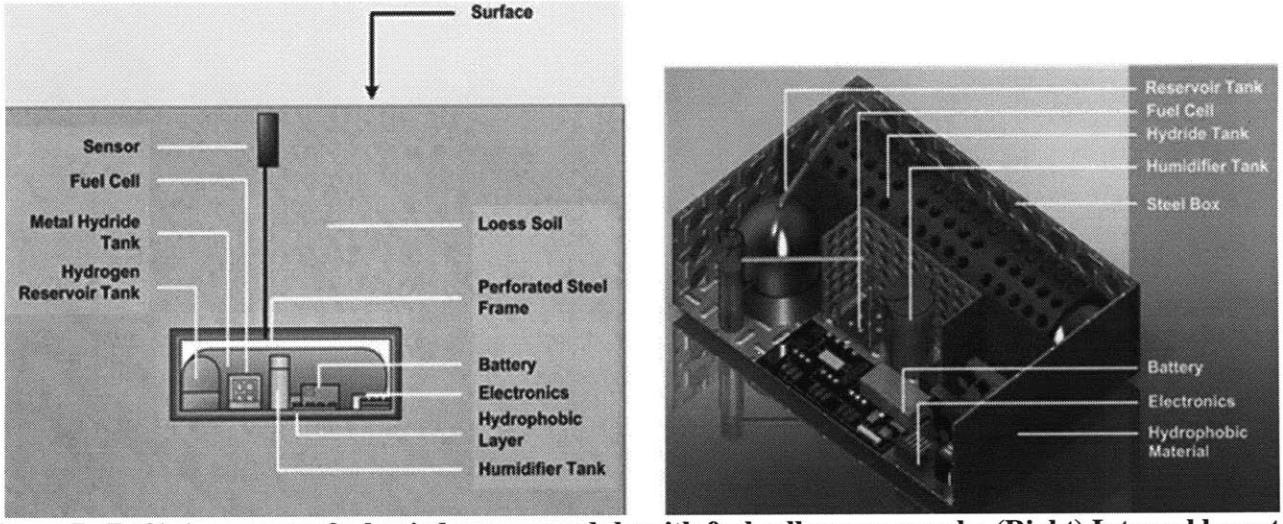

Figure 7. (Left) A concept of a buried sensor module with fuel cell power supply. (Right) Internal layout.

1.4. Thesis Organization

The main objective of this research is to demonstrate the feasibility of using fuel cells for long durations to power sensors in harsh environments. The performance of a PEM fuel cell is analyzed and the feasibility is compared to other technologies. The thermal, air and water management for the power system are studied for two reference missions.

Chapter 2 focuses on the feasibility of using fuel cells for long-duration missions. The chapter summarizes the operation of fuel cells and discusses the advantage of using fuel cells over competing mobile power systems.

Feasibility analysis for using fuel cells for Unmanned Aerial Vehicle (UAVs), Autonomous Underwater Vehicles (AUVs) and all-terrain rovers is performed and reported in Appendix A.

Chapter 3 discusses the model developed for predicting the performance of a PEM micro fuel cell as a function of operating parameters such as pressure, temperature and humidity. This is followed by experimental demonstration and validation of the fuel cell model.

Chapter 4 discusses thermal management system for the two reference missions. Unique passive system concepts for thermal insulation are discussed and analyzed. The thermal insulation system for the reference mission on the moon is tested experimentally.

For a buried field sensor concept, two critical issues are air and water management. Chapter 5 presents design concepts that address these two issues.

In summary, this thesis demonstrates the feasibility of using fuel cells for long life missions, on the order of years to power distributed sensor networks with a focus on two potential applications. This study shows that the power system designs that are developed here are able to provide proper operating conditions to maximize fuel cell life.

CHAPTER 2

FEASIBILITY OF FUEL CELL POWER SYSTEM

This chapter explains the basic operation of the fuel cell and demonstrates the feasibility of using Proton/Polymer Exchange Membrane (PEM) fuel cells for long life sensor applications. Feasibility analysis calculates the number of operating days for a given system mass and volume. Various battery technologies are compared in terms of mass and life with PEM fuel cells. Reduction in mass and increase in operational life using fuel cells as power supplies is demonstrated. Feasibility analyses are also performed for various applications on the ground, in air, and in water.

2.1 PEM Fuel Cells Overview

Fuel cells are electrochemical devices that convert chemical energy into electrical energy. A fuel cell consists of an anode that is negatively charged, a cathode that is positively charged and an electrolyte membrane that separates both the electrodes as shown in Figure 8. A catalyst layer on the electrodes is present to increase the rate of reactions in the fuel cell. There are different types of fuel cells based on the type of electrolyte, fuel and oxidizer used. A summary of these fuel cells and their operating temperatures are given in Table 1 [8, 41]. For this study, PEM fuel cells are chosen for their low operating temperatures (on the order of 10°C to 80°C), high efficiencies (up to 70%), simplicity, feasibility, quick start-up characteristics as well as non-toxic emissions for space and terrain applications [8, 41]. The basic operation of the PEM fuel cell is shown in Figures 8 and 9. The PEM fuel cell takes in hydrogen (H_2) and oxygen (O_2) from air and produces electricity, water and heat. A fuel cell must be constantly fed with fuel and oxidizer to produce electricity. Certain controllable factors such as impurity of reactants, humidity levels can structurally degrade the membrane and the catalyst [19].

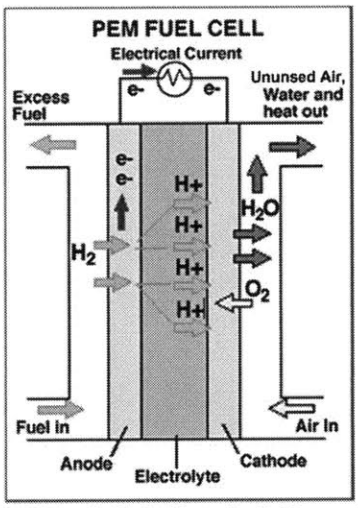

Figure 8. PEM Fuel Cell Detailed Operation [54].

Table 1. Types of Fuel Cell [8, 41].

FUEL CELL	ELECTROLYTE	OPERATING TEMPERATURE	ELECTRICAL EFFICIENCY	FUEL OXIDANT
Alkaline Fuel Cell –AFC	Potassium Hydroxide solution	Room Temperature to 90°C	60-70%	H_2 O_2/Purified air
Proton Exchange Membrane Fuel Cell PEMFC	Proton Exchange Membrane	Room Temperature to 80°C	40-70%	H_2 O_2/Air
Direct Methanol Fuel Cell DMFC	Proton Exchange Membrane	Room Temperature to 130°C	20-30%	CH_2OH O_2, Air
Phosphoric Acid Fuel Cell PAFC	Phosphoric acid	160-220°C	55%	Natural gas, bio gas, H_2, O_2, Air
Molten Carbonate Fuel Cell MCFC	Molten mixture of alkali metal carbonates	620-660°C	65%	Natural gas, bio gas, cool gas, H_2 ,O_2, Air
Solid Oxide Fuel Cell SOFC	Oxide ion conducting ceramic	800-1000°C	60-65%	Natural gas, bio gas, cool gas, H_2, O_2, Air

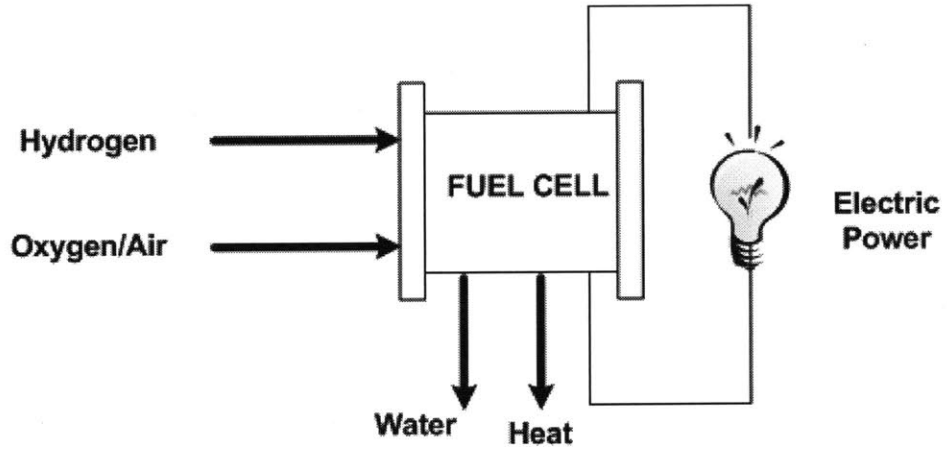

Figure 9. Basic PEM Fuel Cell Operation.

These fuel cells use a special class of proton exchange polymer membrane (PEM) that is impermeable to gases but conducts only protons under nominal conditions. The membrane is sandwiched between the two porous electrically conductive electrodes. To increase the reaction rate, catalyst layers composed of platinum is sandwiched between the membrane and the electrodes. The operation of a PEM fuel cell is shown in Figure 8. Hydrogen is fed on the anode side of the fuel cell. H_2 atoms split into its primary constituents: H^+ protons and electrons. The H^+ protons travel through the membrane to the cathode side of the cell. Oxygen is simultaneously fed through the cathode side of the fuel cell. Either pure oxygen or air can be fed to the cathode side as air contains 21% oxygen. Electrons at the anode accumulate at the electrically conductive collector plates and travel through an electrically conductive load externally, performing useful work in the form of electricity. The

electrons flow back to the cathode and combine with hydrogen protons and oxygen producing water and releasing heat. The basic electrochemical reactions that occur on both sides of the membrane are given by [8],

Anode:	$2H_2 \rightarrow 4H^+ + 4e$	(1)
Cathode:	$O_2 + 4H^+ 4e \rightarrow 2H_2O$	(2)
Overall:	$2H_2 + O_2 \rightarrow 2H_2O$	(3)

PEM fuel cells can be used as single cells or can be stacked in series to provide higher voltage. Each cell is composed of a series of layers, including gas flow channels, gas diffusion, catalyst and membrane layers.

The anode catalyst layer is used to facilitate the splitting of the hydrogen molecule and cathode catalyst is the site of assembly of the water molecules. PEM fuel cells are designed to be thin to reduce resistivity, flat and maximize the electrolyte surface area [8, 41]. The greater surface area of the membrane allows for greater amount of hydrogen protons to pass through the electrolyte and release its electrons, therefore generating more current. Details on the performance of the fuel cell with emphasis on electrochemistry and thermodynamics of the fuel cell are presented in Chapter 3.

2.2. Fuel Cell System Components

Unlike battery technology, fuel cells require additional components to produce power. The basic components required for a fuel cell power system are the fuel cell, fuel storage device, an oxidizer device depending on the oxidizer used (if air breathing this is not required), a power management system for the fuel cell-battery hybrid system (to isolate the fuel cell from the fluctuations of the sensor peak power demands), a fuel/oxidizer management system and environment control system. The fuel/oxidizer management system regulates the flow of reactants into the fuel cell and an environment control system isolates the fuel cell from environmental conditions to maximize life. Figure 10 shows typical components required to operate a fuel cell.

2.2.1. Hydrogen Storage

Hydrogen is a low-density gas that has very high energy density by mass compared to gasoline or other energy sources and low volumetric energy density. Hydrogen has the lowest atomic weight compared to any other molecule (2 grams/mol) and at standard temperature and pressure occupies 22.4L. Therefore extremely high pressures are required to store hydrogen in cylinders to meet typical volume constraints. With conventional approaches, to store small amounts of hydrogen, large storage tanks are required. Hydrogen can be stored either as a pressurized gas or as a cryogenic liquid. Other forms of storing hydrogen include chemical hydrides and metal hydrides where hydrogen is absorbed into metals and alloys [48, 55].

The effectiveness of a storage device is measured by the hydrogen weight-storage-efficiency (the weight percentage of the storage device that is hydrogen) and the volumetric storage efficiency (weight of fuel for a given volume of storage tank)). Table 2 illustrates the storage efficiencies of the different hydrogen storage options that presently exist [32, 48].

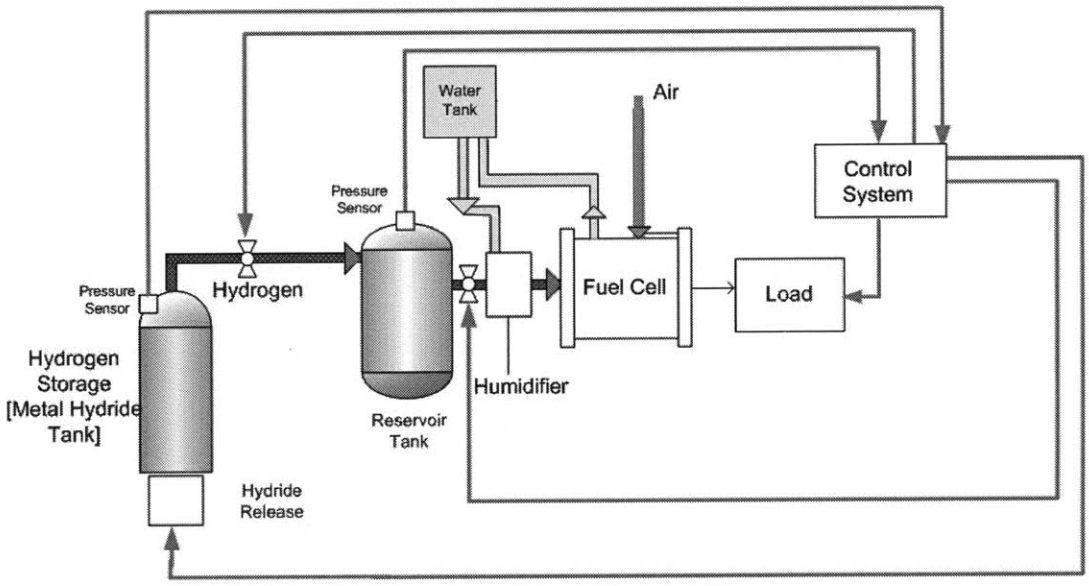

Figure 10. Fuel cell power supply components [19].

Table 2. Hydrogen storage methods and efficiencies [32, 48].

Hydrogen Storage Method	Mass Storage Efficiency (% wt)	Volumetric Storage Efficiency (g/L)
Pressurized Gas (300 bar)	3.1	14
Pressurized Gas (700 bar)	4.8	33
Cryogenic Liquid	14	43
Metal and Chemical Hydride	2-18	28

Table 2 shows that the best storage efficiencies are possible by storing hydrogen in liquid form or in certain hydrides. However, liquid hydrogen needs to be stored at cryogenic temperatures (-253 °C) to remain liquid at atmospheric pressure [55]. For applications being studied in this research, this is not a feasible option as refrigeration of liquid hydrogen requires additional energy and tank insulation, substantially increasing the complexity and mass of the system. Table 2 shows hydrogen must be stored at pressures on the order of 300-700atm in gaseous form for reasonable storage capacity. This is an infeasible option for the small mass and volume applications that are considered in this research. Hence storage as high pressure gas or liquid is not considered and metal hydride storage at moderate temperature and pressure are considered in this research. Certain metal hydrides absorb and discharge hydrogen near ambient temperatures and pressures. Hydrogen is released when heat is added to the hydride or pressure is decreased. Different metal hydrides exist which have varying storage efficiencies on the order of 3-18% [46, 47]. There are also chemical metal hydrides that release hydrogen based on chemical reaction [46, 47, 55]. High thermal release hydrides have good storage efficiencies [48]; however these require proper thermal management and additional components, including valves and external coatings to hold the hydrogen inside the material. Figure 11 shows various metal hydride technologies that are available [46, 48]. The highlighted area in the figure represents the range of metal hydrides that operate

at room temperature within a moderate pressure range. While much research is being done to improve metal hydride storage, this research considers use of commercial off-the-shelf technology with an efficiency of 5.5-6%.

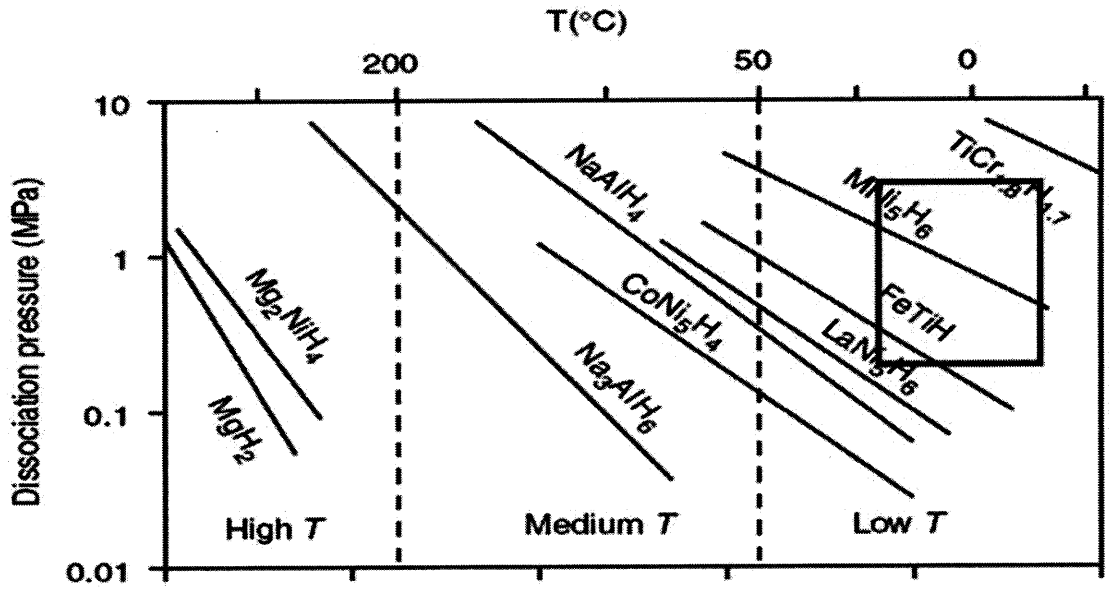

Figure 11. Metal Hydrides operating pressures and temperatures [47].

2.2.2. Oxygen Storage

Oxygen can be stored as compressed gas or as a liquid. Oxygen has an atomic weight of 16 grams/mole, considerably larger than hydrogen. Steel and aluminum tanks are typically used to store oxygen at pressures of 150-200atm [32]. New materials such as gasar materials (metallic material with pores) using magnesium alloys for storing compressed oxygen have been proven to have 58% weight storage efficiencies [36]. Carbon fiber reinforced pressure vessels also exist that can withstand pressures up to 10,000psi [55]. Thus, a high-strength carbon containment vessel can be used for light-weight storage of oxygen. In contrast to storing and extracting oxygen, using an air-breathing system (when possible for terrestrial applications) is expected to reduce mass and system complexity.

2.2.3. Power management, Regulation and Control System

A system-level power management and control system are required to monitor and control the power output to meet the power demands of the payload (field sensor). The power management system needs to meet the power and energy requirements of the sensor while maximizing life of the fuel cell. Hence the power management system needs to isolate the fuel cell from swings in load/sensor power demands. The power management system consists of a rechargeable battery and a DC to DC voltage convertor. A battery or a capacitor can be used to meet the peak powers of the sensor/load (see Figure 5). The fuel cell operates at constant voltage and is used to trickle charge the battery. The fuel cell operates at a voltage of 0.8V, and batteries generally require 3-4V for charging. Hence a DC to DC convertor is required to raise the voltage to charge the battery.

For optimal performance of fuel cells, the power system must be constantly monitored and adjusted to minimize fluctuations resulting from the conditions the fuel cell operates in. It is required to measure and adjust the temperature, pressure, humidity, power output and the reactant flow rates accordingly [45]. The power system components can be designed to fit the specific application to minimize volume, mass and energy constraints. Several control strategies are available in literature, but a simple and efficient control system needs to be designed and developed for ensuring long life operation of the fuel cell power supply.

2.3. Feasibility Analysis

Analysis is performed to demonstrate the feasibility of using fuel cells over existing technologies to provide low, steady power for long durations. Current battery technologies are capable of providing high peak powers but not high energy. Fuel cells are capable of generating large amounts of total energy over a mission. Table 3 lists the energy densities of various electrochemical technologies [8, 23, 41, 42]. Figure 12 shows a comparison of fuel cells and other electrochemical technologies using a chart that plots the energy density versus power density called the Ragone chart [56]. The figure shows that ultracapacitors can deliver very high power but the storage capacity is very limited. In contrast, fuel cells can provide high amounts of energy but have a relatively low power output. Table 3 shows that the energy output of fuel cells using hydrogen is about 35 times that of lithium ion batteries (not considering hydrogen storage).

Two different variations of feasibility analysis are performed. In the first analysis, the operational time is compared for power systems using fuel cells and batteries with the same mass and volume. The power requirement for this analysis is 0.5W that is in the range of powers for the applications considered for this research. The second feasibility analysis is performed to show the feasibility of using fuel cells for the power system concept proposed, for power range between 10mW to 100mW, operating for 3 years. In addition, analysis is performed using fuel cells, fuel cell-battery/photovoltaic hybrid systems for Unmanned Aerial Vehicles (UAVs), Autonomous Underwater Vehicles (AVUs) and rovers and is reported in Appendix A. The metrics used to evaluate feasibility are the system mass and number of operational days.

Table 3. Comparison of Energy Densities of Electrochemical technologies [8, 23, 41, 42].

Technology	Gravimetric Energy Density (WH/kg)	Volumetric Energy Density(WH/L)	Operating Temperatures (◦C)
Hydrogen (PEM Fuel Cells)	33300	530	15 to 80
Lithium Ion	90-150	230-330	-20 to 60
Alkaline	70-100	200-300	-20 to 50
NiMH	40-90	150-320	-20 to 60
NiCd	30-50	100-150	-45 to 50
Lead Acid	20 -40	50-120	-15 to 50

*Note: Hydrogen energy density does not include storage efficiencies which reduces the overall energy density.

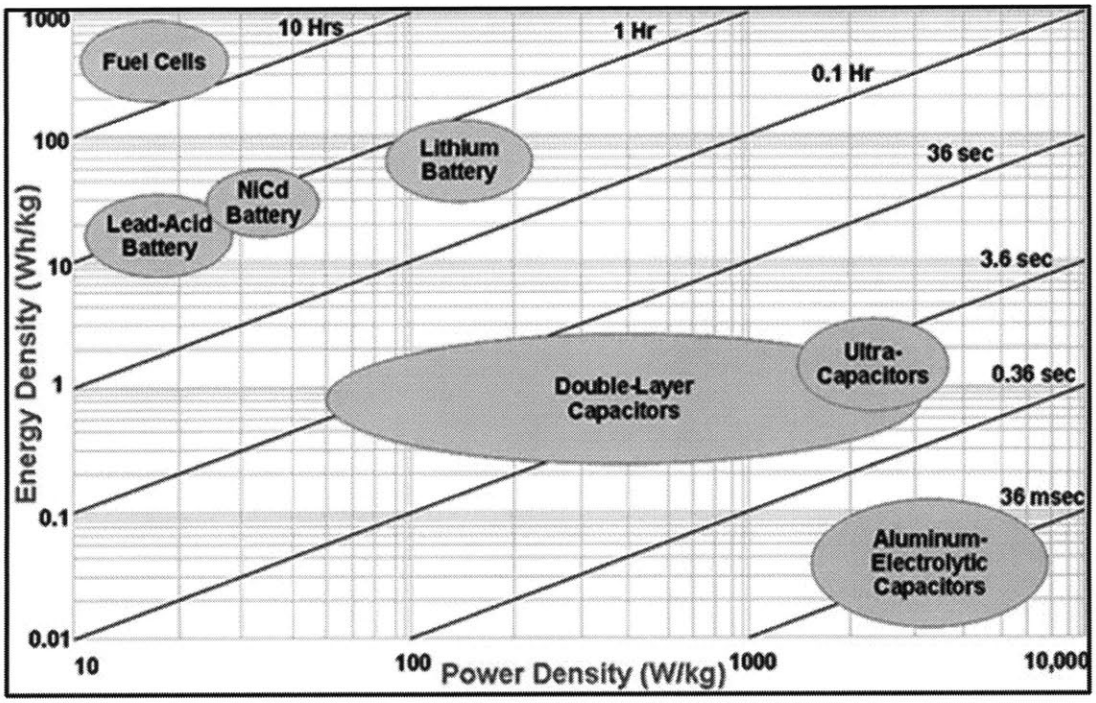

Figure 12. Comparison of energy densities of electrochemical technologies (Ragone chart) [56].

2.3.1. Mass

A general analysis of the system is performed by constraining the power system mass to 1kg and the respective volume and operational times are determined for a power requirement of 0.5W (see Figure 13). The electrochemical technologies mentioned in Table 3 are compared in this analysis. The analysis assumes mass of fuel storage, fuel cells and structure for fuel cell power system, and batteries and casing for the battery technology. Oxygen is assumed to be obtained from ambient air.

The basic equations used in the feasibility analysis are Eq.4 through 9. For a given power (P), and Voltage (V), the current (I) is calculated from Eq.4.

$$I = \frac{P}{V} \tag{4}$$

Since the mass of the power system (M_p) is specified in this case, and the energy densities (E_D) of the power supply technologies are known (Table 3), the total energy supplied (E_S) by the power system is calculated using Eq.5.

$$E_S = \frac{M_P}{E_D} \tag{5}$$

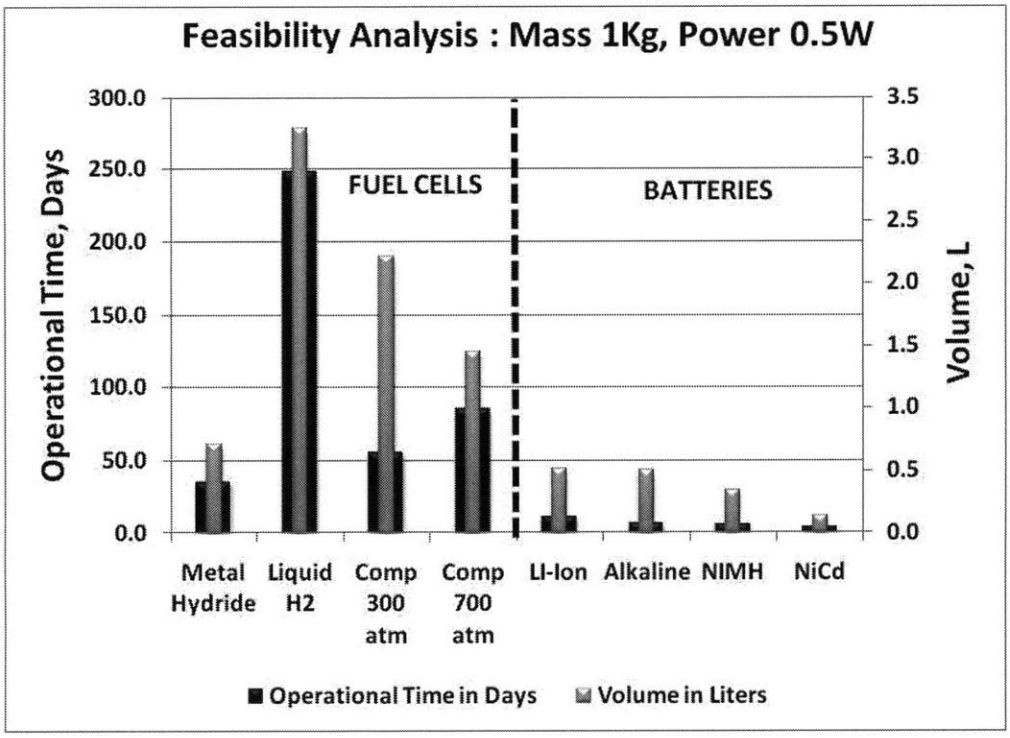

Figure 13. Feasibility analysis results for system mass of 1kg and 0.5W power requirement.

Energy is the integration of power over a period of time. Hence the operational time *(T)* is calculated by dividing total energy by power as shown in Eq.6.

$$T = \frac{E_S}{P} \tag{6}$$

For calculating the area of the fuel cell (A_{FC}), a current density *(i)* is considered and the area is calculated from current by rearranging Eq. 4 and the reference current density using Eq.7.

$$A_{FC} = \frac{I}{i} \tag{7}$$

The mass of hydrogen (M_H) required to produce the power needed is calculated from Eq.8 where the fuel cell efficiency used is 65% (η_{FC}).

$$M_H = \frac{E_S}{\eta_{FC} * E_D} \tag{8}$$

The mass of hydrogen storage (M_{HS}) and the volume of hydrogen storage (V_{HS}) are calculated using the mass and volume storage efficiencies (η_{MHS}, η_{VHS},) (see Table 2) as shown in Eq.9 and 10.

$$M_{HS} = \frac{M_H}{\eta_{MHS}} \tag{9}$$

$$V_{HS} = \frac{M_H}{\eta_{VHS}} \tag{10}$$

From Figure 13, it is evident that fuel cells offer the same amount of power as batteries (in this case 0.5 W) for longer time periods compared to any of the battery technologies for the same mass. Each fuel cell provides 0.8V (η_{FC} = 65%) and hence for 8V output voltage requirement, a stack of 10 fuel cells each with an area 0.31cm^2 and a current density of 0.2A/cm^2 [8] provides the required power. The mass and volume of the fuel

cell is negligible when compared to the storage mass and volume of hydrogen. From Figure 13, it is apparent that liquid hydrogen storage technology operates for nearly 250 days providing continuous power. However, hydrogen storage is a hindrance in terms of volume. Storage of hydrogen in liquid form requires 3.4 L of volume to provide the required power for 250 days. Note, the energy required for refrigeration of liquid hydrogen is neglected in this analysis.

When small size, medium duration applications are considered, Lithium ion (Li-Ion) and fuel cells are good candidates. Li-Ion batteries provide 0.5W power for only 11 days but occupy less volume (~0.5L). Among the fuel cell storage technologies, metal hydrides is the better option since they only occupy 0.7L, but the operational time is less than half of liquid hydrogen storage (35 days). However, for storing hydrogen as liquid, additional energy for cooling and refrigerating hydrogen is required and the overall storage efficiency will be lower than what is used in the calculations. Therefore, to match the operational times provided by PEM fuel cells with metal hydrides, more than double the quantity of Li-Ion batteries would be required. This increases the volume of Li-ion batteries to 1L (double that of metal hydrides). Therefore, it is evident that for short-duration power demands, batteries seem to be a feasible option, but for long-term missions, PEM fuel cells are the best option.

2.3.2. Volume

For the volume constraint analysis, the volume of the power system is limited to 1 L. The operational time and mass of fuel cell and battery power systems are compared. Again, a power requirement of 0.5 W is used. The results of the analysis using Eq.4 through 10 are shown in Figure 14.

It is evident that fuel cells provide the longest operational time for the given volume of the power system. Liquid hydrogen technology is the dominant storage system operating for 76 days and weighing 0.3 kg only. However as mentioned earlier, conditions for storing liquid hydrogen are not feasible for small scale applications. Nickel Cadmium (NiCd) batteries provide power for only 11 days and weigh as much as 10 kg. Metal hydride option provides the same power for 50 days weighing 1.4 kg. Even Li-Ion batteries, known for high energy density among battery technologies, provide only half the operational life of fuel cells (metal hydride storage) and weigh twice as much. For Li-Ion batteries to meet the 50 days operational time of PEM fuel cells, the mass will be 4.2kg, which is 3 times the mass of a fuel cell power system with metal hydride storage.

From the mass and volume feasibility analysis, it is theoretically demonstrated that fuel cells are the best option for long duration missions. Metal hydride storage is shown to be the best choice for missions where volume and mass are critical parameters and the operational complexity needs to be minimized.

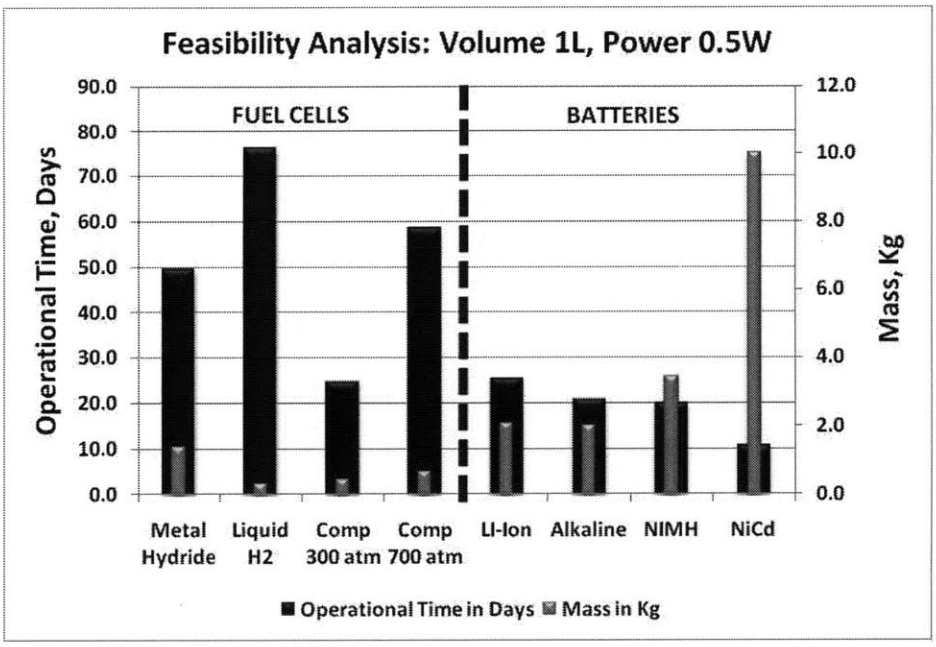

Figure 14. Feasibility analysis results for system volume of 1L and 0.5W power requirement.

2.3.3. Proposed Power system concept feasibility

Analysis is performed to investigate the mass of the power system for 1-5 years operational life. The baseline power requirement is between 10mW to 100mW. The mass of the power system includes power management components, metal hydride storage tank, fuel cell and water for humidification as proposed in the fuel cell power supply concept. Oxygen is assumed to be obtained from ambient air. Figure 15 compares the mass of the system with existing battery technologies for the given power range. Comparison with Li-Ion and Nickel Metal Hydride (NiMH) batteries as the main power source shows that the fuel cell power concept has a significant advantage in terms of mass and volume (also see Figures 13-14).

Figure 16 compares the mass of the fuel cell power system for the given power range with respect to the operational life. Results show that the fuel cell power system would weigh about a kilogram for 100mW average power demand for a 5 year life. This preliminary analysis demonstrates the feasibility of using the proposed fuel cell powered sensor concept for small scale, long duration applications.

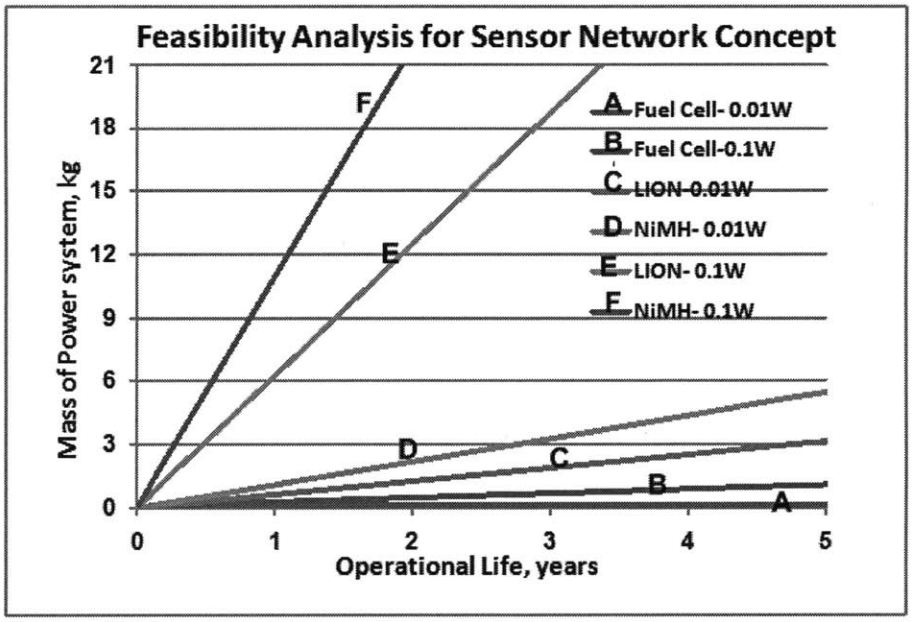

Figure 15.Comparison of the mass of the system for various electrochemical technologies.

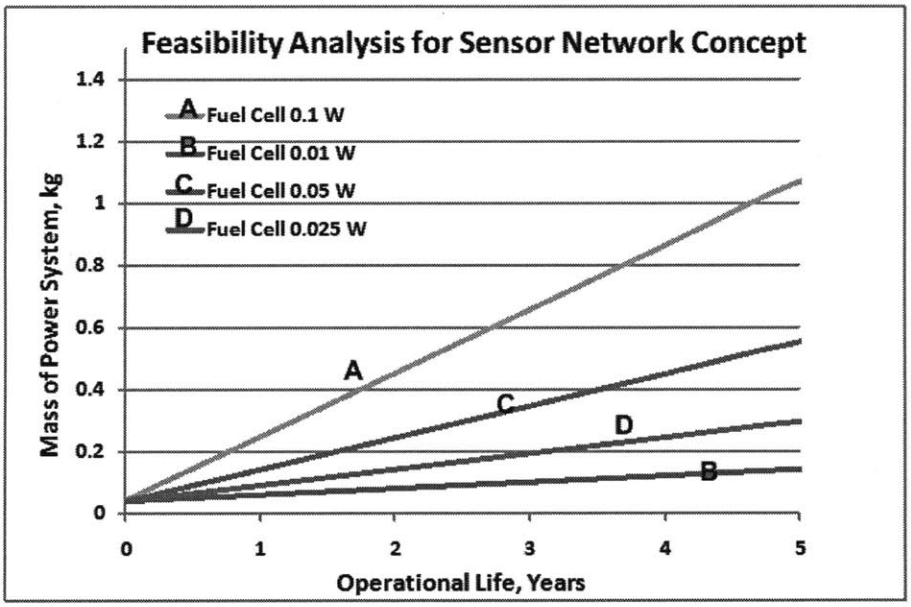

Figure 16. Mass of power supply system verses the operational life of the mission.

2.4. Application Specific Feasibility Analysis

Analysis is performed for other applications such as UAVs, AUVs and all-terrain rovers to evaluate the feasibility of using fuel cells as the power source. Preliminary calculations are performed to compare the mass of the system using the various power technologies.

For UAVs and all-terrain rovers, feasibility is demonstrated by comparing a power system using both fuel cells and photovoltaic cells (solar cells) in combination with batteries as power source. For applications with sufficient exposure to sunlight, solar cells can be used during daytime to power the system as well as electrolyze water to produce hydrogen and oxygen for use by a fuel cell in the absence of sunlight. The study analyses fuel

cell-battery hybrid storage to power the system. The details of the analysis and results are presented in Appendix A as it is outside the scope of this thesis. The results from the analysis for other small scale applications also prove that using fuel cells in combination with solar cells for UAVs is the best option for an operational period of 6 months. Fuel cells with metal hydride storage are best suited for small sized AUVs such as fish robots and all-terrain rovers for long operational times.

Feasibility Analysis Summary

Feasibility analysis is performed to compare PEM fuel cells and batteries for 1) a constant mass of the power system, 2) a constant volume of the power system, as well as 3) for the fuel cell powered sensor network concept requiring 10mW to 100mW of power. The operational life of the power system using fuel cells and existing battery technologies is compared. The results from the analysis prove that a fuel cell power supply system is advantageous in providing powers for long durations when compared to current battery technology. Fuel cells outperform batteries both in terms of mass and volume, for low power demands and for missions and applications that need long operational times in the order of months to years. The feasibility analysis for the fuel cell powered sensor networks show similar results. Although there are certain disadvantages in using fuel cells such as storing hydrogen, the overall operational time obtained by using fuel cells is much greater than batteries as presented in this analysis. To maximize the life of the fuel cell and to meet the peak power demands of the sensor systems, a fuel cell-battery hybrid system is required. For such applications, the fuel cells can provide low continuous powers for trickle charging the battery and the battery provides peak powers for powering the sensors.

CHAPTER 3

FUEL CELL MODEL DEVELOPMENT

This chapter characterizes the performance of a PEM fuel cell based on a steady-state model developed. Modeling facilitates better understanding of the parameters affecting fuel cell operation. The first step in analyzing the performance of a fuel cell is to analytically model and simulate fuel cell operation based on fuel cell operation presented in Chapter 2. A basic steady-state micro PEM fuel cell model is developed as a function of power supply operation which includes the external load current and the voltage demand. The chapter presents various models from literature and describes the model developed for this research with simplifications made from existing models. The chapter demonstrates the validation of these model using data from published literature as well as data from experiments conducted in the laboratory. The effects of the important operating parameters: humidity, temperature and pressure are analyzed.

3.1. Models from Literature

Significant work has been done in the past decade to model the steady state performance of PEM fuel cells [5, 6, 29, 30, 31, 45, 50]. Some models are detailed and complex using elaborate electrochemical, thermodynamic and fluid mechanics principles, modeling individual components of the fuel cell. Such detailed models are not needed for the applications considered here. Spatial variations in temperature and fluid flow can be ignored. Other models are too simple. They do not include the effects of operating parameters and only provide the voltage-current relationship. Mathematical and empirical models found in literature vary in complexity, ranging from simple models that do not account for spatial dimension to complex three dimensional models [29]. A steady state electrochemical model for the PEM fuel cell is proposed in literature [5, 6], but has been used for two particular fuel cells manufactured by Ballard power systems [5, 6]. Another model developed in literature [50] is successful in predicting steady state performance of a PEM fuel cell. However, the model does not include humidity effects. A few commercial ready-to use software models are also available which were designed for particular fuel cells, especially large stacks [29]. In using commercial software models, input specifications can be complex and the code can be inflexible, making it difficult to alter the code and vary system specifications. Other theoretical models [30, 31] do not include a thermodynamic model predicting the change in operating temperature of the fuel cell. Similarly several other models focus only on mass transport or electrochemical reactions. Hence, for this research there is a need to develop a PEM model that accurately captures various characteristics shown by existing models but with reduced complexity. The model developed captures voltage-current relationship, water management, heat, and pressure effects.

3.2. Fuel Cell Model Configuration

The fuel cell model required for this research needs to predict the performance of the fuel cell based on the power, voltage demands of the external load and the operating environmental conditions. The model developed here is the basis for further development of methodologies to control the fuel cell for efficient operation for long life applications.

A one dimensional steady state model of the fuel cell is developed. The model is simplified from several models from literature to fit the overall scope of this research [8, 31, 45, 50]. This model uses empirical formulae from various literature sources [8, 31, 45, 50] and makes an attempt to capture the important aspects of PEM fuel cells while simplifying the complexities (as explained in Section 3.1) in the model. Mathematical equations are used to represent the reactions and processes taking place inside the fuel cell. The model accounts for the electrochemical behavior of the fuel cells, the mass flow of reactants and products and the energy conservation principles. A lumped model is devised where the internal local variations within the fuel cell such as temperature gradients, water gradients within the membrane and the diffusion of fuel in the gas diffusion layers are ignored. The variability of these internal parameters is expected to be minimal for micro fuel cells. The model predicts the performance of a typical PEM fuel cell that uses hydrogen and air or oxygen and is not limited to any particular PEM fuel cell. The model can be scaled up for predicting performance of larger fuel cells as well, provided the variability (gradients) in temperature, humidity and pressure is limited.

The schematic of the fuel cell model developed is shown in Figure 17 and is explained in the following sections in detail. The inputs to the model are pressure *(hydrogen: P_{H2}, air: P_{air})*, temperature *(ambient: T_{amb}, hydrogen: T_{H2}, air: T_{air})*, relative humidity *(hydrogen: φ_{H2}, air: φ_{air})* of the inlet gases and the external load resistance *(R_{Load})*. The internal operations of the fuel cell are divided into sub sections. 1) The Mass Flow block models the anode, cathode flow channels and membrane hydration which are governed by the conservation of mass equations. 2) The Stack Voltage block models the electrochemical processes that are governed by the Nernst equation (which gives the theoretical voltage, V_T) and the voltage loss equations governed by the Volmer-Butler equations (which gives the voltage losses, V_L). 3) The Thermodynamic block models the energy inputs and the heat transfer of the fuel cell operation that are governed by the conservation of energy and heat transfer equations.

The outputs from the model are the fuel cell voltage *(V_{FC})* as a function of current *(I_{St})*, temperature of the fuel cell *(T_{FC})*, mass flow rates of hydrogen *($mdot_{H2}$)*, air *($mdot_{air}$)*, and water in the membrane *(W_{vmem})*. Subsequent sections explain the model in detail.

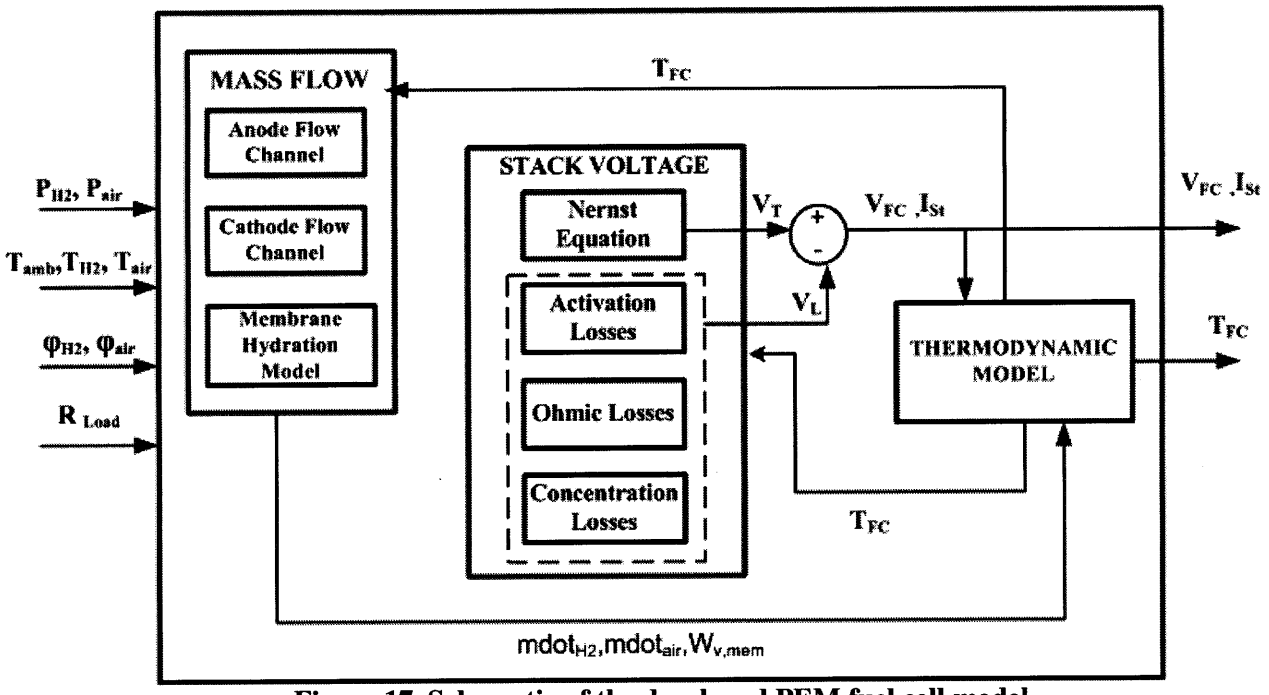

Figure 17. Schematic of the developed PEM fuel cell model.

To simplify the analysis, the following assumptions are made,

- The inlet gases are assumed to be ideal and uniformly distributed in the flow channels.
- Constant pressures are assumed in the fuel cell gas flow channels.
- The hydrogen fuel is assumed to be humidified.
- The oxygen comes from the ambient air.
- The operating temperature is assumed to be between 0°C and 80°C.
- The pressure in the fuel cell gas flow channels are assumed constant.
- The thermodynamic properties are evaluated at the average fuel cell temperature.
- The temperature variations across the fuel cell are neglected.
- The overall specific heat capacity of the fuel cell is constant.

The following sections detail the Mass Flow, Stack Voltage and Thermodynamic blocks of the model.

3.2.1. Mass Flow

Hydrogen is fed into the fuel cell from the anode as explained in Section 2.2 and air enters the fuel cell from the cathode side; any unused gases exit from the same electrodes (see Figure 8). Water that is produced in the fuel cell flows out through the cathode. The flow of the reactant gases into and the fuel cell and the exit of the gases including water are modeled in this section. Mass conservation equations are used to model the flow of gases into the anode and cathode based on relations as described in literature [8, 45].

3.2.1.1. *Anode Flow Model*

In the anode channel, the inlet hydrogen stream is either dry or humidified. The one dimensional mass flow rate of hydrogen ($\dot{m}_{H_2}$) entering the fuel cell is given by Eq.11, as a function of current (I_{st}), molar mass of hydrogen (M_{H_2}), and the Faraday constant (F= 96485 C/mol) [8].

$$\dot{m}_{H_2} = \frac{I_{st} \cdot M_{H_2}}{2F} \tag{11}$$

Water is present in the gas stream when hydrogen is humidified. The mass flow rate of water ($\dot{m}_{H_2OinH_2}$) in the inlet stream of hydrogen is then given by Eq.12 as a function of the saturation pressure of vapor (p_{sat}) at the inlet hydrogen temperature (T_{H2}), the relative humidity of hydrogen (φ_{an}), the molar mass of water (M_{H_2O}) and the partial pressure of hydrogen (P_{H2}) [8].

$$\dot{m}_{H_2O}inH_2 = \frac{M_{H_2O}}{M_{H_2}} \cdot \frac{p_{sat}(T_{H2}) \cdot \varphi_{an} \cdot \dot{m}_{H_2}}{P_{H2} - \varphi_{an} \cdot p_{sat}(T_{H2})} \tag{12}$$

The saturation pressure of vapor is calculated using Eq.13, taken from literature [8, 45].

$$P_{sat}(T_{H2}) = 10^{-2.2+0.03T_{H_2}-9.2e^{-5}T_{H_2}{}^2+1.5e^{-7}T_{H_2}{}^3} \tag{13}$$

The partial pressure is given Eq. 14, taken from references [8, 45] and is a function of current density (i), fuel cell temperature (T_{FC}) and the saturation pressure of water (P_{H2O}) as a function of fuel cell temperature is given by Eq.15 [8,45].

$$p_{H2} = \left(\frac{0.5P_{H_2}}{\exp\left(T_{FC}^{\left(\frac{1.653i}{1.334}\right)} \right)} \right) + P_{H_2O} \tag{14}$$

$$P_{H_2O} = 10^{-2.2+0.03T_{FC}-9.2e^{-5}T_{FC}{}^2+1.5e^{-7}T_{FC}{}^3} \tag{15}$$

Similarly any unused water exiting the anode is given by the difference between the water entering and the water absorbed by the membrane ($\dot{m}_{H_2Omem}$).

$$\dot{m}_{H_2Oout\_anode} = \dot{m}_{H_2OinH_2} - \dot{m}_{H_2Omem} \tag{16}$$

3.2.1.2. *Cathode Flow Model*

At the cathode, air enters the fuel cell and consists of oxygen, nitrogen and water vapor. Water formed due to the electrochemical reaction in the fuel cell, exists from the cathode. The inputs of the cathode model are the flow rates of air and water into the fuel cell, water formed and any unused oxygen (from air). The flow rates of all the individual gas inlets are taken into account in the cathode flow model. The overall mass flow rate equations are similar to that of anode flow model.

Mass flow rate of oxygen ($\dot{m}_{O_2}$) is given by Eq.17, similar to that of hydrogen using molar mass of oxygen (M_{O2}).

$$\dot{m}_{O_2} = \frac{I_{st} \cdot M_{O_2}}{4F} \tag{17}$$

Mass flow of water ($\dot{m}_{H_2OinAir}$) present in the air is given by Eq.18, where the relative humidity of cathode (φ_{cat}), molar mass of air (M_{Air}), molar mass of water (M_{H_2O}), temperature of inlet air (T_{Air}) and the partial pressure of air (P_{Air}) are used [8, 45].

$$\dot{m}_{H_2O}inAir = \frac{M_{H_2O}}{M_{Air}} \cdot \frac{p_{sat}(T_{Air}) \cdot \varphi_{cat} \cdot \dot{m}_{O_2}}{P_{Air} - \varphi_{cat} \cdot p_{sat}(T_{Air})} \tag{18}$$

Mass flow of water ($\dot{m}_{H_2Ogen}$) generated that exists the fuel cell is given by [8, 45],

$$\dot{m}_{H_2O}gen = \frac{I_{st} \cdot M_{H2O}}{2F} \tag{19}$$

The total amount of water exiting the cathode channel ($\dot{m}_{H_2Oout\_cathode}$) is given by Eq.20 as the sum of water generated by the fuel cell and the excess water expelled by the membrane on the cathode side.

$$\dot{m}_{H_2Oout\_cathode} = \dot{m}_{H_2Ogen} + \dot{m}_{H_2Omem} \tag{20}$$

The saturation pressure of vapor ($P_{sat}(T_{air})$) in air inlet and partial pressure of air (p_{air}) are calculated using Eq.21 and 22 [8, 31, 45].

$$P_{sat}(T_{air}) = 10^{-2.2+0.03T_{air}-9.2e^{-5}T_{air}^{2}+1.5e^{-7}T_{air}^{3}} \tag{21}$$

$$p_{air} = \left(\frac{P_{air}}{exp\left(T_{FC}^{\left(\frac{1.653i}{1.334}\right)} \right)} \right) + P_{H_2O} \tag{22}$$

3.2.1.3. Membrane Hydration Model

The membrane hydration block in the model calculates the amount of water content in the membrane. This model has been based on the empirical formulae taken from the experiments conducted in literature [45]. The amount of water in the membrane and the mass flow rates of water across the membrane are a function of the relative humidity of anode and cathode flow channels. This subsection captures the effects of humidification on the fuel cell performance.

Water transport across the membrane occurs because of two distinct phenomena. One is when the water molecules are transported into the membrane by the hydrogen proton from the anode, known as osmotic drag. The other is when the water molecules enter the membrane from the cathode channel due to humidity difference in the anode and cathode flows, known as back diffusion [8, 45, 50].

The average water content in the membrane (λ_{mem}), which is defined as the ratio of water molecules to the number of charge sites is calculated from the average relative humidity (ϕ_{mem}) on the anode and cathode side as shown in Eq.23 and 24 [8, 45, 50].

$$\phi_{mem} = \frac{\phi_{an} + \phi_{ca}}{2} \tag{23}$$

$$\lambda_{mem} = 0.043 + 17.81 \cdot \phi_{mem} - 39.85 \cdot \phi_{mem}^{2} + 36 \cdot \phi_{mem}^{3} \tag{24}$$

The electro-osmotic drag coefficient is a function of membrane water content [45].

$$n_d = 0.0029 \cdot \lambda_{mem}^{2} + 0.05 \cdot \lambda_{mem} - 3.4 \cdot 10^{-19} \tag{25}$$

The water diffusion coefficient for the membrane is defined by Eq.26, which is a function of water content constant (D_λ), given by Eq.27 as a function of membrane water content [8, 45].

$$D_W = D_\lambda exp\left(2416\left(\frac{1}{303} - \frac{1}{T_{FC}}\right)\right) \tag{26}$$

$$\begin{aligned} D_\lambda &= 10^{-6} && for\ \lambda_{mem} < 2 \\ D_\lambda &= 10^{-6}(1 + 2(\lambda_{mem} - 2)) && for\ 2 \leq \lambda_{mem} \leq 3 \\ D_\lambda &= 10^{-6}(3 - 1.67(\lambda_{mem} - 3)) && for\ 3 < \lambda_{mem} < 4.5 \\ D_\lambda &= 1.25 \cdot 10^{-6} && for\ \lambda_{mem} \geq 4.5 \end{aligned} \tag{27}$$

The water concentration at the anode and the cathode ($c_{v,ca}$, $c_{v,an}$) are defined by Eq.28 and 29 as a function of membrane density (ρ_{mem}), membrane dry weight ($M_{mem,dry}$) and anode and cathode water content ($\lambda_{an}, \lambda_{ca}$) [8, 45, 50].

$$c_{v,ca} = \frac{\rho_{mem}}{M_{mem,dry}} \lambda_{ca} \tag{28}$$

$$c_{v,an} = \frac{\rho_{mem}}{M_{mem,dry}} \lambda_{an} \tag{29}$$

The total amount of water in the membrane given by the molar flow rate ($N_{v,mem}$) is the sum of the electro-osmotic drag and back diffusion given by Eq.30. Since in back diffusion water flows away from the membrane, a negative sign is used [45].

$$N_{v,mem} = n_d \frac{i}{F} - D_W \frac{(c_{v,ca} - c_{v,an})}{tm} \tag{30}$$

The overall mass flow rate of water across the membrane using Eq. 30, molar mass of vapor, area of the fuel and the number of fuel cells is given by Eq.31 [45].

$$W_{v,mem} = N_{v,mem} \cdot M_v \cdot A_{fc} \cdot N \tag{31}$$

This membrane hydration model predicting the mass flow rate of water through the membrane is included in the final mass flow model to predict the effects of humidity on the overall performance of the fuel cell.

3.2.2. Stack Voltage Model

The Stack Voltage model has been developed based on the electrochemical reactions taking place in the fuel cell using relations from literature [8, 45, 50, 31]. The stack voltage predicts the voltage of the fuel cell as a function of the stack (single fuel cell or series of fuel cells) current (I_{st}), temperatures of the inlet gases, relative humidity of the inlet gases, inlet gas pressures and the operating temperature of the fuel cell itself.

The overall chemical reaction in a fuel cell is given by the following chemical equation [8].

$$2H_2 + O_2 \rightarrow 2HO_2 \tag{32}$$

The chemical reaction of producing water from hydrogen and oxygen is an exothermic process releasing heat. At 25°C, and at atmospheric pressure this reaction produces water, releasing 286 kJ/mol of heat energy [8]. This thermal energy or so called enthalpy of hydrogen combustion is also termed as hydrogen's higher heating value. For a fuel cell, hydrogen heating value is the measure of energy input into a fuel cell and also this is the

maximum amount of energy that may be extracted from hydrogen [8, 50]. This energy is converted into electricity by a fuel cell given by Eq.33 [8],

$$\Delta G = \Delta H - T\Delta S \tag{33}$$

where G is the Gibbs free energy that is converted into useful work, H is the total enthalpy of hydrogen, T is the temperature and S is the irreversible losses in energy conversion or entropy.

Electrical energy is the product of charge and potential and is calculated using [8],

$$W = qE \tag{34}$$

where W is the electrical work in, q is the charge and E is the potential or voltage. The total charge that is transferred in a fuel cell reaction according to Eq. 32 per mol of hydrogen consumed is given by,

$$q = nN_{avg}q_e \tag{35}$$

where n is the number of electrons per molecule of hydrogen ($n = 2$), N_{avg} is the number of molecules per mole (*Avogadro number=6.022×10^{23} molecules /mol*) and q_{el} is the charge of 1 electron (*1.602×10^{-19} Coulombs/electron*). The product of Avogadro number and charge of 1 electron is Faraday's constant. Therefore the electrical work is,

$$W = nFE \tag{36}$$

Since the maximum amount electrical energy generated in a fuel cell is equal to the Gibbs free energy.

$$W = -\Delta G \tag{37}$$

Thus the theoretical potential of a fuel cell is given by [8],

$$E_0 = \frac{-\Delta G}{2F} \tag{38}$$

Using the values from above (*G=237.34 kJmol^{-1} at 25 ^{o}C*), the theoretical potential of a fuel cell is,

$$E_0 = 1.23\ Volts \tag{39}$$

Therefore at 25 °C , the theoretical potential of a PEM fuel cell is 1.23V [8, 50]. The equation that relates the potential of the fuel cell and inlet pressures is given by the Nernst equation as shown below [8, 50].

$$V_T = E_0 + \frac{RT}{2F} ln\left[\frac{P_{H_2} P_{O_2}^{0.5}}{P_{H_2O}}\right] \tag{40}$$

where P is the partial pressure of the respective reactant and product species and E_0 is the theoretical potential at 25°C and 1atm, and T is the temperature of the fuel cell. Using Eq.15 and 22 the partial pressures of hydrogen and oxygen/air can be calculated.

The voltage V_T calculated is actually the open circuit voltage of the fuel cell. In practice, the open circuit voltage of a fuel cell is lower than the theoretical voltage, generally less than 1V. That means even when there is no external current being generated losses occur in a fuel cell. With a closed circuit further losses occur in a fuel cell which are caused by the following reasons [8, 50],

- Kinetics of the electrochemical reactions.
- Internal electrical and ionic resistance.
- Difficulties in getting the reactants to reaction sites.

- Internal currents and crossover of reactants.

The voltage losses that correspond to the drop in the voltage are the 1) Activation losses, 2) Ohmic resistance losses and, 3) Concentration losses shown by the voltage-current curve known as the polarization curve in Figure 18 [50]. Polarization curve is the most common method of testing the performance of a fuel cell [8, 50]. The polarization curve displays the voltage output of a fuel cell for a given current loading. The polarization curve can be used to determine the power and efficiency of a fuel cell under a given electrical load.

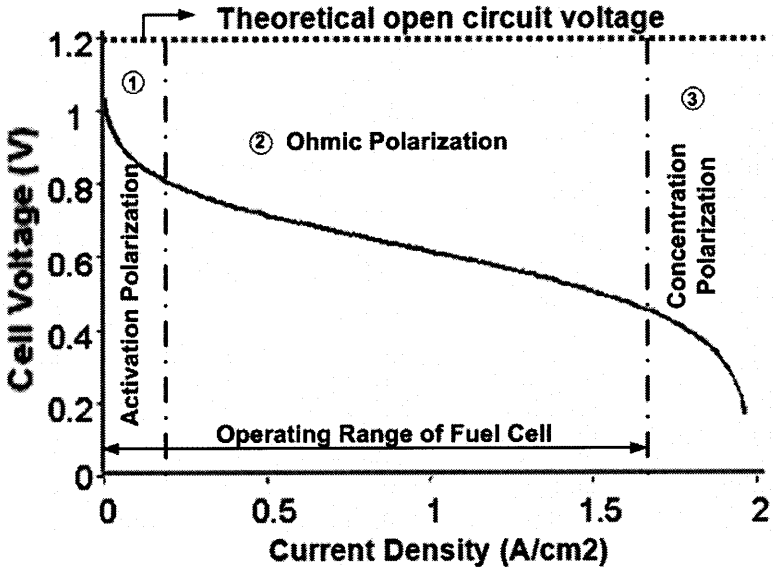

Figure 18. Cell Polarization Curve [8].

The maximum theoretical voltage in a PEM fuel cell is 1.23V and is based on the Gibbs free energy of hydrogen heating value as explained in the Eq.33 to 40. In Figure 18, the theoretical maximum voltage is represented by the straight line. But due to voltage losses the actual voltage is less than 1.23V as seen in the figure. The figure shows that the losses occur in 3 different current ranges of the fuel cell. These losses are explained below.

3.2.2.1. Activation Losses/Polarization

To start the electrochemical reaction, a voltage difference from equilibrium conditions is required and this is termed as the activation polarization. It can also be thought of as the readiness of the electrode to start the reaction. These losses take place at lower current densities. This need for voltage difference causes a reduction in the overall voltage output of the fuel cell. These voltage losses occur both at the anode and the cathode; however, reduction of oxygen requires much higher over-potentials (voltage difference) leading to a much slower reaction than hydrogen oxidation. Therefore, only the voltage loss at the cathode is considered. The equation of the voltage loss (ΔV_{act}) is given as a function of current density and exchange current density (i_o). The exchange current density is the rate of electron transfer in the fuel cell at steady state [50].

$$\Delta V_{act} = \frac{-RT}{\alpha F} \ln\left(\frac{i}{i_0}\right) \tag{41}$$

3.2.2.2. *Ohmic Losses*

There exists a resistance to the flow of ions and electrons through the electrically conductive fuel cell components and the electrolyte. This resistance poses voltage losses that are known as Ohmic losses as they can be expressed in terms of Ohm's law. Ohmic losses occur during the normal operational range of the fuel cell and are given by the following equation [8],

$$\Delta V_{ohm} = iR_i \tag{42}$$

where i is the current density and R_i is the total cell internal resistance which includes ionic, electronic and contact resistance. R_i is a function of the relative humidity of the membrane [8, 45, 50],

$$R_i = \frac{t_{mem}}{\sigma} \tag{43}$$

where t_{mem} is the thickness of the membrane and σ is given by Eq. 44 [58, 60]:

$$\sigma = (0.514\lambda_{mem} - 0.326)\exp\left[1268\left(\frac{1}{303} - \frac{1}{T_{FC}}\right)\right]. \tag{44}$$

3.2.2.3. *Concentration Losses/Polarization*

Concentration losses occur when the reactant is consumed faster than it can reach the surface of the electrode. These losses mainly occur in the higher current density regions. The higher the current generated, the lower the surface concentration of the reactants. A limiting current value is defined when the surface concentration reaches zero and when the rate of consumption exceeds the diffusion rate. This is the maximum current that a fuel cell can generate. This voltage loss is defined in terms of the limiting current density (i_L) [50].

$$\Delta V_{Conc} = \frac{RT}{nF}\ln\left(\frac{i_L}{i_L - 1}\right). \tag{45}$$

3.2.2.4. *Fuel Cell Terminal Voltage*

The actual fuel cell terminal voltage is obtained by combining the voltage obtained from the Nernst equation (Eq.40) and the voltage losses. The total voltage losses that an operating fuel cell experiences is the sum of all the losses explained above. Hence, the actual voltage that a fuel cell produces is less than the theoretical voltage. To obtain a required voltage, a number of fuel cells are stacked into groups based on the power and voltage requirements. The terminal voltage of the fuel cell is then given as follows,

$$V_{FC} = V_T - \Delta V_{act} - \Delta V_{Conc} - \Delta V_{ohm}. \tag{46}$$

The model contains voltages as unknowns; a known load resistance that is grounded on one side is connected to the fuel cell (see Figure 18). Writing Kirchhoff's voltage law for the loop gives the following equation used to determine the fuel cell voltage.

$$V_{FC} - I_{st}.R_{load} = 0 \tag{47}$$

3.2.3. Thermodynamic Model

Most parameters for calculating the fuel cell terminal voltage are a function of the fuel cell operating temperature. A thermodynamic model is developed such that the temperature changes of the fuel cell are taken into account. The generic heat balance of the fuel cell is written as follows [50],

$$\Sigma Q_{in} = W_{el} + Q_{dis} - \Sigma Q_{out} \tag{48}$$

where Q_{in} is the enthalpy (heat) of the input reactant gases, Q_{out} is the enthalpy of the unused reactants and the heat produced by the product (water), W_{el} is the generated electricity and Q_{dis} is the heat dissipated to the surroundings in terms of conduction, convection and radiation.

The enthalpies of the inlet gases (Q_{in}) are given by Eq.49-52 [8]. The net enthalpy of hydrogen and air is given by,

$$Total\_H_2\_energy = \dot{m}_{H2} \cdot (cp_{H2} \cdot T(H_2) + h_{HHV}) \tag{49}$$

$$Total\_Air\_energy = \dot{m}_{O_2} \cdot \left(cp_{Air} \cdot T(Air)\right) \tag{50}$$

The enthalpies of water coming in through the reactants are given as follows [8],

$$Energy_{H2O_{from_{H2}}} = \dot{m}_{H_2O}inH_2 \cdot \left(cp_{H2O\_gas} \cdot T(H_2) + h_{ofg}\right) \tag{51}$$

$$Energy_{H2O_{from_{Air}}} = \dot{m}_{H_2O}inAir \cdot \left(cp_{H2O\_gas} \cdot T(Air) + h_{ofg}\right) \tag{52}$$

$Energy_{H2O_{from_{H2}}}$ and $Energy_{H2O_{from_{Air}}}$ represent the energy of water coming in through hydrogen and air streams. The enthalpy equations are a function of the mass flow rates of the individual gases ($\dot{m}_{H2}, \dot{m}_{O_2}, \dot{m}_{H_2OinH_2}, \dot{m}_{H_2OinAir}$), specific heats of individual gases ($cp_{H2}, cp_{Air}, cp_{H2O\_gas}$), temperatures of the inlet gases ($T(H_2), T(Air)$), higher heat value of hydrogen at 25 °C (h_{HHV}) and heat value of water vapor (h_{ofg}).

The enthalpies of unused hydrogen and air are captured in terms of enthalpy, and the enthalpy of the water generated is given by,

$$Energy_{H2O_{out}} = \left(\dot{m}_{H_2O}out_{cathode} - \dot{m}_{H_2O}out_{anode}\right) \cdot \left(cp_{H2O_{gas}} \cdot T(fc) + h_{ofg}\right) \tag{53}$$

The heat dissipated into the surroundings $\dot{Q}_{dis}$ is the sum of heat transfer from conduction ($\dot{Q}_{Cond}$), convection ($\dot{Q}_{Conv}$ and radiation ($\dot{Q}_{Rad}$) and is given by Eq.55 through 57. The net energies of hydrogen and air flowing in and out of the system are captured in Eq.49 and 50 [8, 50, 13].

$$\dot{Q}_{dis} = \dot{Q}_{Cond} + \dot{Q}_{Rad} + \dot{Q}_{Conv} \tag{54}$$

$$\dot{Q}_{Cond} = \frac{K \cdot A_{fc} \cdot (T_{FC} - T_{amb})}{t\_plate} \tag{55}$$

$$\dot{Q}_{Rad} = \varepsilon \cdot \delta \cdot \left({T_{FC}}^4 - {T_{amb}}^4\right) A_{fc} \tag{56}$$

$$\dot{Q}_{Conv} = hA(T_{FC} - T_{amb}) \tag{57}$$

where T_{FC} is the fuel cell temperature, K is the thermal conductivity, A_{fc} is the area of the conducting surface (fuel cell area), *t_plate* is the thickness of the base plate that holds the fuel cells, ε is the emissivity constant, δ is Boltzmann's constant given by $5.67e^{-8}$ $W \cdot m^{-2} \cdot K^{-4}$ and h is the heat transfer coefficient.

The electricity generated (W_{el}) is given by,

$$W_{el} = N \cdot R_{load} \cdot {I_{st}}^2 \qquad (58)$$

where R_{load} is the electrical load resistance in ohms, N *is* the number of fuel cells in the stack and I_{st} is the fuel cell stack current.

By substituting Eq.49-58 into Eq.48, the energy balance is obtained. All the equations in the model blocks (Mass Flow, Stack Voltage and Thermodynamic) described above are simultaneously solved for the unknown parameters: terminal voltage, temperature of the fuel cell, mass flow rates. The performance of the fuel cell is predicted using this model for various operating conditions. The effects of humidity, pressure and temperature are analyzed in the next section.

3.2.4. Effects of Operating Parameters

As an example, analysis of a PEM fuel cell of area 9 cm^2 and parameters taken from a literature source is used to simulate power curves using the model [24]. The effects of humidity, pressure and temperature are analyzed.

3.2.4.1. Humidity Effect

The effect of humidity on the performance of the fuel cell is demonstrated by Figure 19. The curve is obtained for changing relative humidity of air, and hydrogen (H_2) simultaneously. The figure indicates that an increase in humidity increases the performance of the fuel cell (increase in the power generated by the fuel cell as seen in the figure).

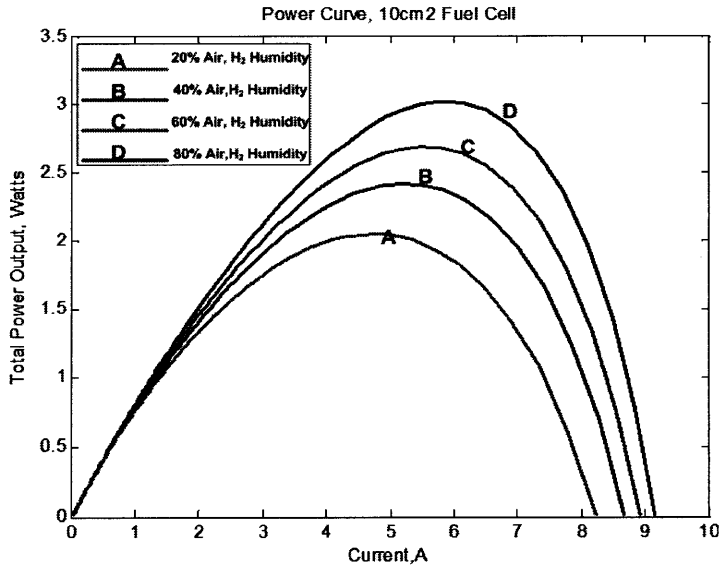

Figure 19. Humidity effect on power generated.

3.2.4.2. *Pressure Effect*

The effect of pressure on the performance of the fuel cell is analyzed by changing the inlet pressure of H_2 into the fuel cell with 50% relative humidity of air and H_2. Figure 20 shows that the increase in pressure results in a higher power output from the fuel cell. This is expected with the Nernst equation given by Eq.40, where the voltage is directly proportional to the hydrogen pressure. However, the increase is very minute within 5%.

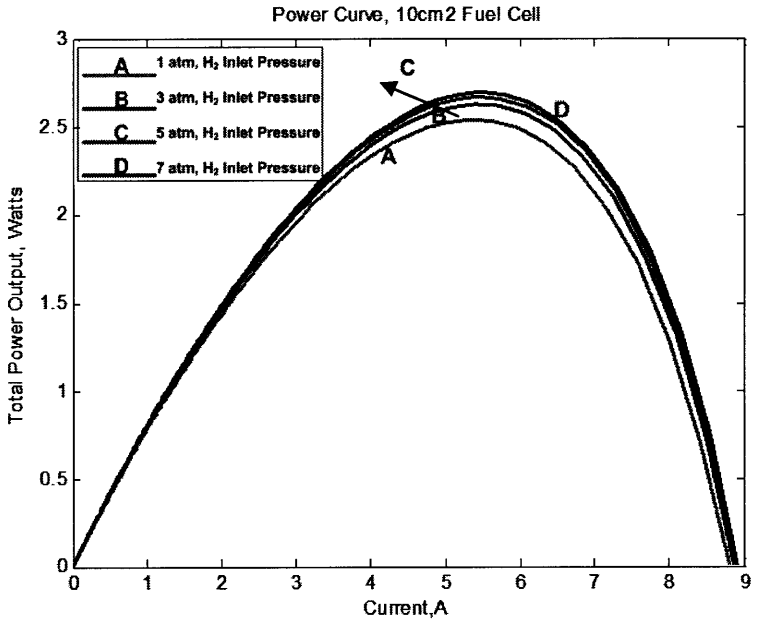

Figure 20. Pressure effect on power generated.

3.2.4.3. *Temperature Effect*

As shown in Eq.59, where, V_{fc} is the fuel cell voltage, T is the temperature, S is the entropy, F is the Faraday's constant and n is 2. With an increase in temperature, the voltage of the fuel cell decreases [8]. However, increase in temperature, results in exponentially higher exchange current density (i_0) according to Eq. 60, where T is the operating temperature and significantly improves the mass transport properties at higher temperatures. This increases the fuel cell voltage. The effect of temperature on the fuel cell is simulated using the model on the same fuel cell used for the humidity and pressure effects. The temperature is varied from 20°C to 60°C for 50 % relative humidity of air and hydrogen. Figure 21 indicates increased power performance with increase in the operating temperature of the fuel cell.

$$V_{fc} = -\left[\frac{\Delta H}{2F} - \frac{T\Delta S}{2F}\right] \tag{59}$$

$$i_o = i_o^{ref}\, a_c\, L_C \left(\frac{P_r}{P_r^{ref}}\right)^{\gamma} exp\left[-\frac{Vf_c}{RT}\left(1 - \frac{T}{T_{ref}}\right)\right] \tag{60}$$

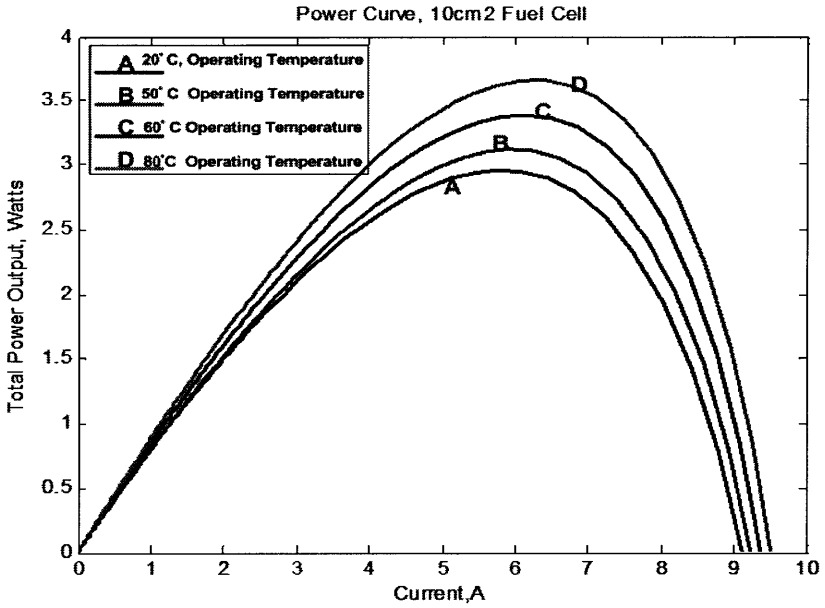

Figure 21. Temperature effect on power generated.

3.3. Model validation

Model validation is performed to verify the accuracy of the model under expected conditions. Validation for the developed fuel cell model is performed in two ways, one by using published literature data and the other using data from experiments conducted at FSRL. Figure 22 shows the polarization curve obtained from the model compared to the published experimental data by Fabian et al. [24]. The fuel cells used in the publication are of area $9cm^2$ operating at 21°C with a relative humidity of 50%. The figure shows that the model developed agrees with the published data within 15% error.

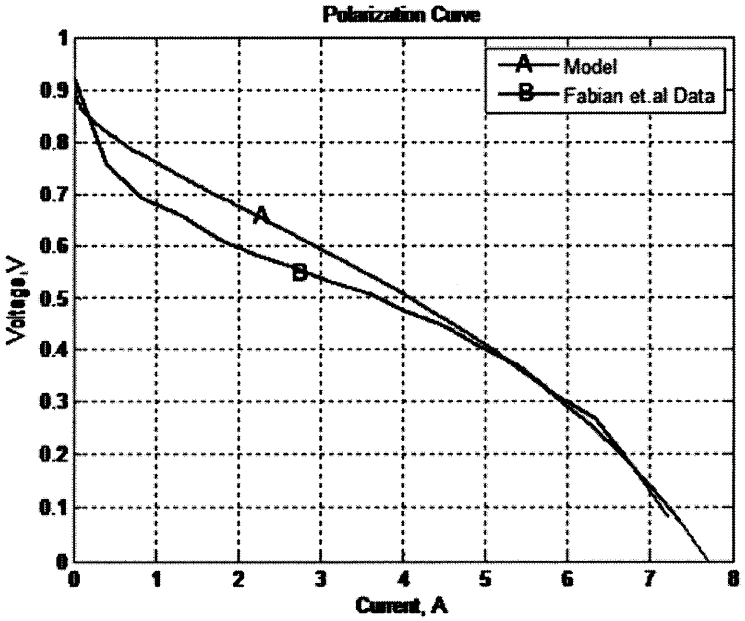

Figure 22. Validation of model results with published literature model.

3.4. Experimental Characterization

Experiments are conducted in the lab to characterize the fuel cells and understand the performance of fuel cells in real time operation under variable environmental conditions. It is critical to experimentally validate these models in terms of fuel cell voltage, power outputs, efficiency and long term degradation.

3.4.1. Experimental Setup

Experiments are conducted in FSRL using PEM fuel cells. The schematic of the experimental system assembled in the laboratory is shown in Figure 23 [25]. The fuel cells are supplied with 100% humidified hydrogen from a pressurized tank and humidified ambient air (see Figure 23). The humidity of air can be adjusted using a humidity generator (wet sponge used for the experiment). The experimental setup is shown in Figure 24 where the fuel cells are maintained in an environmental chamber to maintain desired humidity levels [25]. The fuel cells are connected to an electrically resistive load that simulates circuitry powering low power devices or for charging a battery. The voltage, current and power varies as a function of the load. The fuel cell performance has been characterized as a function of ambient temperature, ambient humidity, hydrogen pressure and hydrogen flow rate. The effects of humidity are recorded and the polarization curves for varying humidity levels are measured.

3.4.2. Experimental Procedure

The first step in the experimental procedure is to adjust the humidity in the environmental chamber to the desired value before the fuel cells are activated. The multimeter is then turned on. Then, the hydrogen flow valve is released and the pressure is adjusted until it meets the desired value. To condition the fuel cells, they are operated for 15 minutes in open circuit configuration, followed by a 10 minute period of operation at approximately 450mA. After conditioning, the polarization procedure begins [25]. A ladder network of resistors is used as the external load to measure the voltage for the experiment. The largest resistance in the resistance network as shown in Appendix B is connected to the fuel cells for five minutes. The output voltage of the fuel cells, along with the ambient temperature, fuel cell temperature, and relative humidity are recorded after five minutes. Then, the next lowest resistance in the resistance network is connected to the fuel cells for five minutes. The process of connecting decreasing resistances to the fuel cells and measuring the output voltage, ambient temperature, fuel cell temperature, and relative humidity is continued until all resistances in the resistance network have been tested. At this point, the experiment is completed, and the output voltage versus resistance data can be used to obtain a polarization curve. More details on the fuel cell start-up and shut down procedures can be found in Appendix B [25].

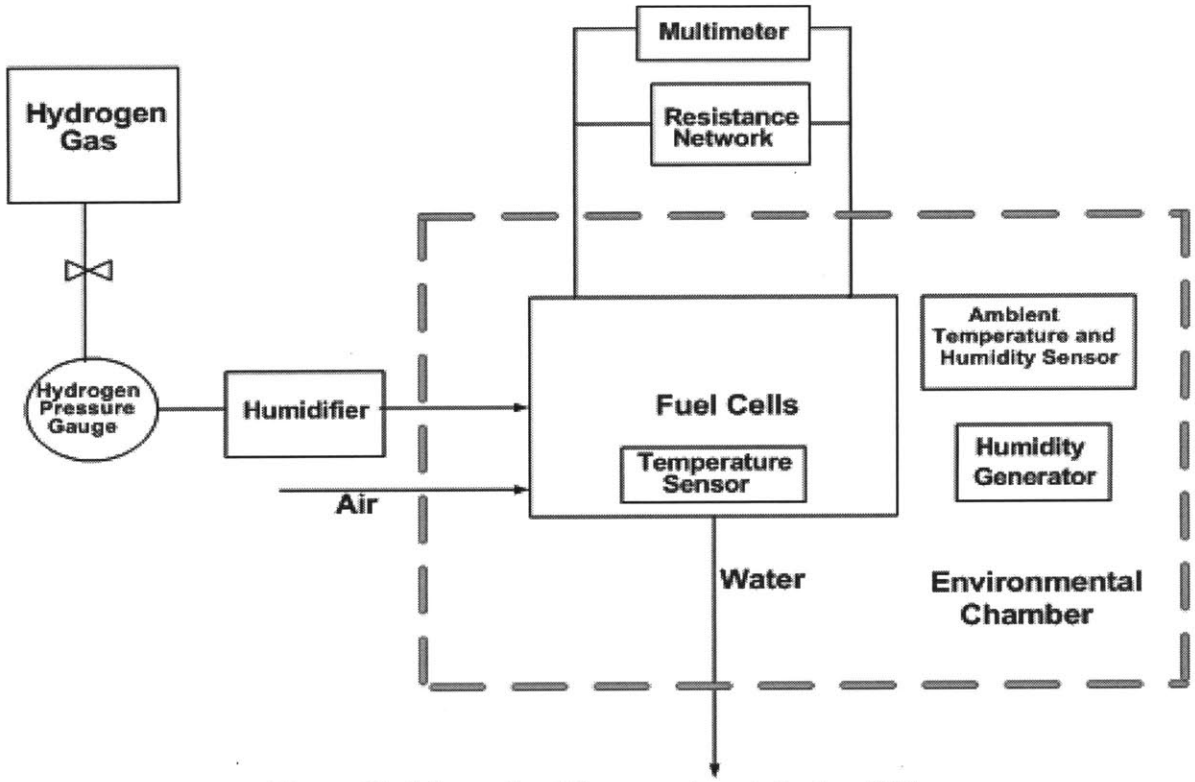

Figure 23. Schematic of the experimental setup [25].

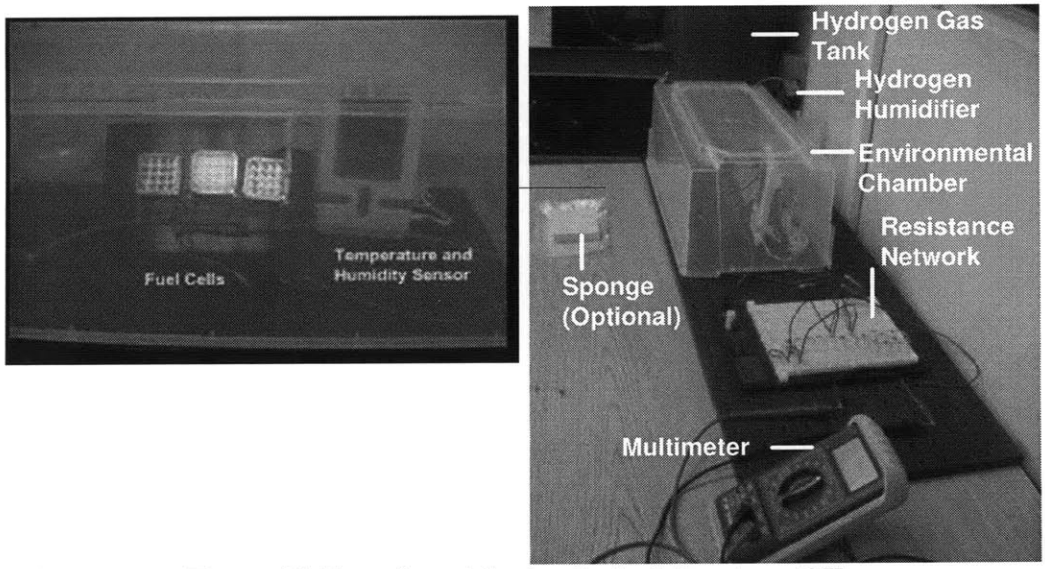

Figure 24. Experimental setup in the laboratory [25].

3.4.3. Experimental Results

The goal of the experiments is to determine the effects of change in the operating parameters, humidity being the most important. The humidity of hydrogen remains saturated (100 %) at all times by passing hydrogen into a beaker filled with water. The humidity effects on the fuel cell performance are studied using the humidity changes in the inlet air. Figures 25-26 show the change in performance of the fuel cell with increasing air humidity. One can observe from the figures that with the increase in humidity, the voltage curve (polarization

curve) shifts up, increasing the power output. Figures 27-28 show the comparison between the experimental data acquired and the performance curves from the model using the parameters from the experiment. The figures below indicate a good agreement between the model and the experiments.

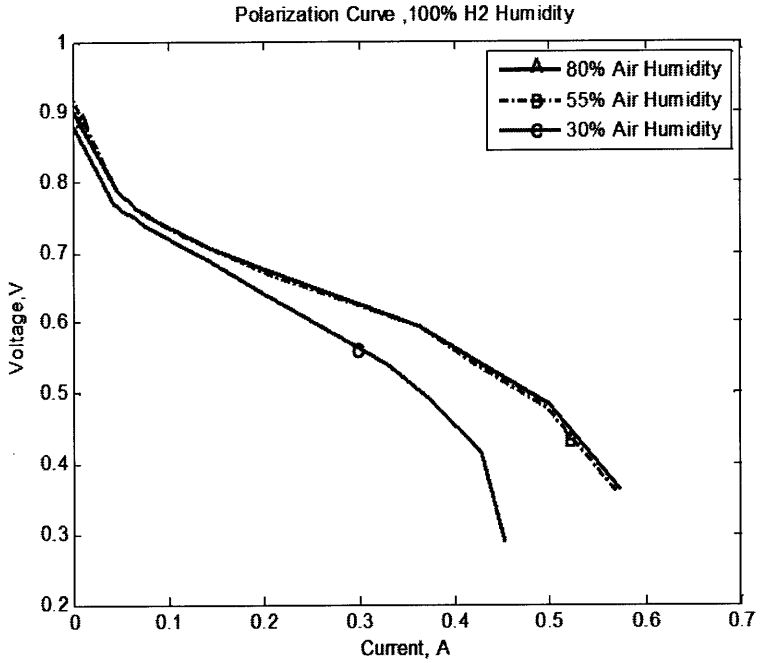

Figure 25. Experimental results of the polarization curve for varying humidity levels in inlet air.

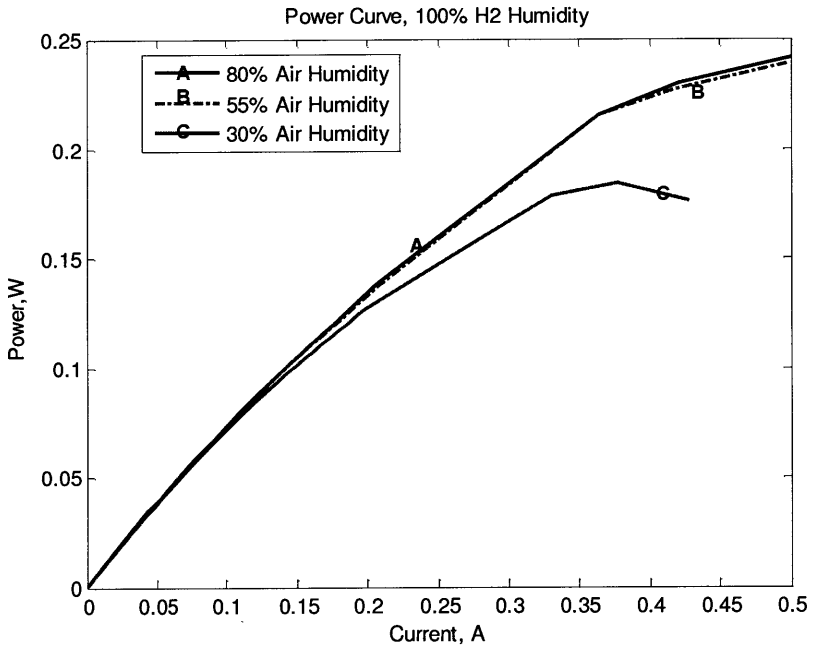

Figure 26. Experimental results of the power curve for varying humidity levels in inlet air.

Figure 27 gives the polarization curve for 30% air humidity giving a maximum power of 0.18W at 0.49V. Figure 28 shows the polarization curve for 80% humidity with an increased maximum power of 0.24W at 0.49V. The model agrees with the change in the humidity levels observed via experiments within 10% error.

The model shows good agreement with experimental data and published results and effectively predicts the performance of a PEM fuel cell as a function of operating parameters and the external load demands.

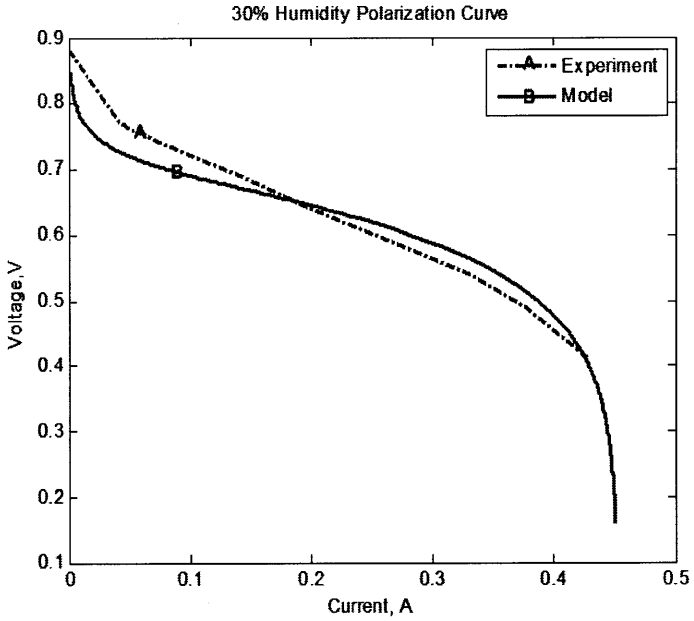

Figure 27. Experimental validation of the model for 30% humidity level of air (100% H_2).

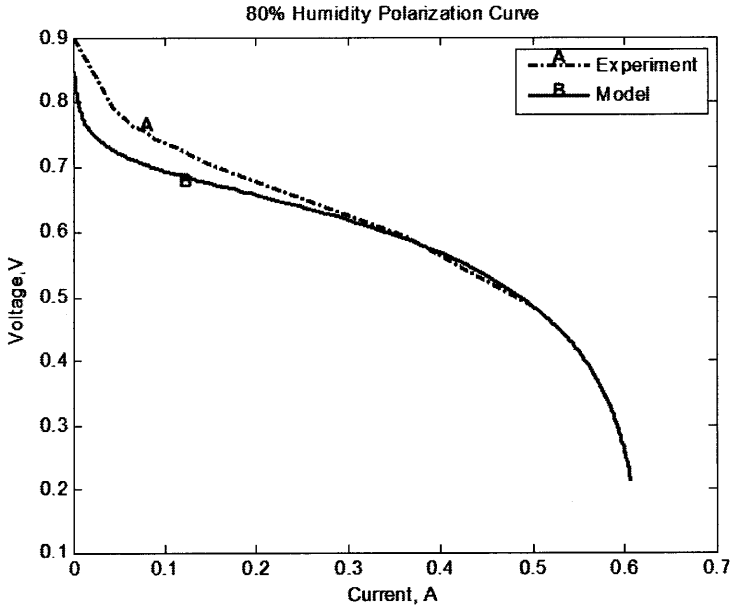

Figure 28. Experimental validation of the Model for 80% humidity level of air (100% H2).

Fuel Cell Model and Experiments Summary

In this chapter it is shown that the steady state model developed can predict PEM micro fuel cell performance within 10 to 15% error. PEM fuel cells have high efficiency values and this has been shown from the experiments conducted. Figure 29 shows the efficiency values from the experiment and the model. At an operating voltage of 0.8V, the fuel cell efficiency is 65% (using Lower Heating Value) which makes fuel cells the best choice for long duration applications with low power demands.

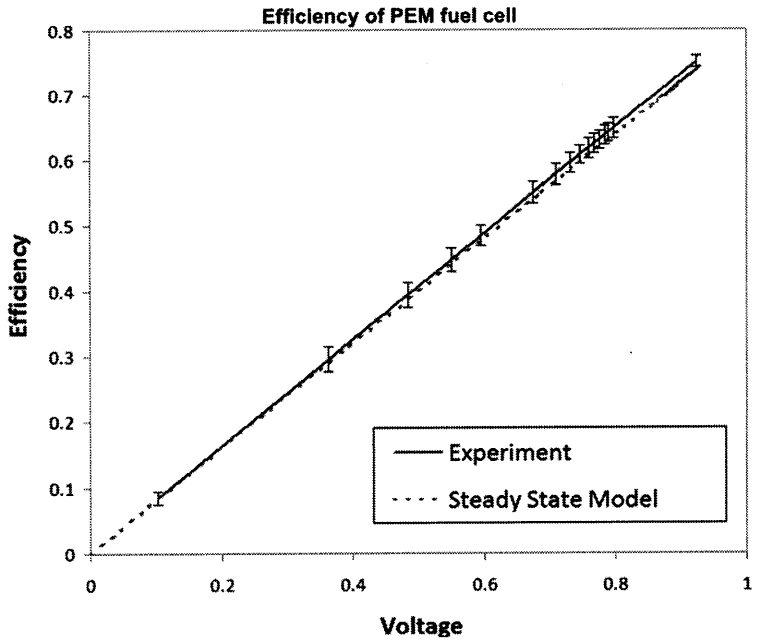

Figure 29. Lower heating value efficiency of PEM fuel cell from model and experiments.

Apart from predicting fuel cell performance, it is necessary to maintain ideal operating conditions for the fuel cells to maximize life. Fuel cells produce electricity and waste heat. Depending on the operating efficiency, the fuel cell system needs to effectively manage the waste heat generated. Hence a thermally conducive environment for the operation of fuel cells needs to be maintained. Similarly, fuel cell produces water; hence an effective water management system should be designed for humidifying the reactants and handling the water produced. For applications where the system might be either buried or in remote locations without open atmosphere available, air management needs to be analyzed. These challenges are further investigated in Chapters 4 and 5. Passive air and water management strategies are proposed for the fuel cell powered systems.

CHAPTER 4

THERMAL ARCHITECHTURE FOR FUEL CELL POWERED SENSOR SYSTEMS

This chapter presents the feasibility of innovative thermal management architectures for fuel cell powered sensor systems in extreme environments. Passive thermal architecture concepts for both space and terrestrial applications are proposed. Experimental evaluation of these simple concepts to demonstrate their feasibility is conducted. Passive thermal designs for the various environments are based upon minimizing heat loss by using a combination of insulation and minimally radiating surfaces. Minimization of heat loss is required in cold environments and heat rejection is required if excessive heat is produced inside the system by the fuel cells and electronics. This is achieved by employing passive thermal design solutions that require as little external energy input as possible. Passive control is advantageous as it does not involve moving parts and is feasible to employ and manage. Active control systems on board add complexity to the system, especially if these sensor systems are to be self-contained and remotely implemented with no supervision.

4.1. Thermal Isolation System for Space Applications

For missions such as planetary surface exploration, water detection on the moon and other small bodies in the solar system, the exploration equipment (devices) will need to function in extreme conditions under low temperatures. Various components of the exploration systems, such as the sensors, electronics and power source (fuel cells), require operating temperatures that are between 0°C and 80°C. This research evaluates the feasibility of using a passive thermal management system for operating in the cold environments for a reference mission on the lunar surface.

4.1.1 Environment on the moon

The reference mission on the moon requires the fuel cell powered sensor systems to be able to operate at the polar regions. The biggest challenge posed by the lunar environment is the extreme cold temperatures. The temperatures at the polar regions of the lunar surface are as low as -153°C [39]. The temperature for operating PEM fuel cells is between 0°C and 80°C [8]. The electronics and sensors operate between 0°C and 50°C [18]. Therefore, a robust system that would protect the power supply and other electronic components from the cold temperatures is required. A concept of the fuel cell powered sensor network on the surface of the moon is shown in Figure 30.

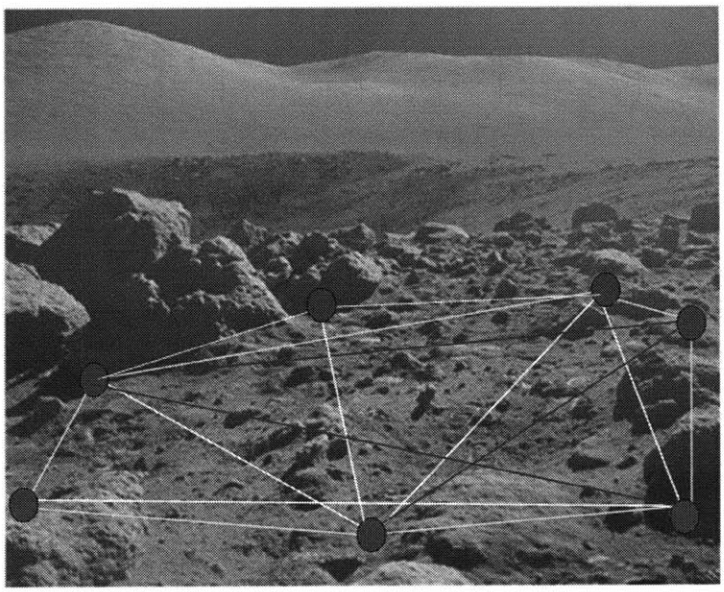

Figure 30. A concept of a fuel cell-powered sensor network on the lunar surface [39].

4.1.2 Thermal system model description

The goal of the thermal architecture is to maintain a broad thermal range inside the system that would prevent either freezing or overheating of the system components. The design of the system has been adapted from previous studies of small hopping robots for planetary exploration [10, 21, 32, 33]. From these previous studies, the use of a spherical design for planetary exploration is expected to be efficient particularly when employing hopping, bouncing and rolling locomotion [10, 21]. Small spherical sensor systems can access and explore subterranean areas such as craters, caves, etc. on the moon.

Based on previous studies the thermal design proposed here is spherical in shape, with a set of concentric spheres that hold the power system (fuel cell) and other components (fuel storage elements) and electronics inside the inner sphere. The thermal encapsulation proposed is shown in Figure 31. The inner sphere is held together by an inner ring made of acrylic. The outer sphere is 7 inches in diameter and the inner sphere is 4 inches in diameter. Both the spheres are connected by a one-inch thick acrylic outer ring. A thin ring of 0.11-inch thickness with four evenly spaced fins is designed and fabricated; where the width of the fins is 0.17 inches. This thickness is to limit the extent of thermal conduction on to the ring. Acrylic has low thermal conductivity and hence is chosen as the system material to minimize system conductivity. Table 4 gives the relevant system geometric values and Figures 32 and 33 show the inner and outer ring drawings.

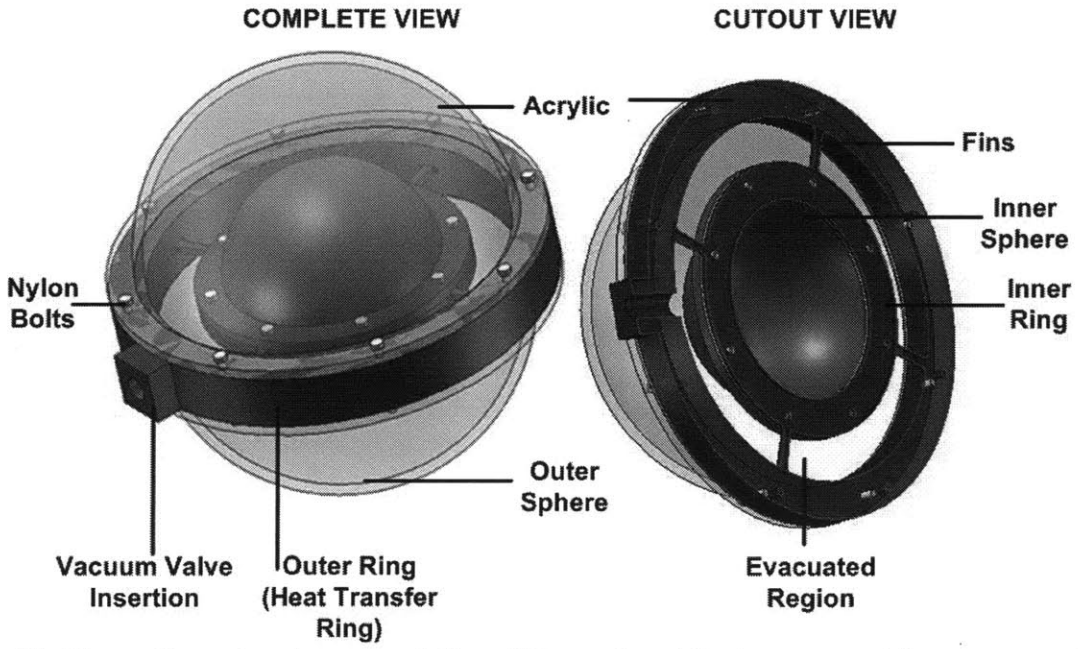

Figure 31. Three-dimensional representation of thermal architecture concept for sensors on lunar surface.

Table 4. Thermal Isolation system parameters.

Geometric Parameter	Value
Outer Sphere Diameter	7 in [0.18 m]
Inner Sphere Diameter	4 in [0.10 m]
Sphere Thickness	0.1575in [4 mm]
Outer Ring Thickness	1 in [0.025 m]
Ring and Sphere Material	Acrylic

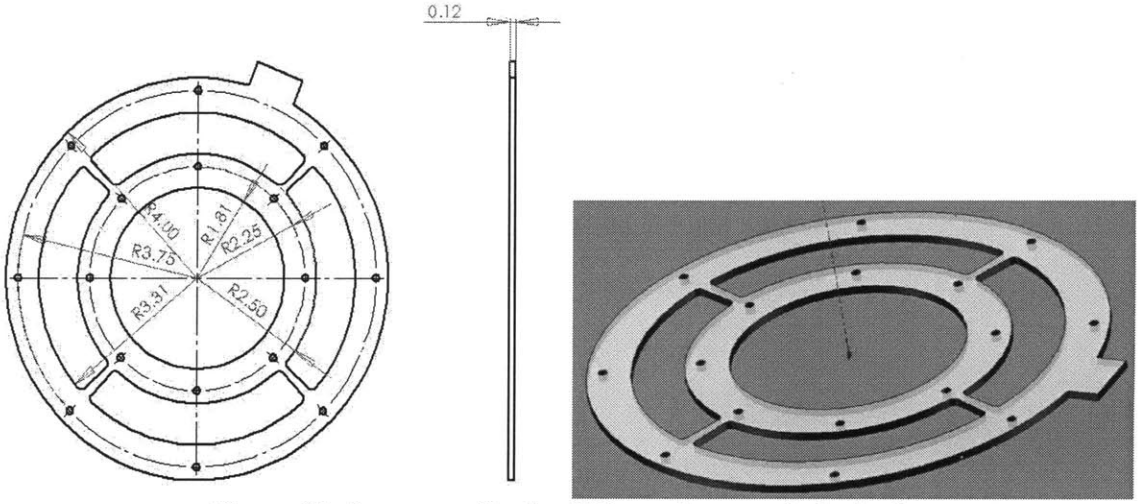

Figure 32: Inner acrylic ring [Dimensions are in inches].

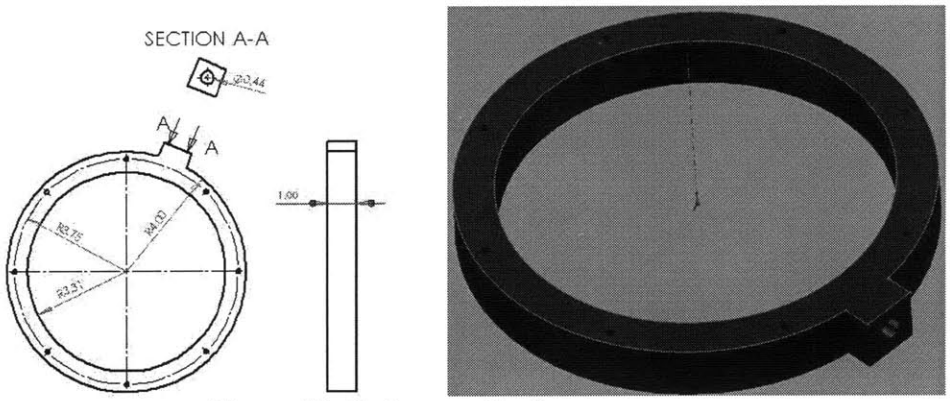

Figure 33: Outer acrylic ring.

The spheres at the flanges and the rings are sealed together with polytetrafluoroethylene (PTFE) (see Figure 47) gaskets. The inner sphere is maintained at atmospheric pressure. Vacuum is drawn in the space between the inner and outer spheres to minimize convection. As seen from Figure 33, the heat transfer ring (outer acrylic ring) has a tapered hole drilled where a vacuum valve (0.25" male NPT) is inserted to facilitate drawing air from the outer sphere. There are concerns with regard to air leakage into the container through any of the many separations between the surfaces. The pressure of the atmosphere against the vacuum helps to provide a clamping force minimizing air leakage. The PTFE gaskets are chosen as they are rated upto -212°C [13]. Basic calculations are performed to prove that acrylic can withstand the pressure difference between vacuum and the atmosphere. Acrylic is rated for 10,000 psi [2], where as the effect of pressure difference is 140 psi. Hence the stress due to the vacuum will not be an issue. Nylon bolts are used to seal the gaskets, rings and the spheres together to minimize thermal conduction, since nylon has a thermal coefficient of expansion close to acrylic and the bolts are rated for low temperature operations. To minimize radiation heat transfer, the outside of the inner sphere should be coated with a material that has very low emissivity value of 0.01. However, obtaining such a low emissivity material is not practical, so the spheres are coated with gold, which has an emissivity of 0.02.

4.1.3. Heat Transfer Model

The design of the thermal architecture consists of a basic heat transfer model mimicking a thermos flask. The three modes of heat transfer, convection, conduction and radiation, are included in a lumped parameter model with conduction and radiation being the major drivers of the system. Figure 34 shows the heat transfer model of the concept where the internal temperature needs to be maintained at above freezing temperature. A thermal system for withstanding external temperatures of -40°C is built and tested for evaluating the feasibility. Improvements in this design will focus on maintaining a minimum temperature of 20 °C. Figure 34 shows the heat transfer modes and the effective thermal resistance at each node of the system. T_∞ is the external/ambient temperature and T_i is the internal temperature to be maintained above 0 °C. Heat is generated inside the system as a result of operating the fuel cell and other electronics.

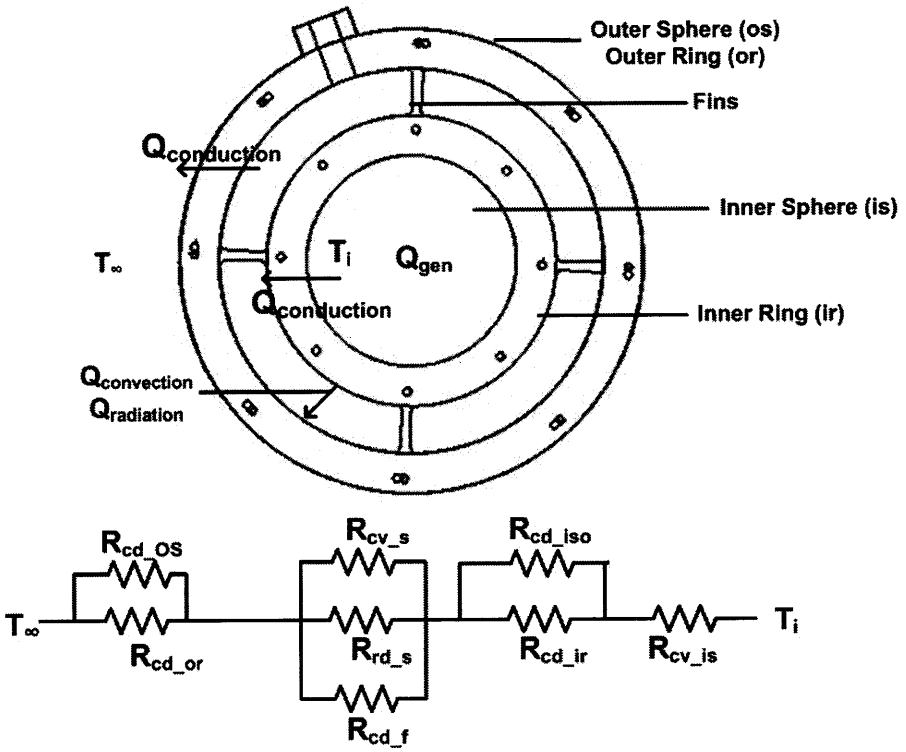

Figure 34: Heat transfer modes at each node in the system.

In this model, R_{cd} is the conductive heat resistance, R_{cv} is the convective heat resistance and R_{rd} is the radiative heat resistance. Each node is represented as a subscript to the resistance in the figure. The subscripts, *is, iso, ir, f, s, or* and *os* represent, the inner sphere, outer side of inner sphere, inner ring, fins, sphere and outer ring and outer sphere respectively. From initial heat transfer analysis it is concluded that significant heat transfer occurs through conduction and heat losses due to radiation and convection are given less consideration. However, due to the extreme temperature gradients between the external temperature and the internal system, heat radiation cannot be ignored. Because the space between inner and outer spheres is evacuated, convection is minimized. A systematic heat transfer model is developed to analyze the heat transfer occurring between the two spheres and the environment while maintaining internal temperature. As seen from the Figure 34, all three modes of heat transfer occur in parallel between the spheres. Analysis is performed with heat transfer modes defined for every node and the steady-state temperature of the system internally is calculated for a given amount of heat being generated in the system.

4.1.4. Heat Transfer Modes in the thermal architecture

4.1.4.1. Conduction

Heat transfer via conduction occurs through the fins, and is defined as [13],

$$\dot{Q}_{cond} = \frac{nk_{acr}A_c}{L}(T_{in} - T_{out}) \tag{61}$$

where k_{acr} is the thermal conductivity of acrylic, A_c is the cross sectional area of the fin, L is the length of the fin, T_{in} is the temperature of the inner ring, and T_{out} is the temperature of the outside ring, n represents number of fins that are designed into the model (4 in this case).

4.1.4.2. Convection

Although vacuum is drawn in the space between the inner and outer spheres, it is not practical to have an absolute vacuum due to air leakage and the limitations of vacuum drawing pumps. Hence, it is possible that some air at low pressures is present. To precisely model the real system it is reasonable to determine the extent of heat transfer that occurs due to natural convection between the spheres from the air remaining in the space. Heat transfer through natural convection is complex and requires making various correlations to predict the magnitude of heat transfer. The following equations are used in determining the convectional heat transfer between concentric spheres [13, 15].

$$\frac{k_{eff}}{k} = 0.74\left(\frac{Pr}{0.861+Pr}\right)^{1/4} Ra_{sph}^{1/4} \tag{62}$$

$$Ra_{sph} = \left(\frac{\frac{1}{2}(D_o - D_i)}{D_o D_i}\right)\left(\frac{Ra_L}{\left(D_o^{\frac{-7}{5}} + D_i^{\frac{-7}{5}}\right)^5}\right) \tag{63}$$

$$\dot{Q}_{conv} = \frac{4\pi k_{eff}(T_{in} - T_{out})}{\frac{1}{r_i} - \frac{1}{r_o}} \tag{64}$$

where Pr is the Prandlt number, and Ra is the Raleigh number, both dimensionless quantities. D_o, D_i, r_o, r_i are the diameters and radii of the inner and outer spheres, respectively. Using these geometric values in the above equations gives a value for Ra_{sph} of approximately 0.03. The above correlations are only valid for $10^2 < Ra_{sph}$, hence there is not an accurate correlation describing this mode of heat transfer. Ideally, the existence of a full vacuum should eliminate convection.

4.1.4.3. Radiation

Since the space between the two spheres is almost a vacuum, radiation is the dominant heat transfer mode in the system and is given by [13],

$$\dot{Q}_{rad} = \varepsilon\sigma A_s\left(T_{in}^{\ 4} - T_{out}^{\ 4}\right) \tag{65}$$

where ε is the surface emissivity of the inner sphere, σ is the Stefan-Boltzmann constant, and A_s is the surface area of the inner sphere. The higher the emissivity of a material, the higher the heat lost through radiation. The emissivity of acrylic is as high as 0.94, so a low emissivity coating on the outside of the inner sphere or a highly reflective coating on the inside of the outer sphere should minimize radiation heat loss.

Thermal resistances due to conduction, convection and radiation are calculated before determining the overall heat loss from the system. The thermal resistances are given by the following equations [13],

$$R_{cond} = \frac{L}{4k_{acr}A_c} \tag{66}$$

$$R_{rad} = \frac{2}{\varepsilon\sigma A_s (T_{in} + T_{out})^3} \tag{67}$$

Here, the value for R_{rad} is only approximate because the temperature difference goes to the fourth power. By comparing the magnitudes of the thermal resistances, one can determine which mode of heat transfer dominates. Finally all the heat transfer modes are modeled in parallel by using the thermal circuit analogy and Newton's Law of Cooling as given in the following equation [15],

$$\dot{Q}_{net} = \frac{(T_{in} - T_{out})}{R_{eq}} \tag{68}$$

where R_{eq} is the equivalent thermal resistance, defined by:

$$R_{eq} = \frac{R_{cond}R_{rad}}{R_{rad} + R_{conv}} \tag{69}$$

where R_{cond} , $R_{conv,}$ R_{rad} are the thermal resistances due to conduction, convection, and radiation, that can be found from Eq.66 and 67.

4.1.5. Transient Heat Analysis

Heat transfer in a system occurs until the system reaches equilibrium (steady-state) with its environment, where the heat flux dissipated equals the heat generated inside the system. The objective is to keep both the transient and steady-state within the desired,above freezing temepratures. A lumped thermal capacitance model is used for the inner sphere and its components, because there is a high thermal resistance between the inner and outer sphere. In the lumped parameter model, the inner sphere and its components are assumed to be at uniform temperature. The general formula for a lumped thermal capacitance model is given by [15],

$$\frac{\theta}{\theta_i} = \frac{T(t) - T_{amb}}{T_i - T_{amb}} = \exp\left[-\left(\frac{1}{R_{eq}\rho V c_p}\right)\cdot t\right] \tag{70}$$

When this formula is applied to the experimental system, the resulting equation for the temperature of the inner sphere over time is given by,

$$T_{is}(t) = (T_{is0} - T_{amb} + R_{eq}\dot{Q})\exp\left[-\left(\frac{1}{R_{eq}(Mc_p)_{tot}}\right)\cdot t\right] + T_{amb} - R_{eq}\dot{Q} \tag{71}$$

where the heat production rate, $\dot{Q}$ is negative as heat will be flowing out of the system. Mc_p is the total thermal capacity of the system (Table 6). Table 5 lists the appropriate values that are used in the analysis. The details of the experimental work for the proposed thermal architecture concept are given in Section 4.3.

Table 5.Values used in thermal transient analysis.

Parameter	Value
Heat Generation Rate	0.5 W
Ambient Temperature	249.2 °K, -24 °C (Average temperature)
Surface emissivity of Acrylic	0.94

4.1.5.1. Heat Transfer in the inner sphere

For modeling purposes, the dominant heat transfer mode within the inner sphere is assumed to be convection due to presence of air. However, in a real system heat is dissipated by the fuel cell and heat is conducted through the support structures of the system and is radiated. An experiment is conducted to validate the heat transfer model. In the experiment, 0.5W of heat is generated using a simple electric circuit with resistors powered by alkaline batteries. It is assumed that the inner sphere and components contained therein are at uniform temperature. It is necessary to determine the heat capacity of the components in the system to predict the transient response of the system. The heat generation components inside the electric circuit consist of 2 AA Alkaline batteries with a holder, a small silicon circuit board, a piece of foam to hold the items, and the data logging device. The heat capacity of an object is defined by the product of its mass and its specific heat capacity. Table 6 gives the various components and the heat capacity that are used for the model and experiments. Section 4.3 presents details on the experiment.

Table 6: Heat capacity of various components inside of sphere.

Component	Mass [kg]	Specific Heat Capacity [J/kgK]	Total Heat Capacity [J/K]
Inner Sphere	0.15	1500	226
Circuit Board	0.007	700	5
2x AA Batteries	0.046	200*	9
Data Logger	0.050*	1000*	50
Total	0.3	N/A	293

Note: * indicates an approximated value

4.2. Thermal Isolation System for Terrain Applications

For terrestrial applications such as border patrol and security monitoring, the fuel cell powered sensor system is assumed to be buried underground for a period of 3 years. A passive thermal control system is an ideal solution for this application as it does not require external energy input to control the thermal environment inside the system. This requires having a good understanding of the climatic conditions. The reference mission assumes that the system will be buried between 0.3-0.9m (1ft-3ft) below the surface, so the environment underground needs to be understood. The fuel cells are known to operate between 0°C to 80°C, while the electronics and the battery are expected to operate between 0°C to 50°C [18]. However, for long life operation of fuel cells, the operational temperature should be maintained above 10°C [19].The objective is to design a robust passive thermal management system that maintains a system temperature in the range of 10°C to 50°C, preventing overheating during the summer and overcooling during the winter.

4.2.1. Environment of the desert regions

A reference mission in Nizzana, in the desert regions of Negev, Israel is considered. Nizzana can be a potential location for deploying sensor networks for border protection as it lies on the territorial border with Israel's neighboring countries (see Figure 35). The temperatures at Nizzana range from an average of 12.5°C during winter to a high of 49°C during summer with August being the warmest month [40]. The annual mean temperatures and monthly average (earth skin) temperatures at Nizzana, Israel are shown in Table 7 [40].

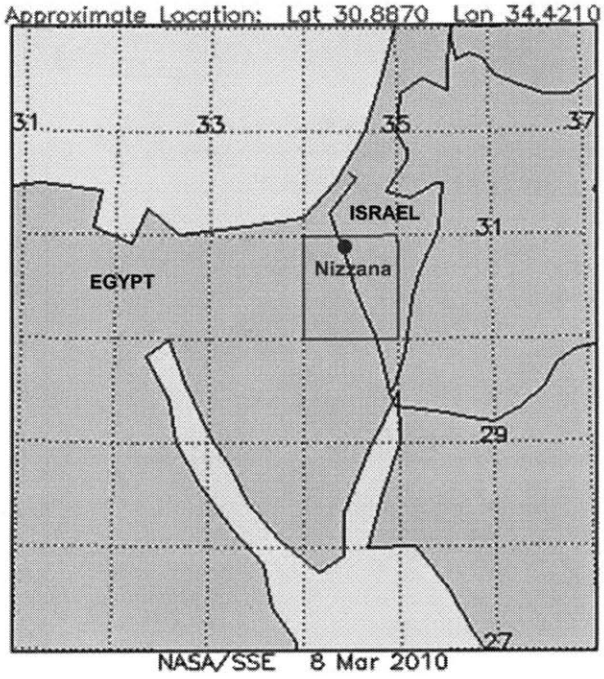

Figure 35. Location of Nizzana, Israel [40].

Table 6. Temperatures at Nizzana, Israel [40].
Monthly Averaged Earth Skin Temperature (°C)

Lat 30.88	**Jan**	**Feb**	**Mar**	**Apr**	**May**	**Jun**	**Jul**	**Aug**	**Sep**	**Oct**	**Nov**	**Dec**	**Annual**
Lon 34.42													**Average**
25-year Average	12.5	14.2	18.5	24.3	28.1	30.7	32.8	32.7	30	25	19.1	13.9	23.5

Average Minimum, Maximum and Amplitude Of The Daily Mean Earth Temperature (°C)

Lat 30.88	**Jan**	**Feb**	**Mar**	**Apr**	**May**	**Jun**	**Jul**	**Aug**	**Sep**	**Oct**	**Nov**	**Dec**	**Annual**
Lon 34.42													**Amplitude**
Minimum	5.22	5.41	8.23	12.2	15.3	17.9	20.2	20.9	19.5	16.3	11.5	6.86	
Maximum	24.6	27.6	33	40.7	44.6	46.7	49.1	48.6	45.5	38.4	31.8	25.8	
Amplitude	9.73	11.1	12.4	14.2	14.6	14.3	14.4	13.8	13	11	10.1	9.49	21.9

4.2.2. Thermal System Model

The spherical design proposed for the moon reference mission is considered for terrestrial applications in the desert. Because the temperature ranges on the moon and the Negev desert differ greatly, certain design modifications for thermal management using passive strategies are made to suit the terrestrial version. In addition, the design has been further simplified and a rectangular configuration, in the shape of a typical shoebox is analyzed. The fuel cell powered sensor system concept can be implemented in either configuration.

Preliminary thermal analysis is performed to obtain design parameters, such as the dimensions of the sensor system and thermal insulation material for the sensor system. Thermal analysis is carried out in two steps that account for annual temperature variations. First, the temperature at 0.61m (2 feet) below ground is extrapolated from the surface temperature data. Note that the surface temperature is affected by many factors such as (a) the ground structure and physical properties, (b) ground surface cover (e.g. bare ground, lawn, etc.) and (c) weather conditions (e.g. ambient temperature, wind speed, solar radiation, relatively humidity, etc) [57]. Here, a simplified model published in literature is used and is based on the solution for transient heat conduction in a semi-infinite solid [57]. For this case, the temperature of the ground, t_g (surface $x = 0$) is varying periodically with time and depth (x).

$$t_g = A_s \cos[2\pi(\tau - \tau_0)/365]) \tag{72}$$

The model can be expressed as:

$$t(x,\tau) = (t_m \pm \Delta t_m) - B_1 K_v A_s \exp(-B_2 x \alpha^{-0.5}) cos\left[\frac{2\pi}{365}(\tau - \tau_o + B_3 x \alpha)\right] \tag{73}$$

where, $B_1 = 1.07$, $B_2 = 0.0031552$, $B_3 = 0.018335$ and A_s is the annual amplitude of temperature, x is the distance from the surface of the earth, t_m is the annual mean temperature, α is thermal diffusivity of the sand and τ is the day of the year (ranging from 0 to 365) and τ_0, is the reference temperature that is 1/8 multiplied by the warmest day of the year. K_v is the vegetation coefficient, which depends on how much projective shade (soil covered by vegetation) is generated by ground vegetation. For this analysis, K_v is set to 1.0, which represents bare ground in full sun [57].

Figure 36 shows the soil temperature during the warmest and coldest days of the year for a depth of 0.61m (2 feet). During the coldest day of the year (Feb), the average temperature at the surface is 13°C. The temperature increases with increasing depth and plateaus at 25°C. A similar but opposite trend is observed in the summer during the months of July and August. The average surface temperature is 38°C and decreases with depth until reaching 2°C. This condition is expected because the thermal conductivity of sand (0.2 W/Km) is low and there is a significant time lag before the temperature of the subsurface sand reaches the ambient surface temperature. From this model, the temperatures at a depth of 0.61m (2 feet) on the coldest day of winter and warmest summer day are 16.6°C and 34°C respectively.

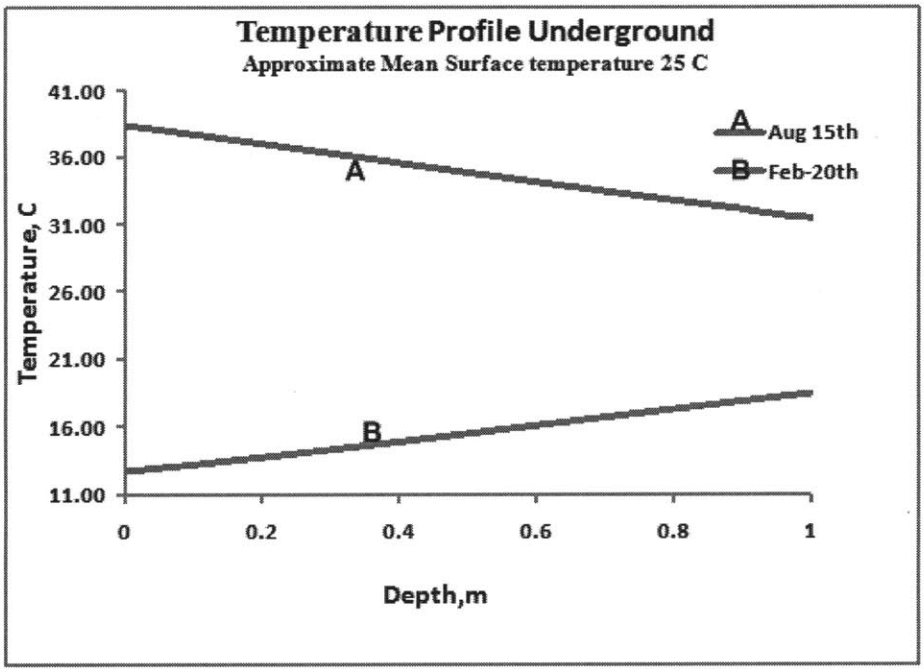

Figure 36. Temperature profiles at varying depths during summer and winter at Nizzana, Israel.

4.2.2.1.1 Spherical Configuration

Thermal analysis for the terrestrial spherical design configuration is presented in this section. The temperatures in the desert are not as extreme as the lunar surface and hence radiation is not the dominating heat transfer mode. Hence the inner sphere from the reference lunar design is unnecessary (Figures 37-38).

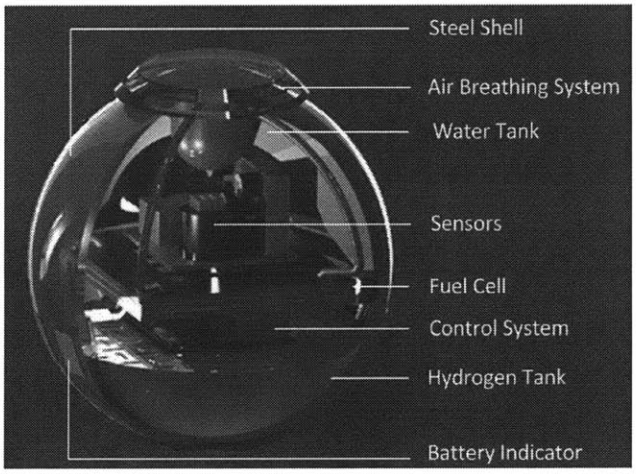

Figure 37. Three dimensional representation of fuel cell-powered sensor system in a spherical configuration.

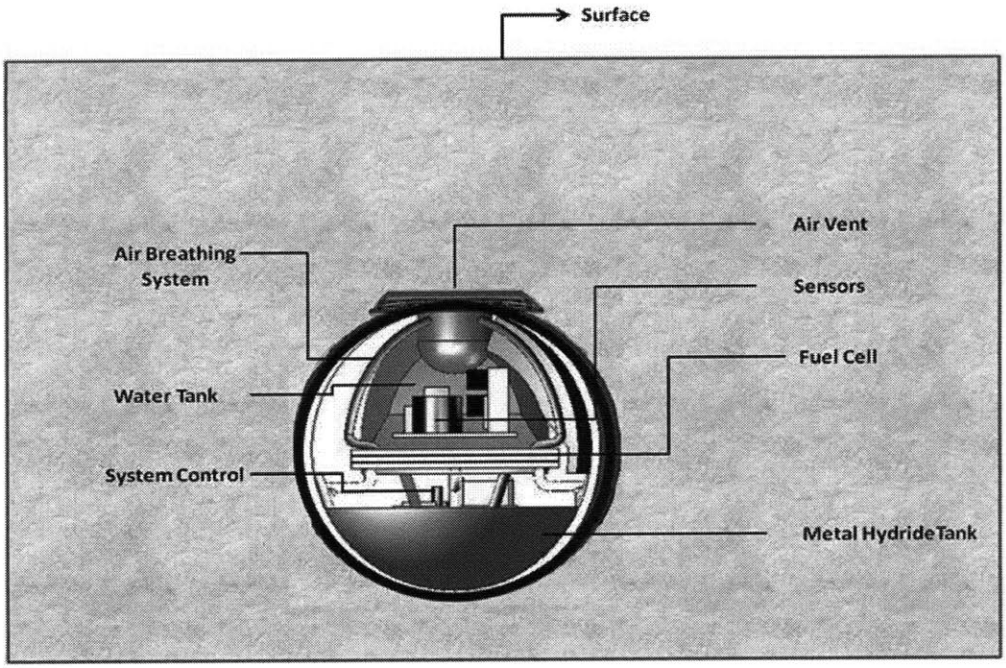

Figure 38. Representation of the fuel cell-powered sensor system buried underground.

Thermal analysis is performed on the system at a depth of 0.61m (2ft). The calculations use steady state heat transfer analysis. The efficiencies of the fuel cells and electronics inside the sensor module affect how much heat is generated. The fuel cells powering the sensor networks operate at 65% efficiency. For a fuel cell producing 10mW power, the amount of heat released is approximately 5mW. The maximum heat released from the electronics is approximately 18mW at 85% efficiency. Therefore it is safe to approximate that the total heat released for the system will not exceed 25mW. Based on these assumptions, heat transfer analysis is performed for steady-state heat dissipation of 25mW. For higher power sensors in the range of 100mW-5W, the heat released will be between 100mW-1W. For comparison heat transfer analysis is also performed for heat dissipation values of 100mW and 1W.

Figure 39 shows the heat transfer model of the system buried underground. T_1 is the temperature inside the system and the objective is to ensure this temperature stays within 10°C and 50°C. T_∞ is the temperature of the sand surrounding the system at the buried depth, and $\dot{Q}$ is the conductive heat flow from the system to the soil. The following assumptions are made for the heat transfer analysis, 1) The temperature inside the system is uniform, 2) The variation in temperature of the sand is assumed to be small (< 5°C). Because the heat generated in the sphere is very low, a one dimensional approximation for radial heat transfer is sufficient. The parameters used in the model are shown in Table 8. Eq.74 gives the steady-state differential equation for a spherical object, where r is the radius of the sphere and T is the temperature [13].

$$\frac{d}{dr}\left(r^2 \frac{dT}{dr}\right) = 0 \tag{74}$$

Imposing boundary conditions for the system, the differential equation is solved for temperature. The two boundary conditions used are: 1) the temperature T_1 in the system is given an initial value, 2) the other boundary

condition is calculated by equating the heat transfer through the walls of the spherical system to the heat flowing out from the spherical system into the surrounding given by [13],

$$\dot{Q} = -kA\frac{dy}{dx} = -k(4\pi r^2)\frac{C_1}{r^2} \tag{75}$$

where $\dot{Q}$ is the heat flow, k is the thermal conductivity of the material and A is the thermally conductive area. Solving the above equation for T_2 gives the constants C_1, C_2 (Eq. 76), that give the particular solutions to the differential equation (Eq.74). The heat transfer across the system is simply the heat dissipated and is obtained by solving for T_1.

$$C_1 = \frac{r_2(T_1 - T_\infty)}{1 - \frac{r_2}{r_1} - \frac{k}{Sksr_2}} \quad \text{and} \quad C_2 = T_1 + \frac{C_1}{r_1} = T_1 + \frac{T_1 - T_\infty}{1 - \frac{r_2}{r_1} - \frac{k}{Sksr_2}}\frac{r_2}{r_1} \tag{76}$$

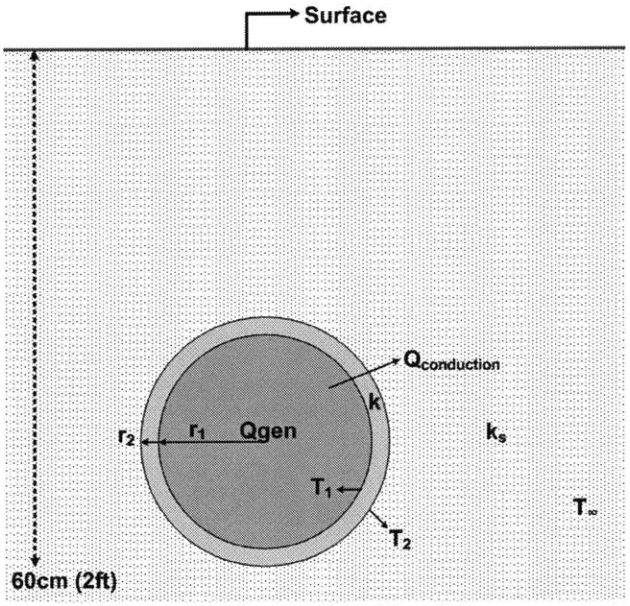

Figure 39. Heat transfer model of buried sensor system.

Table 7. Values used for heat transfer analysis.

Parameter	Value	Description
r1	9.7 cm	Inner radius of the sphere
r2	10 cm	Outer radius of the sphere
K	16	Thermal Conductivity of Aluminum
Ks	0.3	Thermal conductivity of sand
T_∞	34°C, 16.6°C	Temperature of sand in summer and winter

The baseline for the calculations is taken as the coldest day of winter. The radius, insulation thickness and thermal conductivity of the insulation material are varied to ensure the system internal temperature stays above 10°C. An aluminum shell of 3 mm thickness is sufficient to maintain the desired thermal environment. This design is then verified for the warmest day to ensure the temperature stays within 50°C. Figures 40 and 41

plot the radial temperature profile from the interior of the spherical wall into the surrounding soil for winter and summer conditions respectively.

As the distance from the system increases, the temperature exponentially decays. A temperature range of 12.7°C to 36°C is maintained inside the system throughout the year. These results suggest the soil temperature assists in maintaining a relatively stable and favorable thermal environment for the operation of the fuel cell powered sensor system.

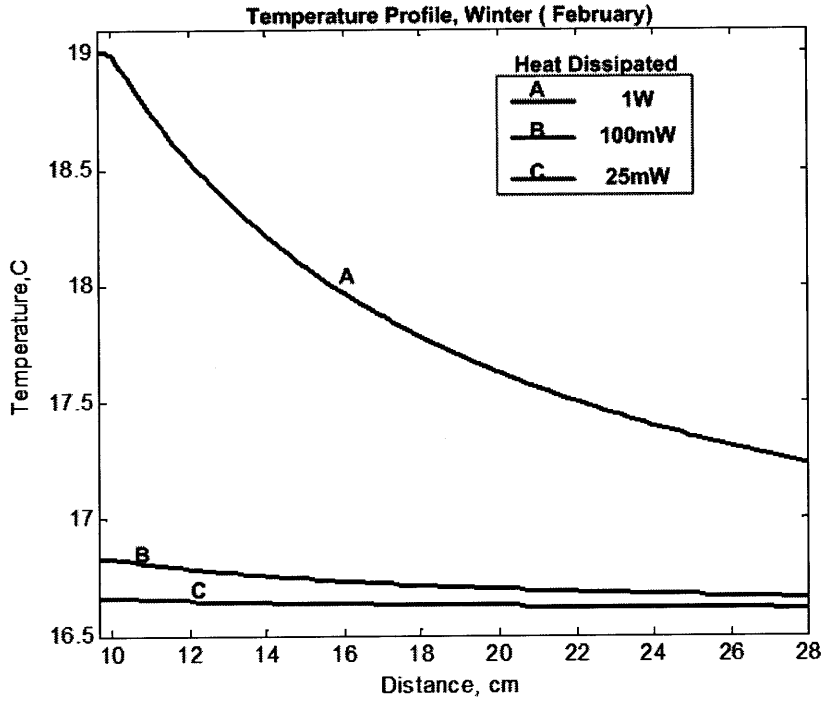

Figure 40. Temperature profile radially outward into the surrounding during winter.

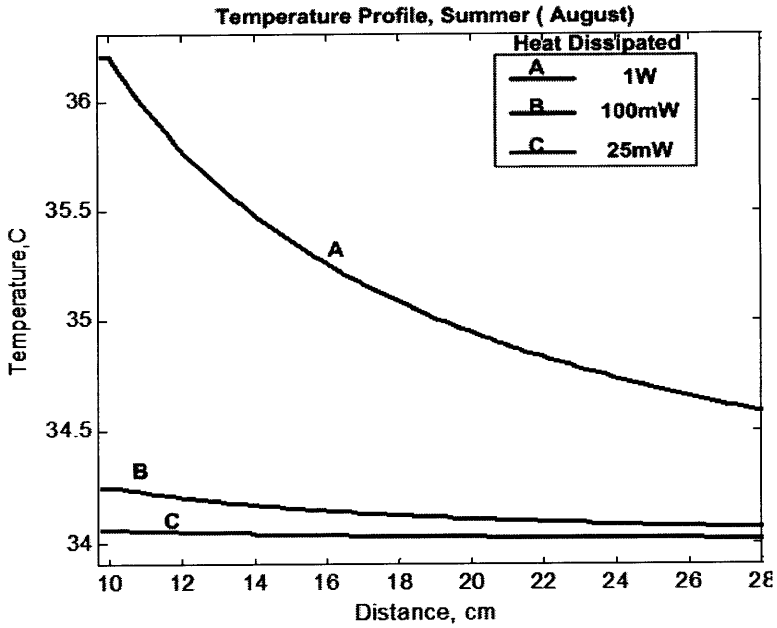

Figure 41. Temperature profile radially outward into the surrounding during summer.

4.2.2.2. Rectangular (Shoe box) Configuration

A rectangular configuration is also considered for the fuel cell power system and is shown in Figures 42 and 43. This configuration reduces the complexity of manufacturing the sensor system and simplifies transportation and/or deployment on the ground. Heat transfer analysis is performed for this configuration to determine if the soil temperature affects the fuel cell power system operations.

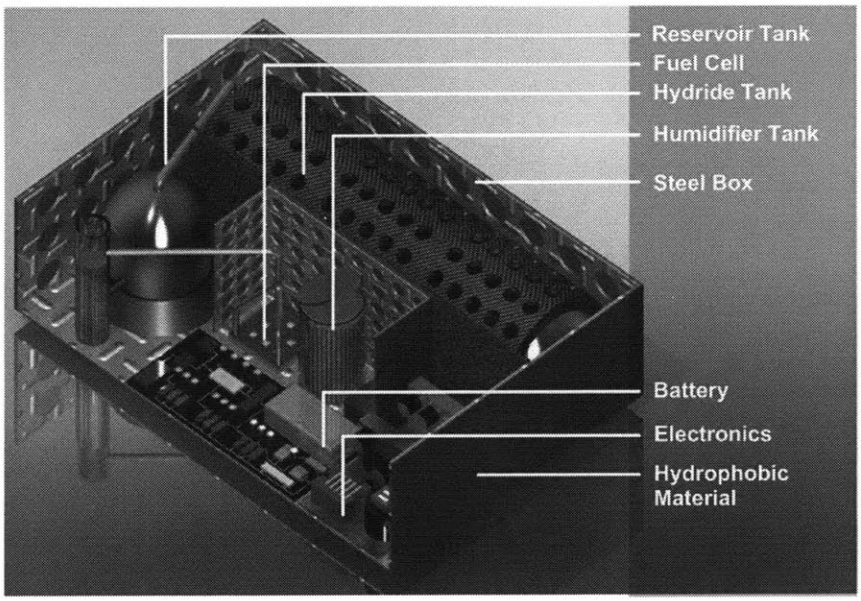

Figure 42. Three-dimensional representation of fuel cell-powered sensor system in a rectangular configuration.

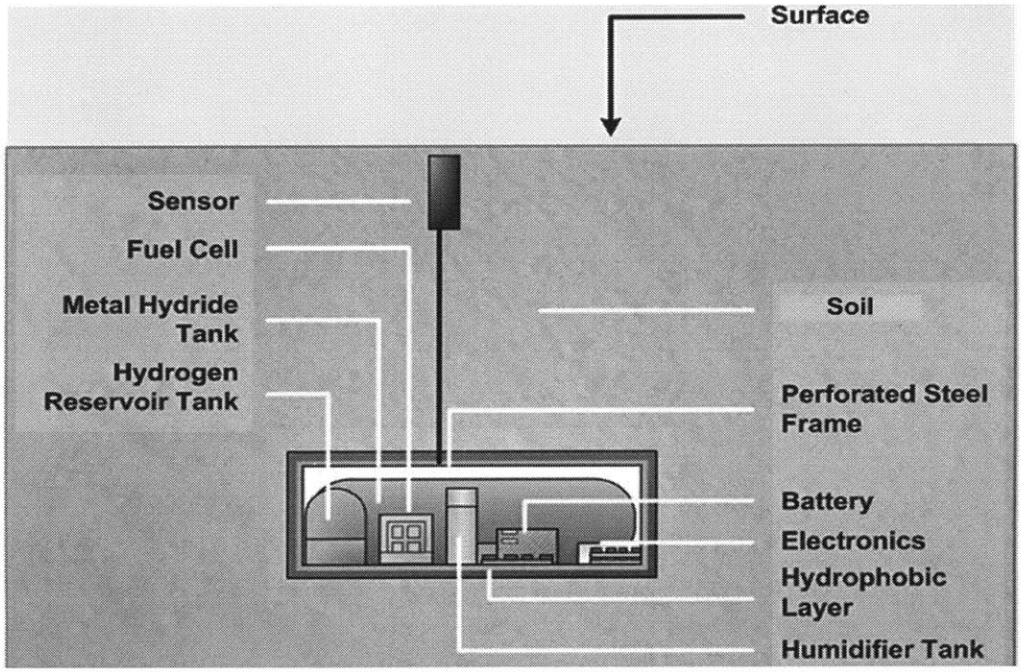

Figure 43. Representation of the fuel cell powered sensor system buried underground.

A steady-state three-dimensional heat transfer analysis is performed using an approach similar to the spherical configuration. For the rectangular configuration, the following assumptions are made, 1) the

temperature inside is uniform, 2) the surrounding soil temperature is assumed to be uniform, 3) the heat generated in the system is small, on the order of 25mW. It is further assumed that the heat conduction in the system is the same in every direction. Figure 44 represents the heat transfer model of the system buried underground. The steady-state heat conduction equation for a three dimensional rectangular object is given by [13],

$$\frac{\partial^2 T}{\partial x^2} + \frac{\partial^2 T}{\partial y^2} + \frac{\partial^2 T}{\partial z^2} + \frac{\dot{g}}{k} = 0 \tag{77}$$

where $\dot{g}$ represents heat generation inside the system, T is the temperature and k is the thermal conductivity of the system. Because the system is buried, a shape factor (S) is defined for a rectangular system in the semi-infinite medium given by [38, 35],

$$S = 1.685L\left[Log[1+\frac{b}{a}]\right]^{-0.59} * \left[\frac{b}{c}\right]^{-0.078} \tag{78}$$

where a is the length, L is the width and c is the height of the system. b is the buried depth. Using the shape factor, the heat dissipated from the system into the surrounding is given by,

$$\dot{Q}_{sand} = Sks(T_2 - T_\infty) \tag{79}$$

where $\dot{Q}_{sand}$ is the heat transfer between the system and the surrounding, ks is the sand thermal conductivity, T_2 is the surface temperature of the system and T_∞ is the temperature of the surrounding soil.

To simplify the analysis, the heat conducted through each wall is calculated individually and superimposed to determine the total heat conducted through the system. Eq.80-82 give the heat conducted though each wall and the total heat from the system is given by Eq.83.

$$Q_{1x} = \frac{kLc}{t}(T_1 - T_2) \tag{80}$$

$$Q_{1y} = \frac{kaL}{t}(T_1 - T_2) \tag{81}$$

$$Q_{1z} = \frac{kac}{t}(T_1 - T_2) \tag{82}$$

$$Q_{system} = 2Q_{1x} + 2Q_{1x} + 2Q_{1x} \tag{83}$$

where T_1 is the temperature inside the system, T_2 is surface temperature of the system, t is the thickness of the insulating wall and A is the surface area of each wall.

At steady-state, heat conduction through the system walls is equal to the heat conduction from the system to the surroundings, given by Eq.84. Using an initial value of T_1, the heat generated is determined by iteratively solving for T_1, This process determines the internal temperature of the system (T_1) for the amount of heat generated by the system.

$$\dot{Q}_{system} = \dot{Q}_{sand} \tag{84}$$

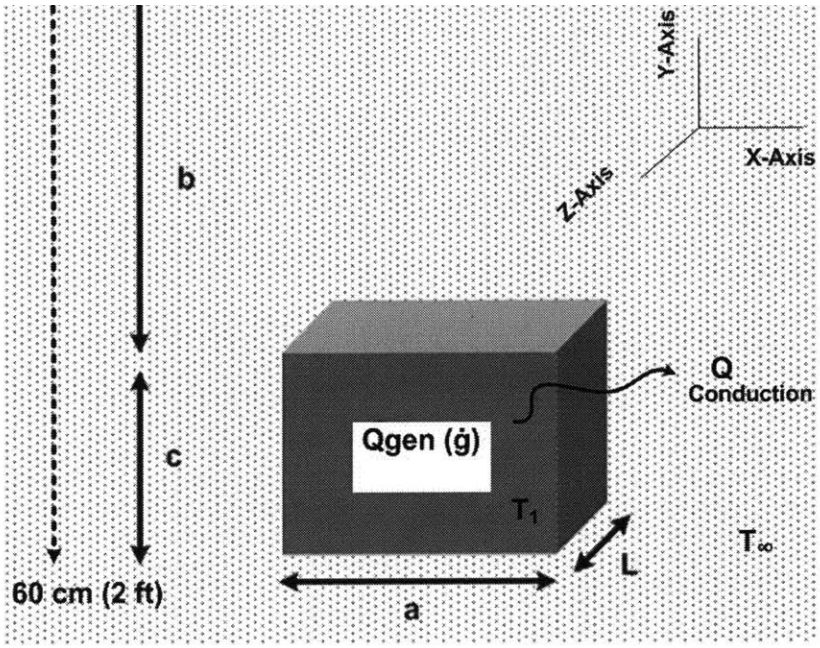

Figure 44. Representation of the heat transfer model for the rectangular configuration.

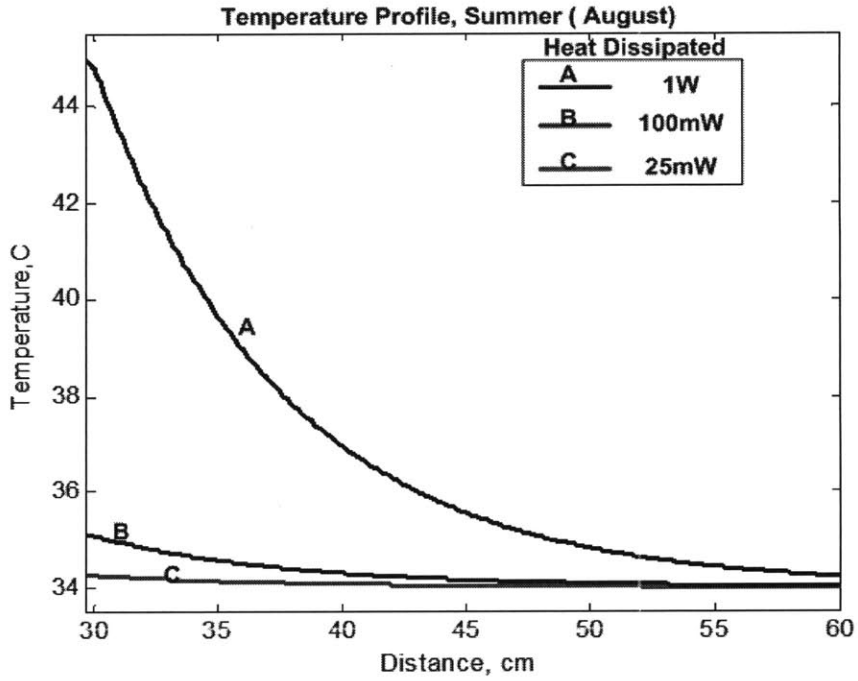

Figure 45. Temperature profile radially outward into the surrounding soil during summer.

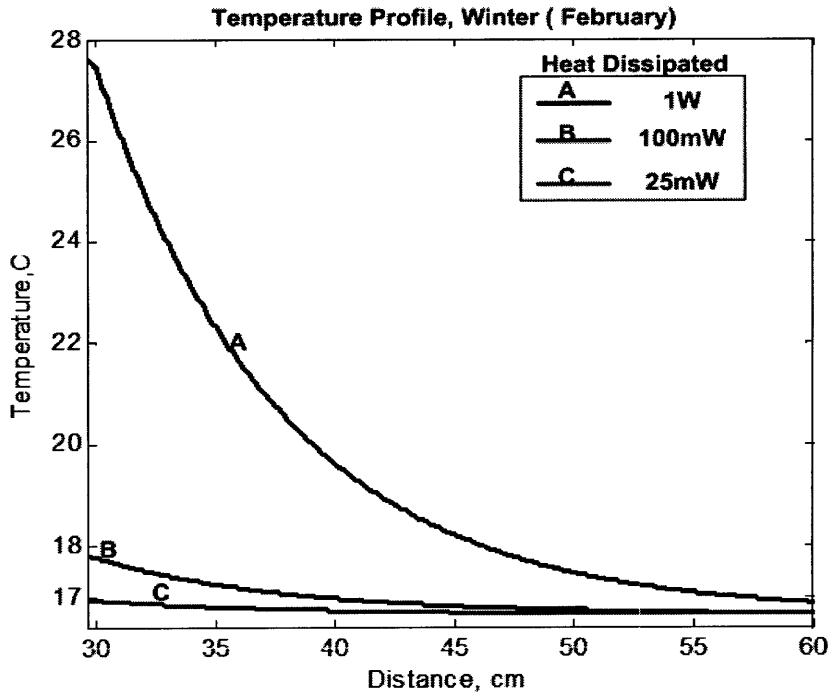

Figure 46. Temperature profile radially outward into the surrounding soil during winter.

The temperature inside the buried field sensor system is determined for 25mW, 100mW and 1W of heat generated. Figures 45 and 46 plot the temperature profile from the interior wall surface into the surrounding soil for summer and winter conditions respectively. The figures show that the temperature inside the system ranges between 17°C and 45°C and is suitable for the operation of the fuel cells and power electronics. A small, simple steel encapsulation for the fuel cell-powered sensor is sufficient in maintaining the desired temperature inside. The slight temperature variations between the spherical and the rectangular configurations are observed. This difference can be accounted by the one dimensional heat transfer approximation made for the spherical configuration. Also, for the rectangular configuration, detailed analysis for the corners of the system is omitted. It is expected that, this approximation predicts slightly higher temperatures inside the system. However, the internal temperature of the system lies within the required range. The results of the heat transfer analysis for both configurations show that a passive thermal management system is feasible for fuel cell power system. However, operating in the field poses additional challenges, such as air and water management, that are discussed in Chapter 5.

4.3. Experimental Validation of the Thermal Model

Experimental validation of the spherical thermal architecture for space applications is presented in this section. It includes details on the fabrication of the experimental setup and testing of the system in a cold chamber.

4.3.1 Experimental Setup

The experimental system consists of a power generation unit within a small acrylic sphere, placed within a larger acrylic sphere. The large and small spheres are linked attaching two small and two large hemispheres to a

ring made of acrylic, such that the power generation unit and small sphere are centered within the large sphere (Figure 48). The ring is machined on an EZ-Trak CNC mill. Two gaskets made of PTFE material are sandwiched between the hemispheres and the ring to form a seal. The heat generation unit consists of two batteries, a resistor and wires connecting them. A temperature data logger with a sampling frequency of 0.05Hz is used to record the internal temperature of the inner sphere as shown in Figure 47. The completed assembly of the experiment is show in Figure 48.

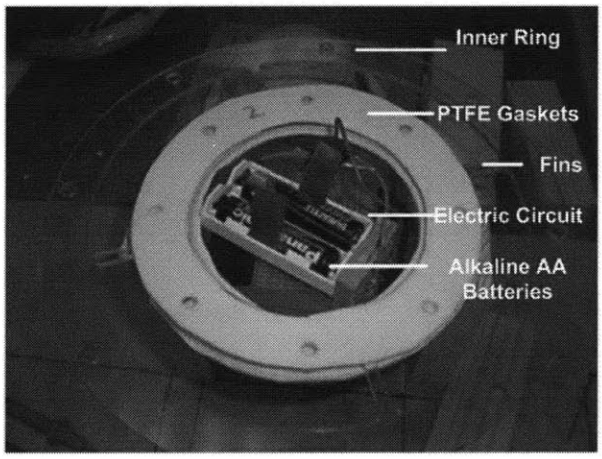

Figure 47. Electrical circuit embedded inside the inner sphere.

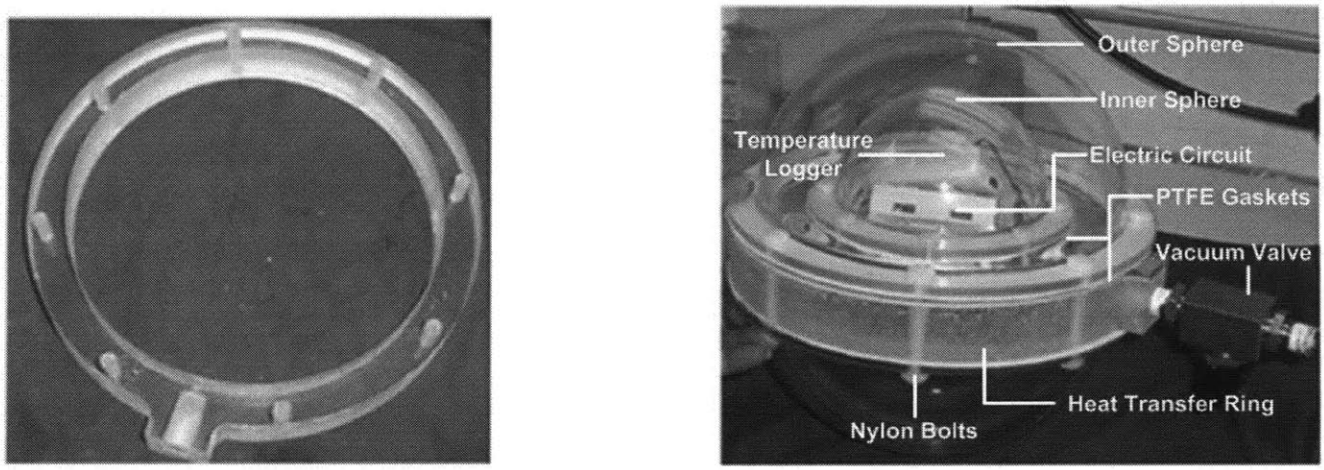

Figure 48. (Left) External ring holding the outer domes (Right) Completed Assembly.

A simple electric circuit is used to generate 0.5W of heat. Basic calculations are performed to determine the electrical load needed to emit 0.5W. Electrical resistors in series powered by two Alkaline AA batteries, in series, are used to generate the required heat. The total resistance required is calculated using the following equation,

$$P = \frac{V^2}{R} \tag{85}$$

where V is the voltage from the batteries and R is the resistance of the system. Each AA battery initially outputs 1.5V, leading to a total voltage of 3V. The voltage output for the battery over time is shown in Figure 49 [43], however for the experiment the heat generation is assumed to remain constant with a battery voltage of 3V.

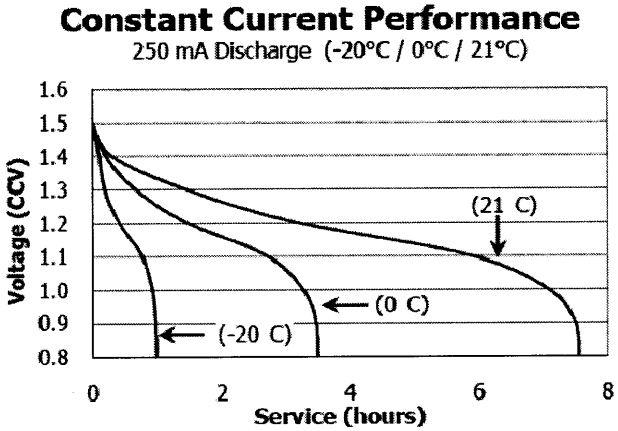

Figure 49. AA Alkaline Battery Performance [19].

Several experiments are conducted, with slight modifications to improve the thermal resistance of the system. The following table outlines the changes made for the various tests.

Table 8. Sequence of experimental tests.

Test 1	No gold coating, PTFE gaskets
Test 2	Gold Coated spheres, Sealant Tape, nylon bolts
Test 3	Gold Coated Spheres, Sealant Tape, metal bolts

Tests are conducted in the freezer located in FSRL. The freezer temperature is adjustable and can go as low as -30°C. The temperature of the freezer is set to an average temperature of -15°C for the initial tests without the gold coating on the inner sphere, and an average temperature of -24°C for the experiments with gold coating. The freezer thermal control circuitry caused the temperature to vary as a sine wave between -17°C and -30°C.

4.3.2 Testing Procedure

1. The heat generating circuit is assembled and the data logging device is initialized. Both are then embedded into the inner sphere. Nylon bolts are used to seal the inner domes carefully with the inner ring that includes the PTFE gaskets for Test 1 and sealant tape for Tests 2 and 3. Tests 2 and 3 used rubber washers to provide more sealing.
2. System assembly is carefully completed, using nylon bolts to seal the outer domes, PTFE gaskets (Test1) and outer ring. Sealant tape in place of PTFE gaskets, and metal bolts/washers in place of the nylon bolts are used for Tests 2 and 3 for additional sealing.
3. Once the system assembly is complete, the valve is installed into the heat transfer ring and the other side is attached to a vacuum pump. The vacuum pump is run for approximately 15 minutes.
4. The valve is closed and the system is disconnected from the vacuum pump.
5. The system is then placed inside the freezer.

6. After 12 hours the system is removed from the freezer, disassembled, and the temperature captured by the data logger is transferred to a computer.

The procedure is identical for each test except for mounting the specified gasket. In the test case using sealant tape, the inner rim of the dome flanges and the rings are covered with the sealant tape and the parts are compressed together with bolts and nuts. The sealant tape acts as an adhesive and sticks strongly to itself.

4.3.2. Experimental Results

4.3.2.1. Test 1

The first experiment is conducted without gold coating to the inner sphere. The emissivity of the acrylic domes is 0.94, leading to substantial heat loss due to radiation. Figure 50 shows both the experimental results and the theoretical estimates. The experimental system reached a steady-state of -10 °C (263K) after 4 hours. The theoretical model given by Eq.71 matches the experimental steady-state values to within 1°C. The drop time in temperature predicted by the theoretical model is 1.2 hours (~ 83 minutes), which is faster than the time it took the experimental system to reach steady state. This indicates that there is additional thermal resistance within the inner sphere (between the point of heat generation and the data logger) that is not accounted for in the theoretical analysis. The sinusoidal oscillations observed in the experiments are due to the refrigerator thermal control system maintaining a fixed average temperature. The average value of the ambient (refrigerator) temperature is also presented in the figure.

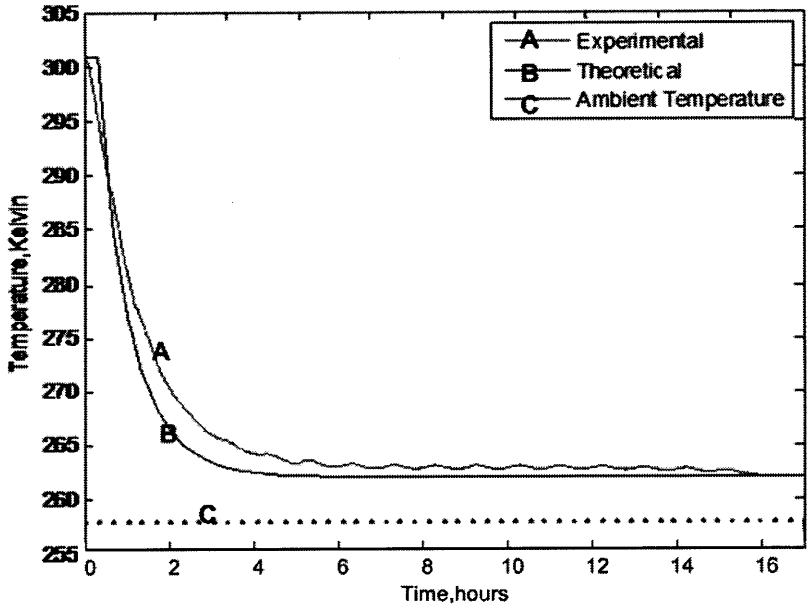

Figure 50. Test 1 experimental results: 0.5 W heat production and ambient temperature -15 °C.

Although the internal temperature of the inner sphere is warmer than the freezer, the temperature difference is not significant and is still below freezing. This indicates there might be air leakage through the gasket. The inner sphere is not coated with the low emissivity material and that might have increased the radiative heat transfer significantly.

4.3.2.2. Test 2

For subsequent tests, the inner sphere is coated with gold to minimize radiation (polished gold $\epsilon=0.02$). One major disadvantage in using a gold coating is that gold does not adhere to acrylic. To overcome this, the domes are first coated with metal polish to hold the gold finish. However, this did not help, and the gold coating would flake off if the domes came into contact with any material. This is problematic, because the gold-coated sphere needs to be handled during assembly. Assembling the experiment contaminated the gold coating and marred the smooth finish. This drastically changes the emissivity, so the results from the experiment are not satisfactory, nor are they different from the earlier tests. To account for the change in emissivity of the contaminated gold coating, the value of ϵ for modeling purposes is taken to be 0.48 (the average emissivity). This is the average of the emissivities of acrylic and gold. The PTFE gaskets are replaced by sealant tape, made by Airtech International. Initial tests on the tape are performed to observe how well it adheres to acrylic and to determine its behavior in low temperature environments. Figure 51 shows the results from the experiment.

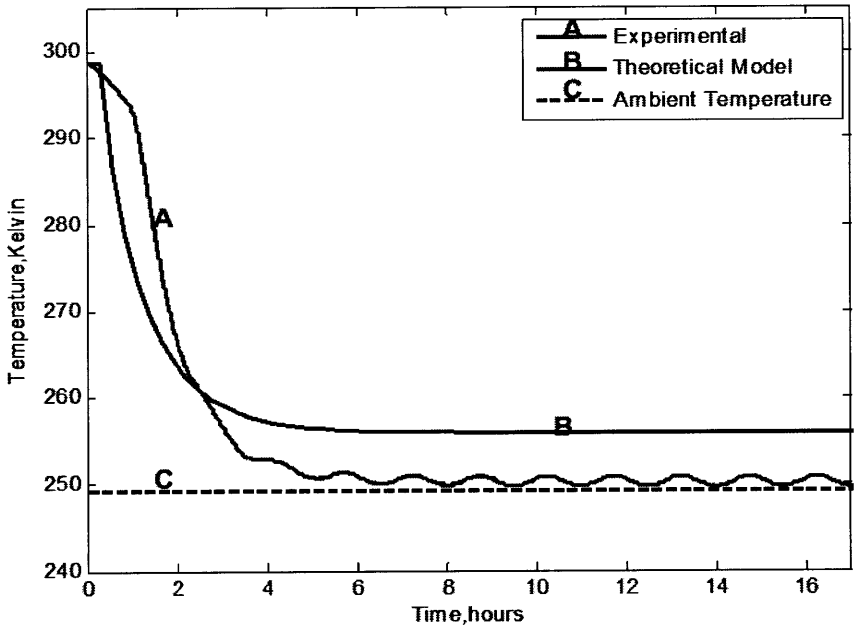

Figure 51. Test 2 experimental results: 0.5 W heat production and ambient temperature -24°C.

Although sealant tape and a vacuum pump are used, vacuum sealing is not sufficient and the system is not capable of holding a vacuum for more than 15 minutes. Hence the results shown in Figure 52, indicate that the average temperature of the inner sphere at steady state is 252 K (-21°C) while the average freezer temperature is -24 °C and steady state is reached in 5 hours. The air leak causes convective heat transfer to dominate and a majority of heat is lost. It is thought that air must have leaked through the bolt holes and that the bolts may not have provided enough compressive force to hold the domes together and to seal the gaps. Another reason could be that the batteries wore out and heat wasn't being generated.

4.3.2.3. Test 3

To overcome the sealing issue, the nylon bolts are replaced with metal bolts and rubber washers in test 3, to achieve better sealing around the holes. This time, the sealant tape is also placed around the holes rather than

only along the inner rim of the flanges as done in test 3. However, the results from this test still show no significant improvement (Figure 52). The average temperature rose by 1°C. The significant difference between the theoretical and experimental model is thought to be caused by the leakage of the vacuum and also the contamination of the gold coating.

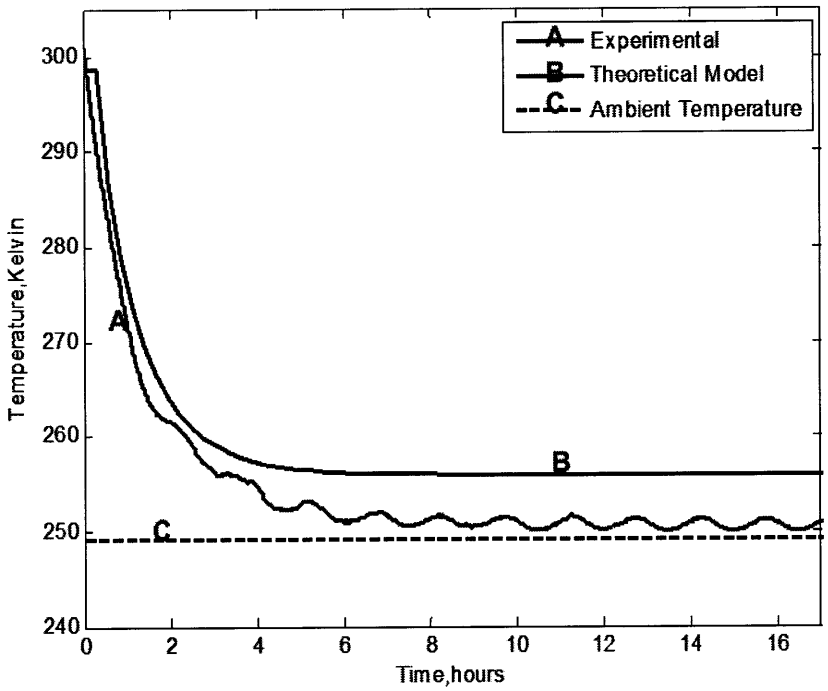

Figure 52. Test 3 experimental results: 0.5W heat production and ambient temperature -24°C.

According to the theoretical models, a passive thermal design of the system is sufficient to maintain a desired temperature range inside the inner sphere. However, the desired temperature range is not maintained experimentally. It is thought that this is due to the inability to seal the system sufficiently to achieve a vacuum. The following recommendations for design and modeling improvement are suggested. Due to time constraints these changes could not be integrated for the experimental analysis.

1. The assumption that the batteries inside the inner sphere provide constant power at temperatures below freezing may not be valid. The behavior of electrochemical energy sources may vary with temperature. Batteries tend to degrade in low operating temperatures and produce significantly lower power, so it is possible that the batteries did not produce 0.5W for the entire duration. Hence with the decrease in power generation the system was not able to maintain desired temperatures. Therefore an alternative source of heat or change to the circuit and power source needs to be considered.
2. An improved gasket system, such as a low temperature O ring, would help achieve the necessary vacuum sealing. A gasket design that incorporates large O-rings both inside and outside of the fastening bolts would be sufficient. The circular cross section of an O-ring would allow more gasket deformation that would likely provide a better seal than the PTFE gaskets and the sealing tape.

3. Acrylic has a low thermal conductivity, so it provides high thermal resistance and helps retain heat inside the system. However, acrylic is brittle, which makes it difficult to machine. It is also prone to cracking at stress concentrations, such as bolt holes, so fastening the spheres and rings must be done carefully. Materials such as Delrin (thermal conductivity 0.31W/m-K) or Polycarbonate (0.2W/m-K) have significantly larger values for fracture toughness and are good alternatives.
4. The assembly procedure needs to be modified to prevent marring the gold coating. Use of standard clean room procedures in handling the gold coated spheres and avoiding any contact of the spheres with external surfaces is expected to mitigate the issue of damaging the gold coating.

Thermal architecture summary

The passive thermal architectures proposed in this chapter based on minimizing heat loss are expected to be a feasible option for fuel cell powered sensor networks for space and terrestrial applications. A spherical configuration implemented with a combination of insulating materials and minimally radiating surface is proposed, analyzed and tested. With ideal materials the concept proves to be feasible analytically. There remain several challenges in testing the concept in the laboratory, particularly coming up with an effective vacuum seal. Nevertheless, the concept can be executed using better vacuum sealing techniques as explained in Section 4.5. For sensor networks operating in the desert regions, the analysis proves that the thermal environment is benign for the fuel cell operation. A desired temperature range between 10°C and 50°C can be maintained throughout the year by using a simple enclosure made of steel.

CHAPTER 5

AIR AND WATER MANAGEMENT FOR A TERRESTRIAL APPLICATION

PEM fuel cells use hydrogen and oxygen and produce electricity, water, and heat. For achieving long-life missions, along with effective thermal, air and water management are also major challenges that need to be addressed. The objective of this chapter is to study the air and water management challenges that the fuel cell powered field sensor system is expected to encounter for the reference mission in the desert regions of Negev.

This chapter presents the environmental characteristics of the desert reference mission. For the reference mission, it is assumed that the sensor system will be buried underground. One option is to carry pure oxygen on board for fuel cell operation, but this poses safety issues. An alternative approach is to use the air present in soil and is the focus of this chapter.

One of the major challenges for the operation of the fuel cell in field is the availability of sufficient air. The amount of oxygen present in the soil is generally less than the amount of oxygen present in the atmosphere. In addition, the percentage level of carbon dioxide is higher than that of the atmosphere. A feasibility analysis is performed for a reference mission in the Negev desert in Israel to learn if sufficient air flow exists underground for operating the fuel cell powered sensors for 3 years.

The water formed by the fuel cell over the life of the fuel cell must be managed efficiently. For 3 years, sufficient water must be provided for air and hydrogen humidification to facilitate efficient performance of the fuel cell. Hence a thorough water management system is required. The chapter proposes passive designs for air and water management for a reference mission in Negev, and analyses the designs to prove the feasibility of using fuel cells for long durations.

5.1. Soils of the Desert Regions

The study of air and water management requires knowledge regarding the local soils where the field sensors will be deployed. Therefore, a basic study of the soils for the reference mission in Negev is conducted. The Negev desert occupies about 60% of the surface of Israel [37, 49]. Desert soils are generally composed of sand or loess depositions like those in the Negev desert. Feasibility analysis is conducted for both sand and loess soil types.

The soil particle size distribution of the loess soil type is that of silt (2-50 μm) [49]. The porosity of the soil, that is the ratio of the volume of open spaces/pores present in the soil to the total volume of the soil, is 35 - 50% for both loess soil and sand [37, 49, 57]. The particle size and porosity levels of sand based deserts

are usually between 0.05 -2mm and 30-50% respectively [49]. The porosity parameter is useful in calculating the amount of air present in the soil because the pores in the soil allow air and water to percolate through the soil. The permeability rate of soil is the ability of air/water to flow through the soil and is an important factor in calculating the amount of air present in the soil. Typical air permeability values measured in soil cores are given in Table 9 [48].

Typical percentages of oxygen and carbon dioxide in the atmosphere are 21% and 0.038% respectively. The percentage of oxygen in soil is less than that in the atmosphere depending on the vegetation growth in the soil. The percentage of oxygen in soil may vary from 15-20%.

Table 9. Air permeability values of soil [48].

Clay % in Soil	Soil Air Permeability, k_a (μm^2)
2.5	14.3
3.7-4.3	36
5.9	22.8
16	1225
21-24	525

5.1.1 Rainfall and Humidity in the Negev Desert

The amount of rainfall in a region also plays an important role in determining how much air is contained in the soil. The amount of water accumulating in the soil changes depending upon the rate of rainfall in any location. The rainfall and humidity data are collected for Nizzana. In sandy desert regions of Nizzana dominated by sand dunes, the water movement is assumed to be predominantly vertical [49, 55]. The average annual rainfall in Nizzana is 95mm [59]. The rainy season usually starts in November and ends in May. Rainstorms tend to concentrate in January-March. From the studies conducted on the rain water percolation rates in Nizzana, it is observed that the maximum depth of water penetration at the end of the rainy period in the soil is in the range of 30-60cm [49, 55]. Figure 53 gives one example of the temporal variations in water movement from the data acquired in the sandy dunes of Nizzana [59]. The average soil moisture values (by volume) at the reference location of Nizzana in the Negev desert are between 5-10% [52, 59].

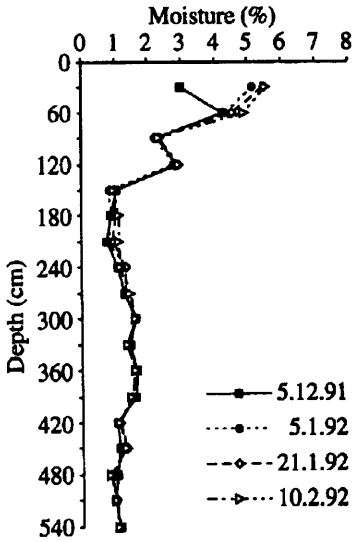

Figure 53. Temporal variation in water movement [59].

5.2. Air Breathing System

5.2.1. System Description

The desert reference mission presented in Chapter 1 requires that the sensor systems are capable of operating for 3 years. The fuel cell power system should provide power to sensors and the electronics. The power requirements mentioned in earlier chapters are 10mW average power and 100mW peak power. The fuel cells are expected to operate at 0.8V, supplying 10mW to charge batteries. Sensors are periodically turned on and powered using the onboard battery using 100mW of peak power. Using Eq.86 and 87 the mass flow rates of air and oxygen required for average power is determined, where I is the current.

$$\dot{m}_{Air\_FC} = \frac{sO_2}{rO_2} * \frac{I*M_{Air}}{4F} \tag{86}$$

$$\dot{m}_{O_2} = \frac{I*M_{O_2}}{4F} \tag{87}$$

where sO_2 is the stochiometric ratio of oxygen, which is1 for this case, rO_2 is the molar ratio of oxygen to air which is 0.20, F is the Faraday constant, and M_{Air} and M_{O2} are the molar masses of air and oxygen.

$$m_{Air/O2} = \dot{m} * time \tag{88}$$

The total amount of air and oxygen required for 3 years is calculated using Eq.88. The mass of reactants required for 3 years operation of the fuel cell is given in Table 10. In addition the amount of air/oxygen required for 100mW average power is calculated. The parameters used for the air flow calculations are in Table 11.

Table 10. Mass of reactants required for 3 years operation of fuel cell.

Power	Mass Flow Rate of Air (g/s)	Mass of Air for 3 Years (g)	Mass of O_2 for 3 Years(g)	Mass of H_2 for 3 Years (g)
10 mW	$4.7e^{-6}$	442	98	15.8
100mW	$4.7e^{-5}$	4420	980.5	158

Table 11. Values of parameters used.

Parameter Used	Value
Molar Mass of Air	28.848 g/mol
Molar Mass of Oxygen	31.998 g/mol
Molar Mass of Hydrogen	2.0158 g/mol
Faraday's Constant	96487 Coulomb/mol
rO_2	0.2
Estimated Fuel Cell Efficiency	65%

The amount of air in the system for the rectangular configuration described in Chapter 4 is calculated. The calculations consider the volume required by other components in the system as well. It is assumed that about 20% of the system volume is occupied by electronic components. The fuel storage of hydrogen is calculated separately for 10mW and the volume of the metal hydride storage is added to the volume of electrical components. The remainder of the volume is occupied by air.

The dimensions of the system and the amount of air present in the system are given in Tables 12 and 13. Without any extra supply of air, the total air present in a completely sealed system would be sufficient to provide 10mW power for 17 days. Hence, for 3 years life, air needs to be supplied to the system. Certain modifications to the system design are needed to allow for air flow into the system from the surrounding soil.

Table 12. Dimensions of rectangular configuration system.

Parameter	Value
Complete System	0.50m x0.10m x0.15m (L, W, H)
Electronic Components Volume	20% of the total box volume
Metal Hydride Storage Efficiency	28g/L

Table 13. Mass of air in the system.

Power	Volume of H_2 Storage (m^3)	Volume of Air in the system (m^3)	Mass of Air in the system (g)	Time to Consume Air (days)
10mW	$5.6e^{-4}$	$5.4e^{-3}$	6.9	17.2

For 3 years life, it is proposed that the system must be perforated and covered with hydrophobic materials on all sides (expect for the bottom to have structural stability and hold the components steady within the system), to ensure continuous flow of air into the power system. Hydrophobic materials such as GORE-TEX® allow the passage of air through them but do not allow soil impurities or liquid water to pass

through them. Figure 54 shows the hydrophobic material on the outer surfaces of the system and the perforations of the steel structure.

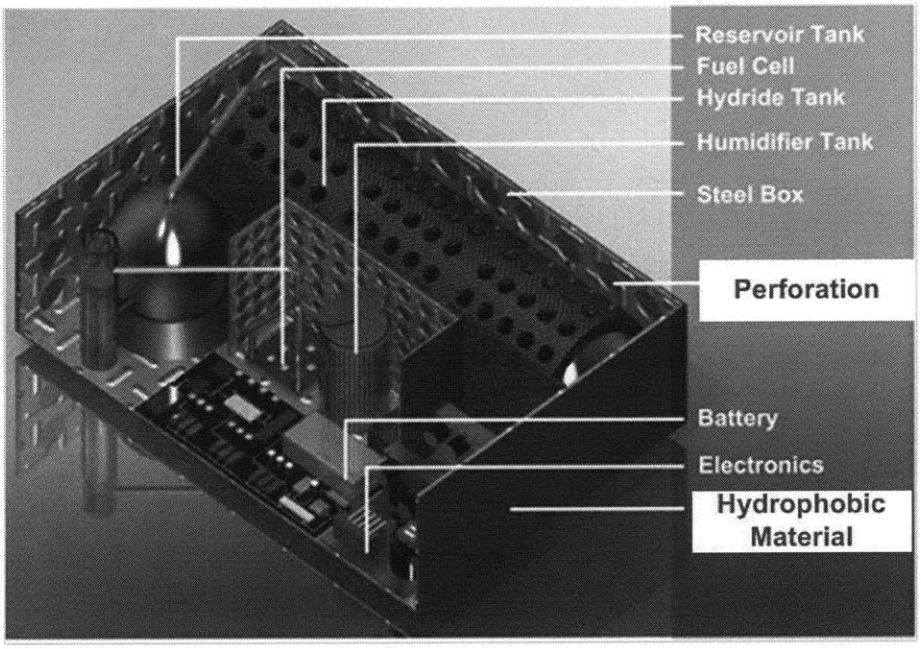

Figure 54. Air breathing system with hydrophobic material on the surface.

5.2.1.1. Hydrophobic Materials

A hydrophobic material is used in the proposed system to ensure enough air flows into the power system, and also to prevent soil particles or any water flowing from the soil into the system. This will prevent damage to the system electronics. Soil impurities lead to degradation of electronics during long operational life.

The hydrophobic material should be selected with a pore size small enough to prevent fine soil from entering. Some hydrophobic materials commercially available that would fulfill these requirements are GORE-TEX® and HST roll [17, 28]. The GORE-TEX® membrane used in fabrics contains over 9 billion microscopic pores per square inch. The pores are 20,000 times smaller than a water droplet, making the membrane waterproof from the outside, as shown in the Figure 55 [17]. The membrane is sandwiched between high performance fabrics to serve various applications and make it breathable.

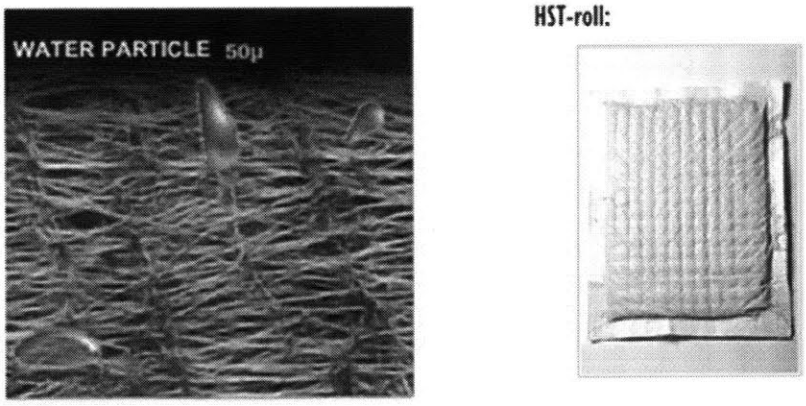

Figure 55. (Left) GORE-TEX® material [28], (Right). HST Roll [17].

Another such material that prevents water flow but has high air permeability is the HST roll [17]. The HST roll has a thickness of 20 mm that allows for air diffusion (see Figure 55 (right)). It has a certified pressure load of 104 N/mm^2 and weighs 36 kg/m^2 [17].

5.2.2. System Analysis

Analysis is performed to verify if the rate of air flow through the system is equal or higher than the mass flow rate of air required for the fuel cell to produce 10mW power. This will ensure that the fuel cells receive the required oxygen from the surrounding soil. The feasibility analysis is based on the air permeability of the soil. Figure 56 shows the model used to calculate the flow rates. The air permeability of soil is given by Eq.89, where k_a is the air permeability of soil (m^2), q is the volume flux per unit area (m/s), η_a is the dynamic viscosity of air in (Pa-s), x is the distance in the direction of flow (m), and p is the pressure of air (Pa)[37].

$$k_a = q\eta_a \frac{dx}{dp} \tag{89}$$

The soil's air permeability rates are known, as given in Table 10 and rearranging the equation above will provide the flow rate of air into the system from each surface of the module (Eq.91), where ρ is the density of air.

$$q = k_a \frac{dp}{\eta_a dx} \tag{90}$$

$$\dot{m}_{air_{system}} = q * a * \rho \tag{91}$$

The pressure at a certain depth can be calculated using Eq.92, as derived from the Bernoulli's equation where Δp is the difference in pressure, z_1 and z_2 are elevation of the two points, g is the acceleration due to gravity (9.8 m/s^2) and v_1 and v_2 are the fluid velocities at two points [37]. In this case, the fluid is air, point 1 is the soil and point 2 is in the atmosphere directly above soil. With zero wind speed, v_2 is 0, the pressure difference from soil to atmosphere is due to difference in elevation that is about 0.61 m (2 ft) multiplied by the density of air and gravitational constant [37].

$$\Delta p = \frac{\rho v_2^2}{2} + (z_2 - z_1)\rho g \tag{92}$$

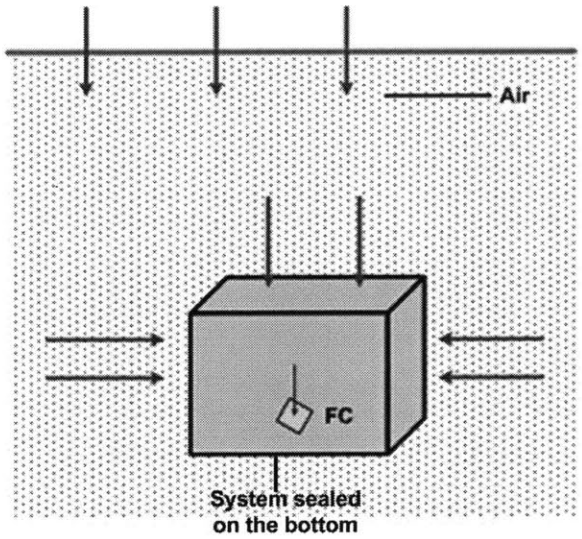

Figure 56. Model for air breathing analysis of the system buried underground.

Table 14 shows the mass flow rate of air into the system compared to the mass flow rate of air required for the fuel cell (Eq. 91).

$$\dot{m_{Air\_FC}} = \frac{sO_2}{rO_2} * \frac{I*M_{Air}}{4F} \tag{93}$$

As the air in the system is used up by the fuel cell, the concentration of oxygen in the system starts decreasing. This difference in concentration drives the oxygen (air) from the surrounding to diffuse into the system. The ratio of the flow rates of air entering the system is much higher than the rate of oxygen consumption by the fuel cell. This shows that the proposed air management strategy is feasible for providing sufficient air for long-term operation of the fuel cell power system. The analysis demonstrates that it is feasible to implement an air breathing system to supply oxygen for a buried fuel cell powered field sensor system.

Table 14. Air breathing analysis results.

Power	Air permeability, ka, (μm2)	Mass flow rate of air into the box (g/s)	Mass flow rate at the fuel cell	Ratio of flow rates
10mW	1225	$1.232e^{-3}$	$4.7e^{-6}$	243
100mW	1225	$1.232e^{-3}$	$4.7e^{-5}$	24

5.3. Carbon Dioxide Accumulation

5.3.1. Carbon Dioxide/Carbon monoxide poisoning of PEM Fuel cells

Carbon dioxide combines with hydrogen and forms carbon monoxide and water. Carbon dioxide and carbon monoxide are a potential hazard to PEM fuel cell operation. The presence of carbon monoxide in the air and hydrogen fuel inlet stream causes the adsorption of carbon monoxide onto the platinum catalyst. This blocks the active sites on the catalyst, hampering the absorption of hydrogen and oxygen on the electrodes.

Some methods to mitigate the effect of carbon monoxide poisoning are i) Using a platinum alloy catalyst such as platinum-rheuthinium, which has improved carbon monoxide tolerance, or ii) increasing the cell operating temperature to 80°C [9]. Increasing the cell operating temperature to a higher value results in membrane dehydration and results in other degradation issues in the PEM fuel cell. This degradation reduces the fuel cell life time [19]. Another option is to use pure oxygen. Using pure oxygen poses safety problems and requires additional components that increases the system mass. Another simple way to prevent carbon dioxide contamination is to use soda lime to absorb carbon dioxide from the air entering the fuel cell. At carbon dioxide concentrations in excess of 25% the voltage losses are high, and the production of carbon monoxide from carbon dioxide is not negligible [9, 16]. To develop methods to prevent carbon dioxide contamination, first the percentage of carbon dioxide entering and accumulating in the system must be determined.

5.3.2. Soil Carbon Dioxide Content

Methods to mitigate carbon dioxide accumulation should be considered for efficient functioning of the fuel cell power system for long life operations. The air entering the fuel cells carries about 21% oxygen by mass, and the remainder is composed of nitrogen, carbon dioxide and other gases. These gases, besides oxygen, are unused by the fuel cell which accumulate over a period of time. Although the percentage of carbon dioxide in atmospheric air is only 0.038%, carbon dioxide levels underground are often 10 times greater that the atmospheric concentration. An ecological process called soil respiration releases carbon from the soil in the form of carbon dioxide by underground roots of plants and vegetation [61]. Hence the amount of carbon dioxide in the soil depends on the vegetation content of the location. An analysis is performed to determine if the amount of carbon dioxide accumulation beneath the soil surface would be a threat to the power system's operation, and if methods to overcome the problem could be implemented.

5.3.3. Carbon dioxide content case study for a terrain application

An analysis is performed to obtain the percentage of carbon dioxide in the system over a period of 3 years. Figure 57 shows the model used for the analysis in determining the percentage of carbon dioxide accumulation. The mass flow rate of carbon dioxide into the system due to soil respiration ($\dot{m}_{CO2_{soil_{resp}}}$) is given by Eq.94 where x is the soil respiration rate and A is the surface are of the entire system.

$$\dot{m}_{CO2_{soil_{resp}}} = x * A \tag{94}$$

Eq.95 gives the mass of carbon dioxide ($m_{CO2soil\ resp}$) accumulated in the system in a given time t.

$$m_{CO2soil\ resp} = \dot{m}_{CO2_{soil_{resp}}} * time \tag{95}$$

If the mass flow rate of the air flowing into the system is greater than the mass flow rate of carbon dioxide into the system, then it is assumed that no carbon dioxide accumulates because of soil respiration (Eq. 94).

$$\dot{m}_{air\_system} > \dot{m}_{CO2_{soil_{resp}}} \tag{96}$$

Carbon dioxide is unused by the fuel cell and exits through the cathode and over a period of time. This is calculated using Eq. 97, where C_{CO2} is the concentration of carbon dioxide in the air and m_{air} is the mass of air in the system.

$$m_{CO2_{air}system} = m_{air} * C_{CO2\,air} \tag{97}$$

The total mass of carbon dioxide in the system is given by the sum of carbon dioxide accumulated in the system due to soil respiration and the unused carbon dioxide in the air by the fuel cell, given by,

$$m_{CO2\,total=} \; m_{CO2_{air}system} + m_{CO2soil\,resp} \tag{98}$$

$$\%\, C_{CO2} = \frac{m_{CO2total}}{m_{air_{remaining}}} * 100 \tag{99}$$

$$C_{CO2} = C_{CO2\,soil\,resp} + C_{CO2air\_system} \tag{100}$$

The criterion for feasibility is to verify that the percentage of carbon dioxide accumulation is below the threshold value of 25%. The mass flow rate of the air into the system should be greater than the mass flow rate of carbon dioxide entering the system to ensure no carbon dioxide accumulation occurs. This ensures at steady-state that carbon dioxide does not accumulate in the system. The total concentration of carbon dioxide accumulated (C_{CO2}) in the system given by Eq.100, that is the sum of carbon dioxide entering the system because of soil respiration ($C_{CO2\,soil\,resp}$) and the carbon dioxide present in the air exiting from the fuel cell cathode (C_{CO2air_system}).

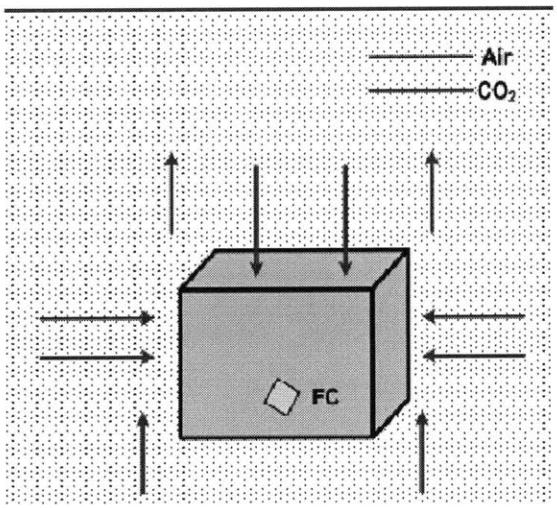

Figure 57. Model for Carbon dioxide accumulation in the system buried underground.

Soil respiration rates of the Negev desert are found to be 60-70 μmol carbon dioxide m^{-2} min^{-1} [61]. Two worst case scenarios are analyzed, where it is assumed that the soil above the system is sealed due to continuous rainfall for 4 and 2 days. Carbon dioxide is assumed to accumulate through the surface areas of the system. The percentage values of carbon dioxide are compared against the 25% threshold values from literature. As seen from Figure 58, carbon dioxide levels for the worst case scenarios do not exceed a concentration of 5%, and is well below the threshold value. For 3 years life, the amount of carbon dioxide

present due to soil respiration is not a hindrance because the mass flow rate of air is higher than that of carbon dioxide leaving the soil due to soil respiration. The mass flow rate of air in and out of the system is $4.4e^{-6}$g/s and the mass flow rate of carbon dioxide is only $1.6e^{-7}$g/s. Hence the higher flow rate of air will not allow carbon dioxide to accumulate in the system. The total percentage of carbon dioxide from the unused air is still 2.6%, which is far below the threshold of posing any problems to the fuel cell's operation.

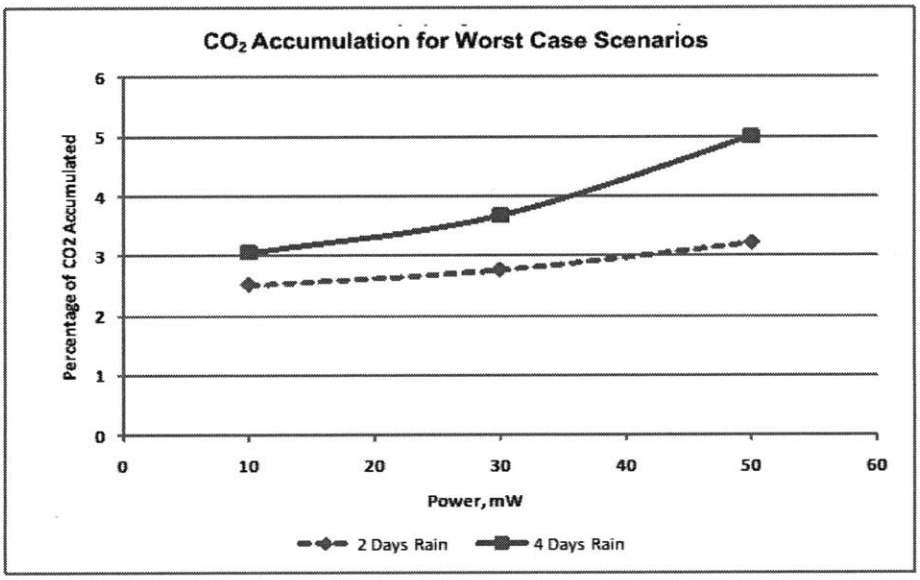

Figure 58. Results from carbon dioxide accumulation analysis.

5.4. Water Management

For efficient performance and longevity of the PEM fuel cells, the inlet air and fuel need to be humidified. The effect of humidity on the performance of PEM fuel cell has been detailed in Chapter 3. Constant humidification of the inlet gases keeps the membrane from drying out and thus aids in extending the life of the fuel cell. Fuel cell also produces heat, water and electricity. For a self-contained, self-sustainable sensor system that works in remote places, the amount of water needed for humidification and the amount of water produced need to be managed.

With the increase in humidity the cell performance increases. However, there is a limited range of humidity level that is favorable for optimal performance of fuel cell. According to fuel cell degradation studies conducted at FSRL, the humidity of air must be maintained in the range of 30-50% for extending the life of fuel cell operation to 3 years [19]. The air entering the system carries some humidity. However, the reference mission is in the Negev, the humidity levels are very low. The average rainfall at Nizzana is about 95 mm [59]. The humidity levels of Nizzana soil range between an average of 5 to 10% during summer and rainy months [52, 59]. This humidity level is not sufficient for long term operation of fuel cell. Therefore, the air flowing into the system must be humidified to 30-50% before it gets fed into the fuel cell cathode. Hydrogen is humidified using a humidifier to 100% for the 10mW power required. The hydrophobic material

used in the air management system allows water vapor to escape from the system into the surroundings depending on the relative humidity levels in the system and the surroundings. Hence an efficient way to control the humidification process and prevent the escape of humidity from the system has to be designed. A simple water management system is proposed here to overcome this challenge.

First, analysis is performed to determine the total amount of water required for humidification of hydrogen and air at an operating temperature of 30°C. The saturation pressure of water at 30°C is determined from the psychometric chart that gives the thermodynamic properties of moist air [44]. The amount of water required for 100% humidification of hydrogen is calculated. The mass flow rate of hydrogen ($\dot{m}_{H_2}$) that is explained Chapter 3 is given in Eq.101. To use the psychometric chart values for hydrogen, the number of moles of hydrogen ($moles_{H2}$) entering the fuel cell should be calculated (Eq. 103). Water required for humidification of hydrogen ($m_{H_2O\_Humidification}$) is calculated using Eq.104, where, the water saturation pressure ($H_2O\ Sat\_pressure$) is derived from the psychometric chart (see Table 16).

$$\dot{m}_{H_2} = \frac{I \cdot M_{H_2}}{2F} \tag{101}$$

$$m_{H_2} = \dot{m}_{H_2} * time \tag{102}$$

$$moles_{H_2} = m_{H_2} * M_{H_2} \tag{103}$$

$$m_{H_2O\_Humidification} = moles_{H_2} * H_2O\ Sat\_pressure \tag{104}$$

A similar procedure is applied for calculating amount of water required for humidifying air to 50%. The amount of water required to humidify 1 kg air to 50% is 8 grams [44]. The total amount of water produced by the fuel cell is determined for 10mW power for 3 years at 65% fuel cell efficiency (see Table 15).

Table 15.Water required and released by fuel cell.

Parameter	Value
Total H_2 needed for 3 years	12.2 g
Water for 100% H_2 humidification	4.6g
Total air needed for 3 years	414.1g
Total O_2 needed for 3 years	96.3g
Water for 50% air/O_2 humidification	4.6g
Total amount of water produced in 3 years by fuel cell	108.4g
Water saturation pressure at 30°C	0.0424 atm
M_{H2}-Molar Mass of Hydrogen	2.0185 g/mol
Voltage	0.82 V (at 65% efficiency)
I-Current (Power/Voltage)	1.2e-^{2} A

The water values in the table suggest that the amount of water that needs to be carried by the system is very minute. The water produced by the fuel cell can be used to humidify the air coming in. Figure 59 shows one simple concept of the proposed water management system. In this setup, the water produced from the fuel cell is collected. A humidity sensor in the system will sense the humidity of the air coming into the

system. A regulator that gets signal from the humidity sensor is attached to the water collector from the fuel cell. If the humidity of air coming into the system is less than 50%, the humidity sensor signals the regulator to release the required amount of water vapor to humidify the incoming air. As mentioned previously, the hydrophobic material lets water vapor escape from the system; a different option of encapsulating the fuel cell with a vapor barrier material around the fuel cell can be adopted (see Figure 59). The vapor barrier minimizes water vapor loss from the incoming air. Feasibility analysis is performed to show that the use of vapor barrier would improve the water management.

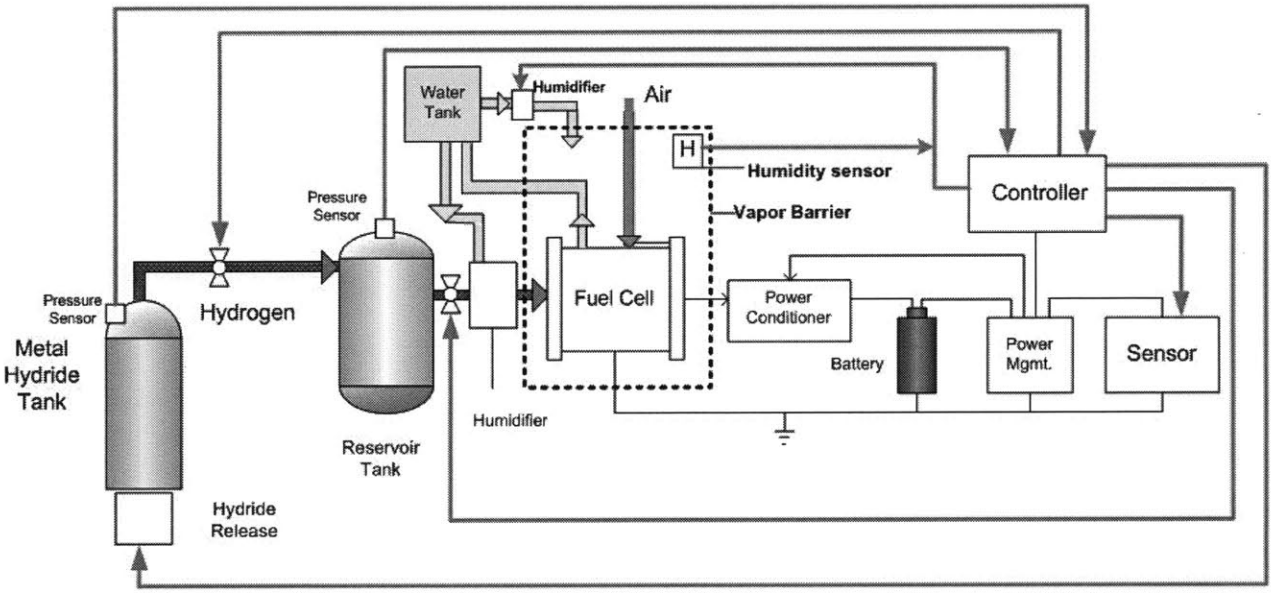

Figure 59. Water management concept for fuel cell powered sensor systems [19].

A spray foam vapor barrier by CertainTeed® is used for analysis [14]. Vapor barriers not only prevent the escape of vapor but also minimize air permeability. Therefore, the thickness of the barrier must be sized to minimize the humidity loss and allow enough air flow for proper operation of the fuel cell. This data is extrapolated from the data provided by the vapor barrier manufacturing company [14]. The mass flow rate of air required by the fuel cell to produce 10mW power is compared to the mass flow rate of air through the barrier. The corresponding vapor mass flow rate escaping from the vapor barrier is calculated. Then the minimum surface area of the vapor barrier that satisfies the vapor flow rates is determined. Figure 60 shows the surface area of the barrier versus the vapor flow rate from the system. Table 16 gives the parameters of the barrier chosen and the permeability rates of air and water for a 0.1 inch (0.26cm) barrier. Figure 61 shows that the air flow into the vapor barrier material is higher than the air flow required for the fuel cell operation.

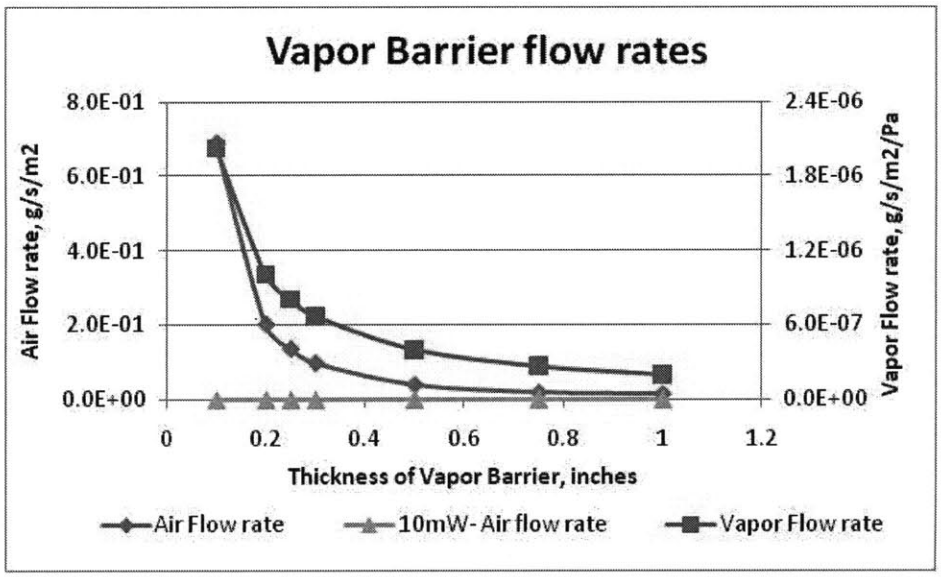

Figure 60. Air and vapor flow rates through the vapor barrier for water management.

Table 16. Parameters used for water management analysis.

Parameter	Value
Vapor barrier material used for analysis	CertaSpray™ Closed cell foam
Thickness of material	0.26 cm (0.1 inch)
Air flow rate though barrier	$2.9e^{-3}$ g/s
Vapor flow rate through barrier	$8.5e^{-9}$ g/s
Surface area of barrier	4.2 e^{-3} m^2

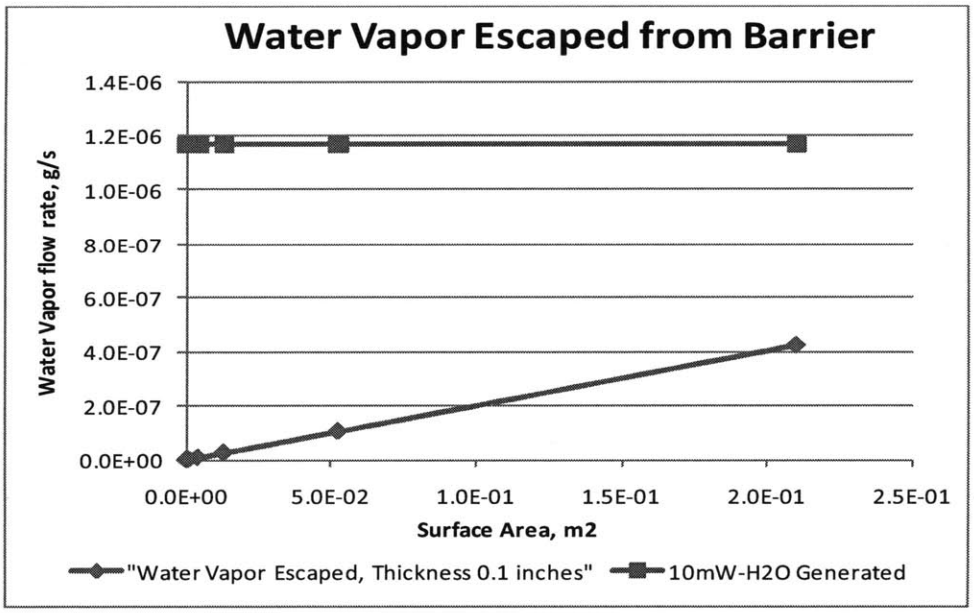

Figure 61. Vapor escaped from the system with respect to the vapor barrier surface area.

Taking into account the escape of vapor from the system, the amount of water required to humidify air for 3 years is determined using the model shown in Figure 62. The flow rates of water are given by Eq.105-

108. Table 17 gives the values of amount of water that needs to be carried onboard the system with and without the vapor barrier. The results show that the water needed in the absence of vapor barrier is very large. Hence, the option of using a vapor barrier is the best option. Using the vapor barrier, only very small amount of water is required to humidify air in the beginning as shown in the table and the rest of the water for air humidification comes from water produced by the fuel cell. The time required to the initial amount of water required is 3.2 minutes. Therefore, overall the total amount of water that should be carried by the system is only 5g and a container to collect the water from the fuel cell should be placed in the system.

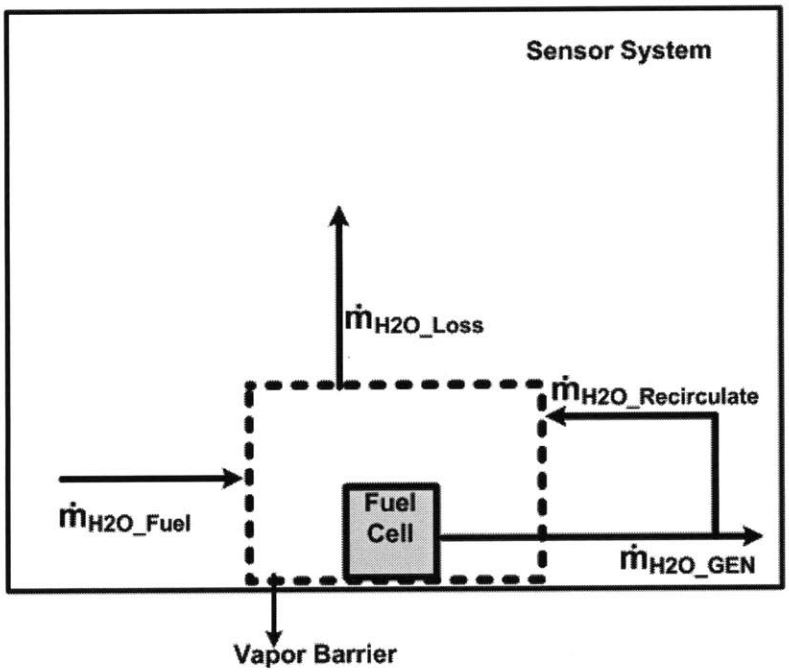

Figure 62. Model for water management analysis.

Flow rates into the vapor barrier

$$\dot{m}_{H_2O\_Fuel} + \dot{m}_{H_2O\_Recirculate} \quad (105)$$

Where, $\dot{m}_{H_2O\_Fuel}$ is the water coming in through humidified hydrogen and $\dot{m}_{H_2O\_Recirculate}$ is the water coming being re-circulated to humidify air.

Flow rates out of vapor barrier

$$\dot{m}_{H_2O\_Loss} + \dot{m}_{H_2O\_GEN} \quad (106)$$

where, $\dot{m}_{H_2O\_Loss}$ is the water vapor lost from the system because of humidity difference between the system and the surrounding, $\dot{m}_{H_2O\_GEN}$ is the water generated by the fuel cell.

At steady state water lost should be equal to water re-circulated as shown below.

$$\dot{m}_{H_2O\_Loss} = \dot{m}_{H_2O\_Recirculate} \quad (107)$$

For recirculation the water generated by the fuel cell should be greater than water lost from the system.

$$\dot{m}_{H_2O\_GEN} > \dot{m}_{H_2O\_Loss} \quad (108)$$

Table 17. Comparison of water required with and without vapor barrier in the system.

Parameter	Without Vapor Barrier	With Vapor Barrier
Water needed for 100% H_2 humidification for 3 years	4.6g	4.6g
Water needed for 50% air humidification	>50kg	2.3e-4 g of water initially required. At steady state water produced from fuel cell will be used
Total water generates in 3 years	108.4g	108.4g

The option of disregarding the use of vapor barrier can be done, if oxygen is carried on board. This would require only 4.6 g of water for humidification of oxygen (Table 15). However, carrying pure oxygen does not seem feasible in terms of storage volume, and complexity of regulating the oxygen storage system.

Air and Water Management Analysis Summary

Passive methods for air and water management for a buried fuel cell powered sensor network system are proposed and analyzed. The results from the analysis show that if the system is buried, it is possible for the fuel cell to breathe from the surrounding soil. For water management, it is proposed that the water produced by the fuel cell can be re-circulated and used for humidifying air and hydrogen. However, there is a need for a simple controls strategy that would integrate the various mechanisms and operations.

CHAPTER 6

CONCLUSIONS AND RECOMMENDATIONS

6.1. Summary of Results

The results of this study support the feasibility of using micro fuel cell systems for distributed sensor networks. The analysis suggests that fuel cell power systems have the potential to provide far more energy than conventional batteries both in terms of mass and volume density, making them favorable for use in long duration missions in the order of months to years.

The study focuses on developing a micro PEM fuel cell model to predict the performance in harsh environments. The effect of field operating conditions such as humidity, temperature and pressure on the fuel cell are simulated and studied. Experimental analysis using fuel cells is performed to generate powers in the range of 10-500mW and the effects of operating conditions are studied and the developed model is validated.

Two reference missions are chosen to study the implementation of the fuel cell power concept in challenging environments. The results strongly support the feasibility of using simple system designs with passive control strategies for thermal, air and water management. For space applications, where large thermal gradients are expected, a novel thermal architecture is proposed and analyzed. An experimental thermal system prototype is developed and tested in a cold chamber to simulate a reference mission in the polar regions of the moon. For terrestrial applications, a reference mission in the desert regions of Negev, Israel is chosen and the challenges of the fuel cell powered sensor system operating in those field conditions are studied. Finally, simple yet effective system designs for air and water management are proposed and feasibility is shown using analytical methods.

6.2 Challenges and Lessons Learnt

Although this study strongly supports the feasibility of using fuel cells for long durations, the premature failures and unreliability of fuel cells have prevented the full potential of this technology from being realized in any field system. An ongoing degradation analysis being conducted in FSRL on fuel cell life suggests that field conditions such as fluctuating load/sensor power demands and operating conditions such as temperature and humidity reduce the life-span of fuel-cells.

As mentioned in Chapter 2, fuel cell technologies also face the challenge of hydrogen and oxygen storage. For very large networks of sensors, the complete fuel cell system needs to be as small as possible for reasons such as transportation (ease of carrying the sensors if required by military personnel). On-board hydrogen storage continues to be one of the most technically challenging barriers for miniaturization of the fuel cell power system. While metal hydrides are currently the best option available to store hydrogen, the

weight storage efficiencies presently do not exceed 6% at room temperatures [46, 47, 55]. Metal hydrides that exhibit high storage efficiencies require high pressures or high temperatures to release hydrogen, placing them beyond the scope of the simple, self-contained sensor packages being studied in this research. In the case of oxygen storage, the current technologies employing pressurized aluminum tanks, carbon composites [5], or gasar materials [36] are not suitable due to the complexity and safety issues that accompany the transport of pure oxygen.

For self-containing sensor networks working with fuel cell power systems in remote places, it is crucial to develop a controls system that would manage the operating conditions of the fuel cell. During the testing of passive thermal architecture for space applications, it is learnt that perfect vacuums do not exist and it is not feasible to maintain a vacuum in an enclosed system for long durations. As a result, it is realized that for self-containing sensor power systems in remote places and extreme environments, it is crucial to develop a controls strategy to manage the operating conditions of the fuel cell and isolate fuel cells from environmental variations. This would augment the life of fuel cells. The challenge then is to design embedded controls system that are relatively simple and reliable and that will reduce the stress on the fuel cells. Although several control strategies exists in literature, none of them address control strategies for small scale power demands over long durations in the field.

6.3 Future work

As described in Section 6.2, there are a number of technologies that need to be developed to further this research. First, a miniaturized version of the fuel cell power system should be developed. Research is being conducted to discover different configurations and components to miniaturize the whole fuel cell power supply system. Much of the controls and hybrid fuel cell-battery technology required to fit within a system no larger than 6 inch diameter sphere or a 6 inch wide cube already exists; however, the components need to be integrated and ideally a plug-and-play system that operates in any environment needs to be developed. A miniature hydrogen storage system appropriate for the sensor package will need to be developed and that has the required storage capacity.

Research is being performed on the implementation of hybrid power systems for electrical load management (sensor power demands). A control strategy to manage and stabilize the operating conditions of the fuel cell must be developed that will the system from disturbances arising from changing external field conditions. The successful implementation and testing of fuel cell systems in field-simulated conditions open doors to various small scale applications in several fields, including robotics, communications, space exploration, and unmanned aerial vehicles.

REFERENCES

1. ABC News, "2008 China Earthquake Devastation". Web, April 2010. Available: http://www.abc.net.au/news/photos/2008/05/13/2242718.htm

2. Acrylic Datasheet, Web Feb 2009. Available: http://www.curbellplastics.com/technical-resources/pdf/acrylic-pop-datasheet-curbell.pdf

3. AeroVironment, Unmanned Aircraft Systems. Web, March 2010. Available: www.avinc.com

4. W. A. Amos, "Cost of Storing and Transporting Hydrogen", National Renewable Energy Laboratory, 1998, Web, Available: http://www1.eere.energy.gov/hydrogenandfuelcells/pdfs/25106.pdf

5. J.C. Amphlett, R.M. Baumert , R.F.Mann, B.A.Peppley, P.R. Roberge, A.Rodrigues, "Parametric Modeling of the Performance of a 5-kW Proton-Exchange Membrane Fuel Cell Stack," Journal of Power Sources, Vol.49, Pages 349-356, 1994.

6. J. C. Amphlett, R. M. Baumert, R. F. Mann, B. A. Peppley, and P. R.Roberge, "Performance Modeling of the Ballard Mark IV Solid Polymer Electrolyte Fuel Cell, I. Mechanistic model development," Journal of Electrochemical Society,Vol.142, Pages 1-8, 1995.

7. Angstrom Power, 2006, V60 Fuel Cell Module. Web, April 2010. Available: http://www.angstrompower.com/products_v60.html

8. F. Barbir, *PEM Fuel Cells: Theory and Practice*, Elsevier Academic Press, 2005.

9. J. J. Baschuk and Xianguo Li, "Carbon monoxide Poisoning of Proton Exchange Membrane Fuel Cells," International Journal of Energy Research, Vol.25, Pages 695-713, 2001.

10. B. Burg, S. Dubowsky, J. Lienhard, and D. Poulikakos, "Thermal Control Architecture for a Planetary and Lunar Surface Exploration Micro-Robot," Proceedings of the Space Technology and Applications International Forum, Albuquerque, NM, February 11-15, 2007.

11. K. A. Burke, "Fuel Cells for Space Science Applications," in First International Energy Conversion Engineering Conference Portsmouth, Virginia, AIAA, 2003.

12. K. A. Burke, "Small Portable PEM Fuel Cell Systems for NASA Exploration Missions," in Proceedings of 3rd AIAA International Energy, San Francisco, CA, 2005.

13. Y. A. Cenegel, *Heat Transfer, A Practical Approach*, McGraw Hill, 2nd Edition, 2003.

14. CertainTeed, "CertaSpray™ Specifications". Web, Jan 2010. Available: http://www.certainteed.com/products/insulation/spray-foam-insulation/317388

15. J.Cravalho, *2.006 Thermal Fluids Engineering II Course Notes*, Oxford University Press, 2005.

16. F.A.de Bruijn, D.C Papageorgopoulos, E.FSitters, and G.J.M.Janssen, "The Influence of Carbon dioxide on PEM Fuel Cell Anodes," Journal of Power Sources, Vol.110, Pages 117-124, 2002.

17. Desalt Innovation Middle-East (DIME Creations), "Hydrophobic Materials". Web, Nov 2009. Available: http://www.dimecreations.com/images/homeanimation2.swf

18. S.Dubowsky, K. Manyapu, D. Gallardo, and J. Thangavelautham,, " Long-Life Micro Fuel Cell Power-Supplies for Field Sensors," FSRL Research Report 1, 2009.

19. S.Dubowsky, K.Manyapu, J.Thangavelautham,and D. Gallardo, " Long-Life Micro Fuel Cell Power-Supplies for Field Sensors," FSRL Research Report 2, 2010.

20. S. Dubowsky, J. Thangavelautham, K.Manyapu, and D.Gallardo, " Long-Life Micro Fuel Cell Power-Supplies for Field Sensors," FSRL Research Presentation 1, 2010.

21. S.Dubowsky, "A Long Life Thermal Architecture of Robotic Mobility and Sensor Modules for Operation in Temperature Low Temperature Planetary Environments", Proposal to NASA, FSRL, 2007.

22. S. Dubowsky, K. Iagnemma, D. Lambeth, S. Liberatore, J.S.Plante, and P. Boston, "Microbots for Large-Scale Planetary Surface and Subsurface Exploration," Proceedings of the Space Technology and Applications International Forum, Albuquerque, NM, February, 2005.

23. Energizer, Energizer Product Data Sheet, "AA 91." Energizer, Web, March 2009, Available: http://data.energizer.com/PDFs/E91.pdf

24. T.Fabian, J.D.Posner, R.O'Hayre, S.K.Cha, J.K. Eaton, F.B.Prinz, and J.G.Santiago, "The Role of Ambient Conditions on the Performance of a Planar Air-Breathing Hydrogen PEM Fuel Cell," Journal of Power Sources, Vol.161, Pages 168-182, 2006.

25. E.S.Field, "Fuel Cell Polarization Curve Experimental Procedure," FSRL Report, 2009.

26. S. Fraser, M. Monsberger, and V. Hacker, "Fuel Cell Power System Options for Mars Rovers," 2nd International Conference on Green Propellants for Space Propulsion, Chia Laguna , Sardinia, Italy, ESA, 2004.

27. A.Gholam, and N.P.Gianfranco, Lithium *Batteries Science and Technology*, Kluwer Academic publishers, Boston, Dordrecht, New York, London 2004.

28. GORE-TEX®, "Hydrophobic Material". Web Nov 2009. Available: http://www.gore-tex.com/remote/Satellite/content/how-does-it-work

29. K.Haraldsson, and K.Wipke, "Evaluating PEM Fuel Cell System Models," Journal of Power Sources, Vol.126, Pages 88-97, 2004.

30. R.O'Hayre, R.Braithwaite, D. Hermann, W. Lee, S.J, T.Fabian, S.K.Cha, Y.Saito, and F.B.Prinz, "Development of Portable Fuel Cell Arrays with Printed Circuit Technology," Journal of Power Sources, Vol.124, Pages 459-472, 2003.

31. Y.Hue, H.Tawfik, and K.El-Khatib, "One Dimensional Mathematical Model for PEM Fuel Cells," Systems, Applications and Technology, IEEE Conference, Long Island, May 2005.

32. S. Kesner, "Mobility Feasibility Study of Fuel Cell Powered Hopping Robots for Space Exploration," Master's Thesis, Massachusetts Institute of Technology, 2007.

33. S.Kesner, J.S.Plante, P.Boston, T.Fabian, and S.Dubowsky, "Mobility and Power Feasibility of a Microbot Team System for Extraterrestrial Cave Exploration," Proceedings of the 2007 IEEE International Conference Robotics and Automation, Rome, Italy, April 2007.

34. A. Kundu, J.H. Jang, J.H. Gil, C.R. Jung, H.R. Lee, S.H. Kim, B. Ku and Y.S. Oh, "Micro-Fuel Cells-Current Development and Applications," Journal of Power sources, Vol.170, Pages 67-78, 2007.

35. J.H.Lienhard, *A Heat Transfer Textbook*, 3rd edition, Electronic copy, 2006. Web, August 2009. Available: http://web.mit.edu/lienhard/www/ahtt.html

36. R.Loutfy, V.Shapovalov, and E.Veksler, "Oxygen Source for Isolated Fuel cells," MER corporation, Web, March 2010, Available: www.springerlink.com/index/v5310445w18035h6.pdf

37. R.Lal, *Encyclopedia of Soil Science*, second edition, CRC Press, 2006.

38. A.F. Mills. *Heat Transfer*, 2nd Edition. Upper Saddle River, New Jersey, Prentice Hall. 1999.

39. Moon Temperatures, Web, April 2009. Available: http://www.universetoday.com/guide-to-space/the-moon/temperature-of-the-moon/

40. NASA Surface Meteorology and Solar Energy, Web, Oct 2009. Available: http://eosweb.larc.nasa.gov/cgi-bin/sse/sse.cgi.

41. R. O'Hayre, S. Cha, W. Colella, and F. B. Prinz, *Fuel Cell Fundamentals*, New York, Wiley, 2005.

42. S. R. Ovshinsky, M. A. Fetcenko, and J. Ross, "A Nickel Metal Hydride Battery for Electric Vehicles," *Science* 260, Pages 176-181, 1993.

43. Powerizer, Powerizer Product Data Sheet, Web, March 2009. Available: http://www.batteryspace.com/index.asp?PageAction=VIEWPROD&ProdID=3989

44. Psychometric Chart US and SI Units, Web, March 2010. Available : www.coolerado.com/pdfs/Psychrmtrcs/0000Psych11x17US_SI.pdf

45. J. T. Pukrushpan, A. G. Stefanopoulou, and H. Peng, *Control of Fuel Cell Power Systems: Principles, Model, Analysis and Feedback Design*, Springer-Verlag London, 2004.

46. G.Sandrock, "A Panoramic Overview of Hydrogen Storage Alloys from a Gas Reaction Point of View," Journal of Alloys and Compounds, Vol.293-295, Pages 877-888, 1999.

47. B.Sakintuna, F.L.Darkrim and M.Hirscher, "Metal hydride materials for solid hydrogen storage," International Journal of Hydrogen Energy, Vol.32, Pages 1121-1140, 2007.

48. Soils and Soil Physical Properties, Web, August 2009. Available: casfs.ucsc.edu/education/instruction/.../unit_2.1a_soil_physical.pdf

49. A.Singer, *The Soils of Israel*, Springer, 2007.

50. C. Spiegel, PEM *Fuel Cell Modeling and Simulation Using Matlab*, Elsevier Academic Press, 2008.

51. C.Spiegel, *Designing and Building Fuel Cells*. McGraw-Hill, New York, 2007.

52. M.Sprintsin, D.G. Blumberg, J.B. Asher, J.Daniels, and M. Linetsky, "Estimation of Soil Water Content in the Negev Desert Open Areas Using Archived ERS SAR Images," Geoscience and Remote Sensing Symposium, IGARSS '02, IEEE International, Vol.4, Pages 2220-2222, 2002.

53. Y.Takada, T.Tamachi, S.Taninaka, T.Ishii, K.Ebita, and T.Wakisaka, "Development of Fish Robots Powered by Fuel Cells: Improvement of Swimming Ability by a Genetic Algorithm and Flow

Analysis by Computational Fluid Dynamics," *Bio-mechanisms of Swimming and Flying*, Chapter 19, 2008.

54. US Department of Energy. HFCIT Fuel Cells: Types of Fuel Cells. Web, April 2009. Available: http://www.eere.energy.gov/hydrogenandfuelcells/fuelcells/fc_types.html

55. US Department of Energy. HFCIT Hydrogen Storage: Metal Hydrides. Web, August 2009. Available: http://www.eere.energy.gov/hydrogenandfuelcells/storage/ metal_hydrides.html

56. US Defense Logistics Agency, Ragone chart, Web April 2010, Available: http://electronicdesign.com/Content/14978/58749_fig_01.gif

57. H.Wang and C.Qi, "Performance Study of Underground Thermal Storage in a Solar-Ground Coupled Heat Pump System for Residential Buildings," *Energy and Buildings,* Vol. 40, Pages 1278-1286, 2008.

58. C.Wang, H.Nehir, and S.R.Shaw, "Dynamic Models and Model Validation of PEM Fuel Cells using Electrical Circuits," IEEE transaction on Energy Conversion, Vol.20, Pages 442-451, 2005.

59. A.Yair, H.Lavee and N.Greitser, "Spatial and Temporal Variability of Water Percolation and Movement in a System of Longitudinal Dunes, Western Negev, Israel," Hydrological Processes, Published Online, Vol.11, Pages 43-58, 1998.

60. Q.Yu, S.Y.Choe, A.K.Srivastava and W.Gao, "Improved Modeling and Control of a PEM Fuel Cell Power System for Vehicles," Proceedings of IEEE South East Conference, Memphis, March, 2006.

61. E.Zaady, U.Kuhn, B.Wilske, L.Sandoval-Soto and J. Kesselmeier, "Patterns of CO_2 Exchange in Biological Soil Crusts of Successional Age," Soil Biology and Biochemistry, Vol.32, Pages 959-966, 2000.

62. J.Zhang, *PEM Fuel Cells Electrocatalysts and Catalyst Layers, Fundamentals and Applications*, Springer, 2008.

63. Y. Zhang, M.Ouyang, Q. Lu, J. Luo, and X.Li, "A Model Predicting Performance of Proton Exchange Membrane Fuel Cell Stack Thermal Systems," Applied Thermal Engineering, Vol.24, Pages 501-513, 2004.

APPENDIX

A

FEASIBILITY ANALYSIS FOR OTHER SMALL SCALE APPLCIATIONS

In addition to the feasibility analysis that was performed in chapter 2, further analysis of using fuel cells as power supply is executed for other small applications such as unmanned aerial vehicles (UAVs), autonomous underwater vehicles (AUVs) and terrain robots. The sections below provide a comparison of fuel cells with other electrochemical technologies including photovoltaic cells (PV) and a combination of fuel cells with PV as well as batteries. The mass of the system and the power demand using the various power sources are analyzed and compared. In all the cases using fuel cells proved to be the best option.

A.1. UAV Feasibility Analysis

The feasibility analysis for UAVs is performed to analyze the mass of the system for a mission operating upto 6 months. Small UAVs are used in applications such as border patrol and search and rescue operations. The goal of the mission assumed for the analysis is that the vehicle should be capable of operating continuously for 6 months at a cruise altitude of 8000 ft with a range of 125 km. The mass of the system should not exceed 200kg. A UAV with a wing span of 4.27m is used.

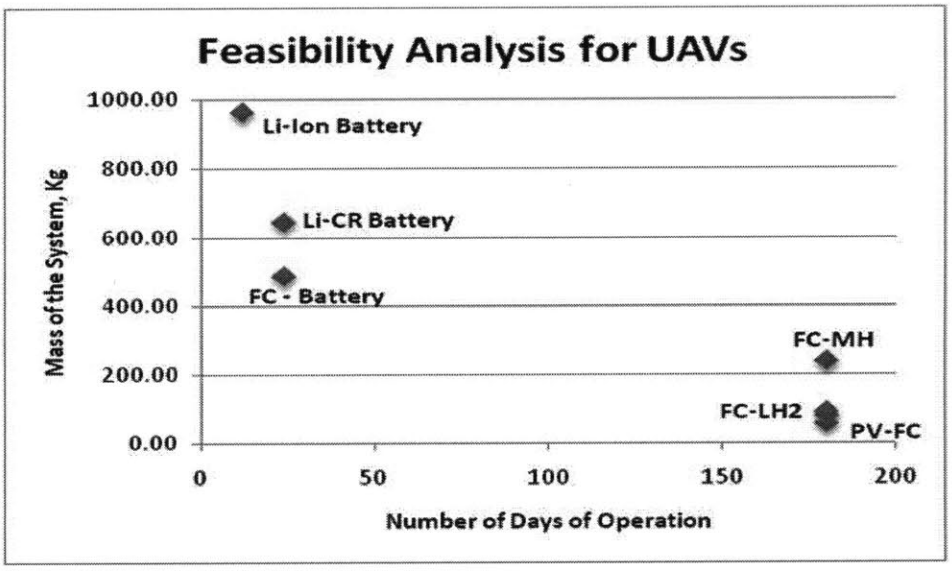

Figure 63. Feasibility analysis results for UAVs.

Figure 63 plots the results of number of operating days versus the mass of the power system. From the figure it is evident that the battery technology is not capable of providing 6 months of sustained power within reasonable mass allocation. The results also show that lithium polymer batteries provide only up to 12-15

days of power with a mass nearing 1000 kg which is an unreasonable mass for UAVs. Even a fuel cell-battery hybrid system does not provide sufficient power for 6 months within practical mass range. Fuel cells with metal hydride storage as well as liquid hydrogen storage are capable of providing sustained long-term power. Analysis also shows that a PV-fuel cell with metal hydride storage provides power for 6 months with a lowest mass of 60kg.

A.2. Terrain Robots

For a reference mission requiring the robot to traverse a distance of 50km in 4 hours and with a 2 5kg restraint on the mass of the system is considered for this analysis. The robot needs to traverse on a rough terrain such as rocky surfaces with hills and boulders. Small terrain robots are useful in border patrol and related applications. The feasibility results for terrain robots, shown in Figure 64 are similar to the UAV feasibility results, fuel cells with metal hydride storage provide the lowest system mass. PV cells in combination with fuel cells are the next competing technology. Batteries fail to keep the mass of the robot below 25kg.

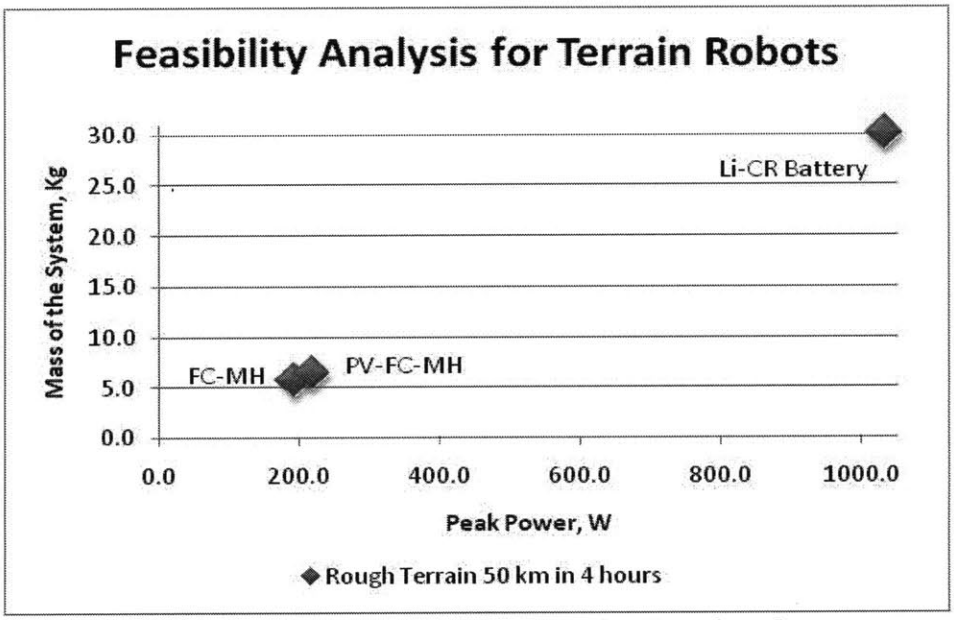

Figure 64. Feasibility analysis results for Terrain robot.

A.3. AUV Feasibility Analysis

An AUV such as a fish robot is considered for the analysis. These devices are used in applications like search and marine rescue operations involving image sensing, Used in the fields of underwater archaeology, photography, mapping, water cultivation and fishing as well as underwater carrying of small-sized object and to explore underwater terrain [53]. A fish robot that is 1 meter long is considered for this analysis. The goal considered for this analysis is that the fish robot should be able to survive for 15 days performing image sensing and transmitting during search and rescue operations. The robot should be able to traverse 15 miles in water and be able to dive to 15 feet into the water. Figure 65 shows that for a fish robot

that is about a meter long and travels a distance of 15 miles, the fuel cell system with metal hydride storage is the best option for powering the system for 15 days. With the use of lithium polymer batteries that are presently used in AUVs, the mass is anywhere from 3-10 times more than that of the fuel cell powered system increasing the overall power demand as well. For the fuel cell system, oxygen can be carried by the onboard system as compressed gas or as hydrogen peroxide. The materials used for the system can be also designed such that the fuel cell system will be able to breathe the oxygen that is present in water. Presently there are no research data available on this subject and could be a major area for further research.

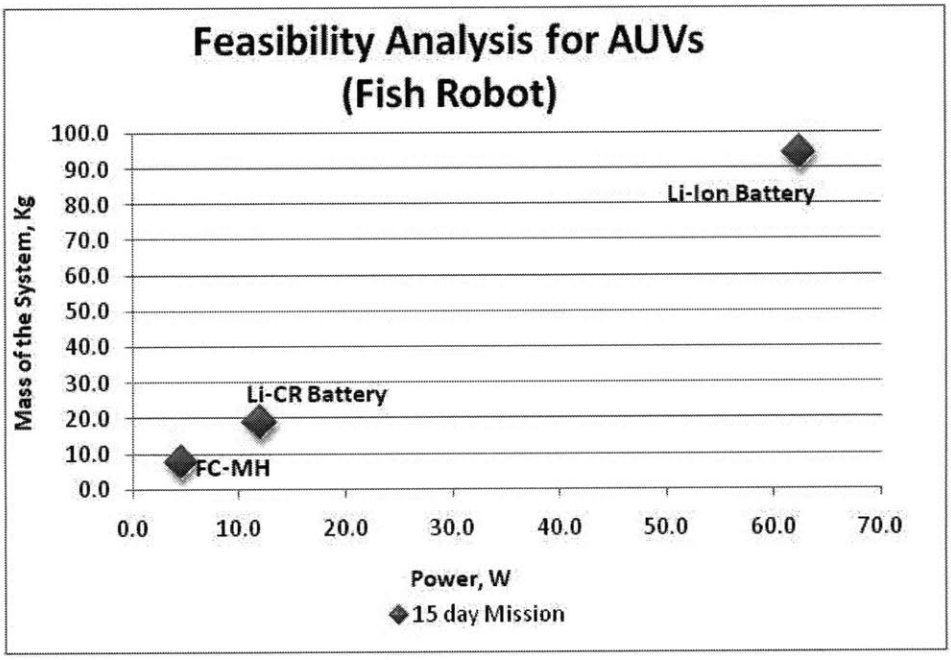

Figure 65. Feasibility analysis for AUVs (Fish Robot).

APPENDIX
B
DETAILS OF FUEL CELL EXPERIMENT

The fuel cell experiment is conducted to characterize the fuel cells in FSRL and understand the performance of the fuel cell with varying operating conditions. The sections below detail the experimental procedures and layouts [25].

B.1.Fuel Cell Equipment

- 3 Fuel cells connected in series, attached to the fuel cell holder
- Environmental chamber
- Hydrogen humidifier
- Hydrogen gas (Airgas industrial hydrogen HY 200)

B.2 Test Equipment

- Multimeter (BK Tool Kit 2703B)
- 2 Alligator clips.
- Resistance network (Figure 66 and Figure 67)
- Hydrogen pressure gauge (Concoa regulator 4021361-01-350).
- Relative humidity sensor (RadioShack 63-1032).
- Ambient temperature sensor (RadioShack 63-1032)
- Fuel cell temperature sensor (RadioShack 63-1032).
- Humidity generator (sponge and sponge holder).
- Clock or timer.

B.3. Resistance Network

The resistance network provides 16 different resistances that are connected to the fuel cells at different times during the polarization process, from highest resistance to lowest. The 16 resistances are labeled in Figure 66. The multimeter measures the voltage across the fuel cells during the experiment.

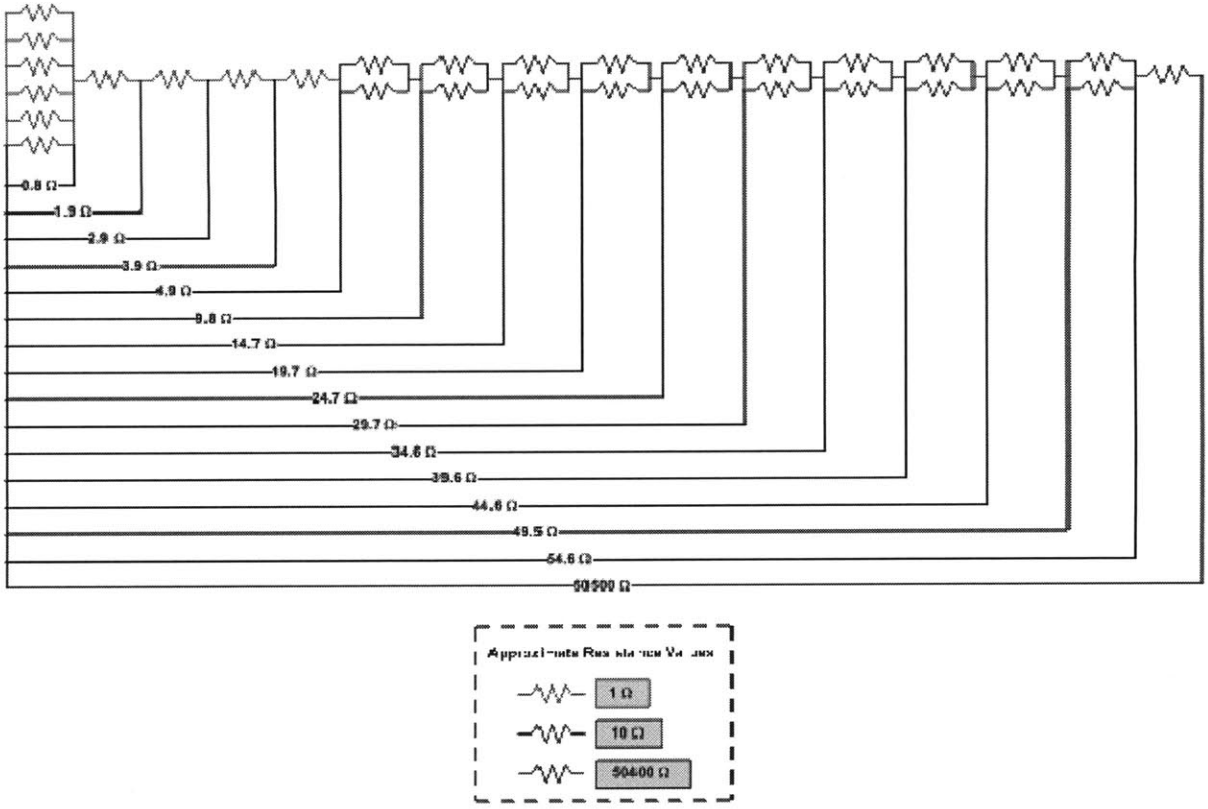

Figure 66. Resistance Network values [25]

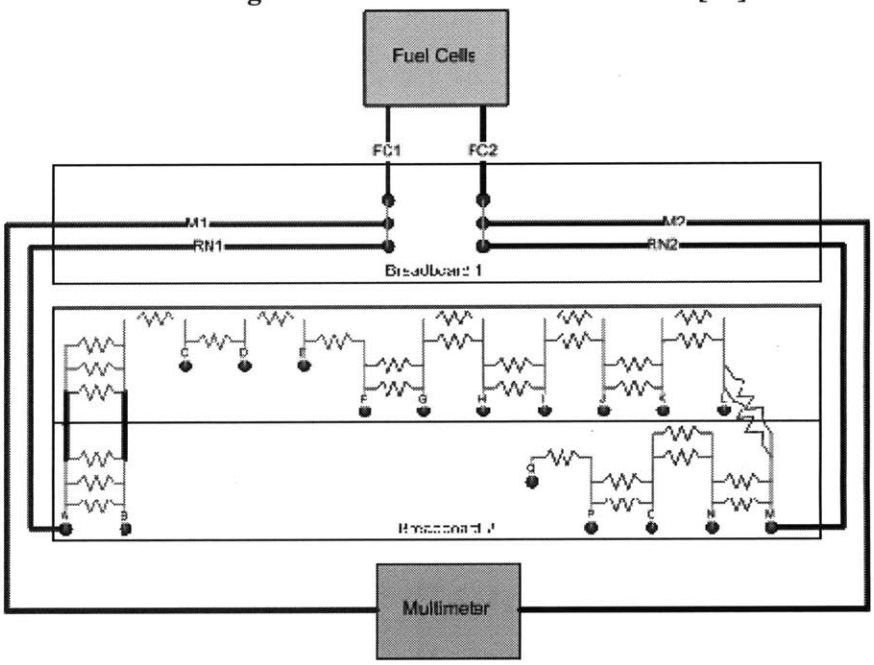

Figure 67: Electrical Schematic of Resistance Network, Fuel Cells, and Multimeter [25].

B.4. Experimental Procedure

The overview of the experimental setup is explained in Chapter 3.

B.3.1. Safety Precautions

- The lab door must be left open whenever hydrogen is used.
- Personnel need to be statically discharged using a grounded wristband or equivalent before starting the experiments.
- Liquids must be kept away from the resistance network and other electronic components.
- Objects (particularly powered electronics) not part of the experimental setup must be kept away from the area (to avoid risk of spark ignition).
- The fuel cells are not to be shorted under any circumstances.
- All emergencies need to be reported immediately to the emergency contact number listed: 617-253-1212 (MIT 24-hour police, ambulance, fire, and first aid).

B.3.2. Fuel Cell Start-Up Procedure

1. The temperature and relative humidity sensor is always turned on. This sensor should be placed beside the fuel cells so that the temperature and humidity readings are visible from within the environmental chamber. The cord of the sensor head measuring the fuel cell temperature needs to be fastened to the fuel cell holder with masking tape, and the sensor head touching the edge of the third fuel cell, as shown in Figure 68.

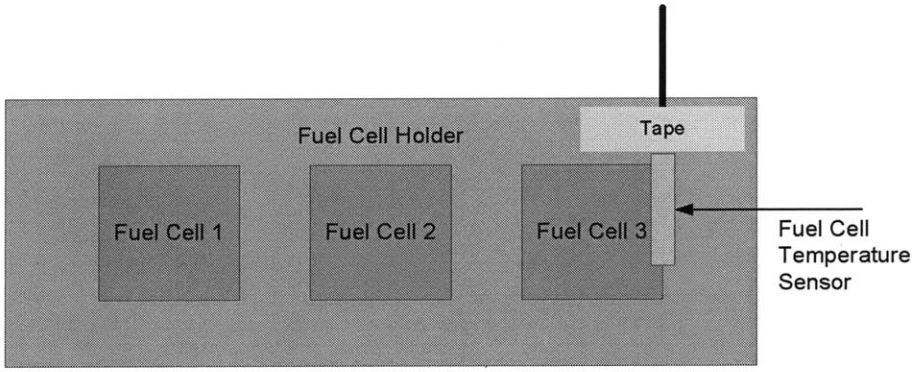

Figure 68. Fuel Cell Temperature Sensor Placement [25].

2. A wet sponge is placed in the environmental chamber if the humidity is below 50%. Water may be added to the sponge periodically before the fuel cells are activated, until the desired humidity of 50% is reached for the particular experiment. The sponge is removed after 50% humidity is reached.
3. The fuel cell leads FC1 and FC2 should be connected to Breadboard 1, as shown in Figure 67. The resistance network leads RN1 and RN2 should also be connected to Breadboard 1, as shown in Figure 67.
4. The resistance network is disconnected from the fuel cells by having RN1 and RN2 unplugged from Breadboard 2. Care is taken to ensure RN1 and RN2 do not touch each other or another object that could cause them to short.

5. Each of the wires M1 and M2 are connected to alligator clips. The free end of the alligator clip connected to M1 is connected to the positive lead of the multimeter and the free end connected to M2 is connected to the negative lead. The multimeter is set to read voltage on the scale of 20.
6. The hydrogen gas tank outlet is opened and the regulator is used to adjust the hydrogen pressure to the desired value for the experiment. The time taken for the pressure to reach the desired value is recorded, along with the voltage reading on the multimeter, the ambient temperature, fuel cell temperature, and relative humidity. This marks the beginning of the open circuit fuel cell procedure.
7. After 15 minutes of open circuit operation, the voltage reading on the multimeter, the ambient temperature, fuel cell temperature, and relative humidity are all recorded.
8. The wire labeled RN1 is connected to 'A' on Breadboard 2, and RN2 to 'C' on Breadboard 2. This corresponds to connecting the fuel cells to the 1.9 Ω resistance in the resistance network and is equivalent to operating the fuel cell at approximately 450mA. After 10 minutes, the voltage reading on the multimeter, ambient temperature, fuel cell temperature, and relative humidity are all recorded.

B.3.3. Polarization Measurement Procedure

1. The wire labeled RN1 is connected to 'Q' on Breadboard 2, and RN2 to 'P' on Breadboard 2. After 5 minutes, the voltage reading on the multimeter, ambient temperature, fuel cell temperature, and relative humidity are recorded.
2. Periodic checks of the hydrogen pressure gauge need to be performed to ensure the hydrogen pressure has not changed from the desired value. If the hydrogen pressure changed, the new pressure is recorded and the regulator is readjusted to meet the desired value.
3. The previous two steps are repeated for decreasing resistances, according to the connections shown in Table 18. Note that RN1 stays the same while RN2 needs to be switched.

Table 18. Connection Guide for RN1 and RN2, and the corresponding resistance [25].

RN1	RN2	Resistance (Ω)
A	P	54.6
A	O	49.5
A	N	44.6
A	M	39.6
A	L	34.6
A	K	29.7
A	J	24.7
A	I	19.7
A	H	14.7
A	G	9.8
A	F	4.9
A	E	3.9
A	D	2.9
A	C	1.9
A	B	0.8

B.3.4. Fuel Cell Shut-Down Procedure

After the last voltage, temperature, and humidity measurements have been recorded, for a resistance of 0.8Ω, the hydrogen gas tank outlet and multimeter are turned off. This marks the end of the experiment.

B.3.5. Data Gathering

The data from the polarization procedure contributes to the creation of the polarization curve of the fuel cells. A polarization curve is a plot of the fuel cell output voltage as a function of output current for a particular load. The fuel cell output voltage is determined experimentally in the polarization procedure. The output current of the fuel cell is equal to the output voltage divided by the resistance. The power output and efficiency of the fuel cell can be determined from the polarization curve. Power is equal to the product of output voltage and output current. Efficiency is equal to the output voltage divided 1.481V or 1.254V depending on the phase of water being generated, the voltage equivalent of the higher heating value or low heating value enthalpy [8].